Mira Geoscience
...modelling the earth

ADVANCED GEOPHYSICAL INTERPRETATION CENTRE

Mira Geoscience Limited
409 Granville Street, Suite 512 B
Vancouver, BC
Canada V6C 1T2

Tel: (778) 329-0430
Fax: (778) 329-0668
info@mirageoscience.com
www.mirageoscience.com

Integrated Geologic, Magnetic and Radiometric Cu-Au-Mo Targeting on the G, K and O Block Properties near Carmacks, Yukon Territory, Canada

Prepared for: Canadian Dehua International Mines Group Inc.

Project Number: 3486

Work Completed by:

Vicki Thomson

Diane Hanano

Patrick van Kooten

Peter Kowalczyk

Date: Dec 20, 2010

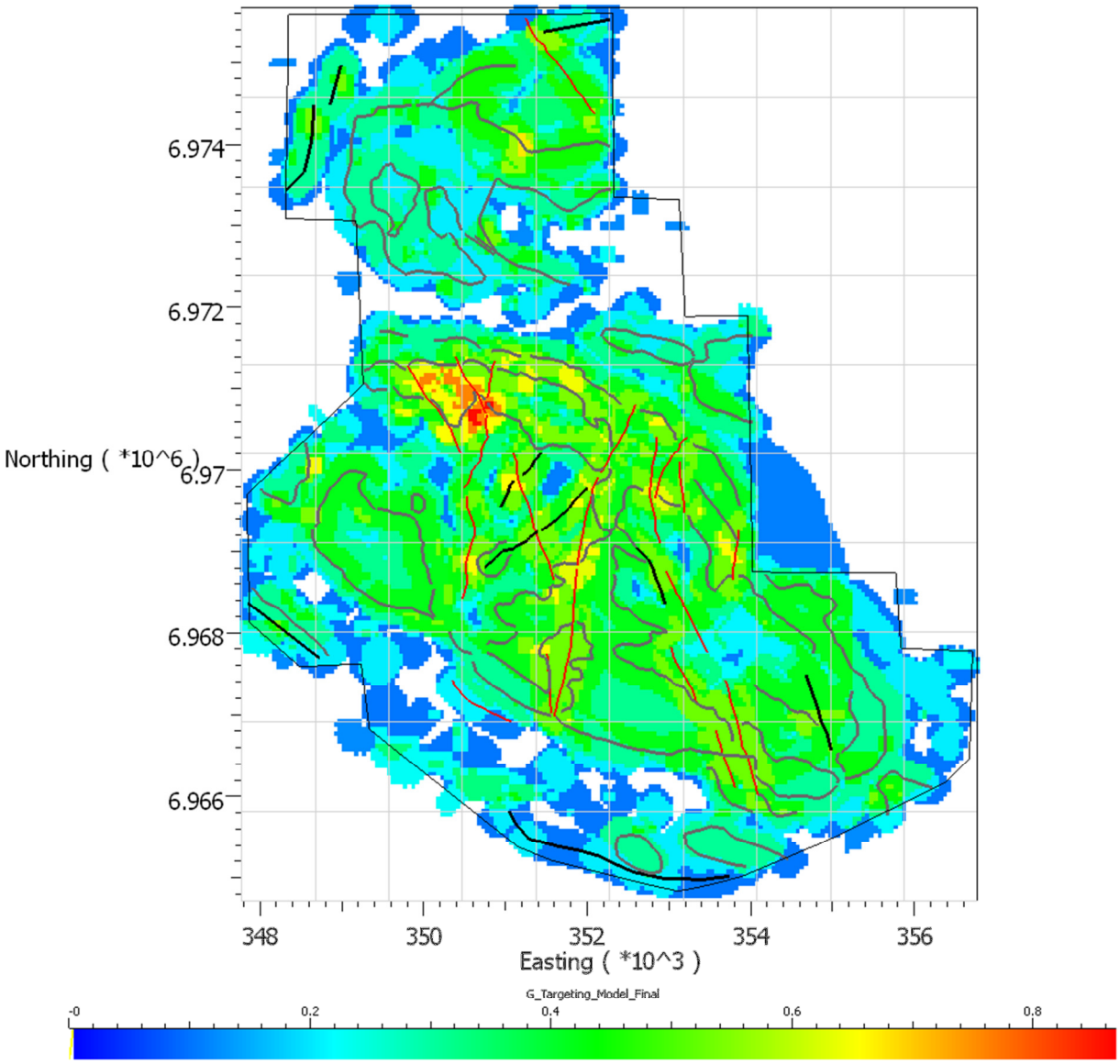

Figure 1: Targeting result for the G Block showing targets coloured by score with structural interpretation shown. Similar maps have been produced for K & O blocks.

Executive Summary

The Advanced Geophysical Inversion Centre (AGIC) at Mira Geoscience has completed integrated geologic, magnetic and radiometric Cu-Au-Mo targeting of the G, K, and O block properties near Carmacks, Yukon Territory, Canada, for Canadian Dehua International Mines

Group Inc. This work has been conducted to aid the geologic understanding of the project areas and for prioritization of exploration targets.

This report provides information on the strategy and method employed for the targeting, the data processing and geophysical interpretation and modelling results, the targeting criteria and results, as well as conclusions and recommendations. The targeting results show that there is the good potential for a large deposit to be found on the G, K and O block properties. All three properties show that a significant number of criteria are satisfied for intrusive-porphyry style mineralization at numerous locations on the properties. The interpretation of the geophysical data and subsequent targeting performed on the survey areas represent a very thorough review.

The models produced in this study should have persistent value to Canadian Dehua International Mines as long as they hold the property. The final model will be adaptable to further targeting studies. Modifications to exploration criteria or target type, definition of training data, or simply the addition of new drilling or other data can all be used to update the existing model easily now that the investment in the model framework for the Carmacks area is complete.

Table of Contents

List of Figures

List of Tables

1. Introduction

The objective of the Carmacks exploration targeting project is to identify zones within the project areas that have the potential to host Cu-Au-Mo style mineralization. These target areas will be identified based on the structural and lithological interpretation of the magnetic and radiometric data. The targeting criteria will be developed from known mineralization in the area, favourable geology, and intrusive-porphyry style deposit model to complement the geophysical data.

Geophysical prospecting methods used in mining exploration provide information about the physical properties of the subsurface. These properties can in turn be interpreted in terms of lithology and/or geological processes. Moreover, the geometric distribution of physical properties can help delineate geological structures and may be used as an aid to determine mineralization and subsequent drilling targets.

The Advanced Geophysical Interpretation Centre at Mira Geoscience has completed a geologic review, 2D structural interpretation of the magnetic and radiometric data, and 3D magnetic inversion modelling of magnetic data from the G, K and O block properties near Carmacks, Yukon Territory, Canada.

This report provides information on the strategy and method employed for the targeting (Section 3), the data processing and geophysical interpretation and modelling results (Section 4), the targeting criteria and results (Section 5), as well as conclusions and recommendations (Section 6). A list of project deliverables can be found in Appendix 1.

The final model will be adaptable to further targeting studies. This can be accomplished by updating the exploration criteria embodied within the model to reflect new exploration concepts or new data as it becomes available. The framework for furthering exploration targeting models and concepts is now in place.

2. Geologic Review

2.1. Regional Geologic Setting

The G, K, and O Properties are located approximately 60-115 km northwest of Carmacks, in west-central Yukon. The properties are located within the Dawson Range Mineral Belt, a 125 km northwest-trending corridor of polymetallic mineral deposits. The belt lies at the northern end of the Intermontane Terranes, and is primarily underlain by assemblages belonging to the Yukon-Tanana and Stikinia terranes. In the Dawson Range region, the Yukon-Tanana Terrane is composed of metasedimentary and metavolcanic rocks, including quartz-mica schist and diorite gneiss. The regional structure and geology is not well understood, due to limited outcrop and lack of detailed geologic mapping. Furthermore, the area is unglaciated and deeply weathered. However, recent exploration and research in the area has significantly improved understanding of this important mineral belt. Geologic data used in this report is the most updated publically available data from the Yukon Geological Survey (M. Colpron, personal communication).

2.1.1. Major Structures

The Dawson Range Mineral Belt is bounded by the Tintina Fault to the northeast and the Denali Fault to the southwest. These faults are crust-penetrating, dextral strike-slip faults with several hundred kilometers of Cenozoic displacement. This fault-bounded domain is cut by numerous older faults dominated by northwest-trending, dextral strike-slip faults belonging to the Teslin fault system. Seismic surveys indicate that the Teslin fault extends to mid to lower crustal depths (Cook et al., 2004). The Teslin extends into northern BC, where it is called the Thibert Fault and is interpreted to have accommodated 125 km of dextral displacement (Gabrielse et al., 2006). In the Yukon however, the fault progressively loses displacement towards the northwest, such that there is no apparent offset at the cities of Carmacks and Minto. This displacement can be accounted for by second-order faults to the east. However, northwest-trending structures (e.g. the Big Creek Fault) that extend westwards into the Dawson Range may also belong to the Teslin system. Faulting is generally constrained at 125-95 Ma, though some evidence suggests that faulting locally persisted until at least the Late Cretaceous (Bennett at al., 2010).

Importantly, these NW-trending structures appear to exert first-order control on mineralization in the region. Two of the major regional-scale NW-trending faults are the dextral Big Creek and Hoochekoo faults, which extend northwest from the Miller Fault for approximately 80 km (Figure 2). Mid to Late Cretaceous displacement on the Big Creek Fault was at least 20 km (Johnston, 1999). Near the Minto Mine, the Hoochekoo fault appears to bend to the west, where it merges with the Big Creek Fault just north of the Sonora Gulch Property; however, overlying Upper Cretaceous and Quaternary volcanic flows obscure part of the fault trace and prevent a conclusive relationship. The east-west-trending portion of the fault makes up much of the southern border of the G Property. A north-trending structure, the Wolverine Creek Lineament, is also present in this area.

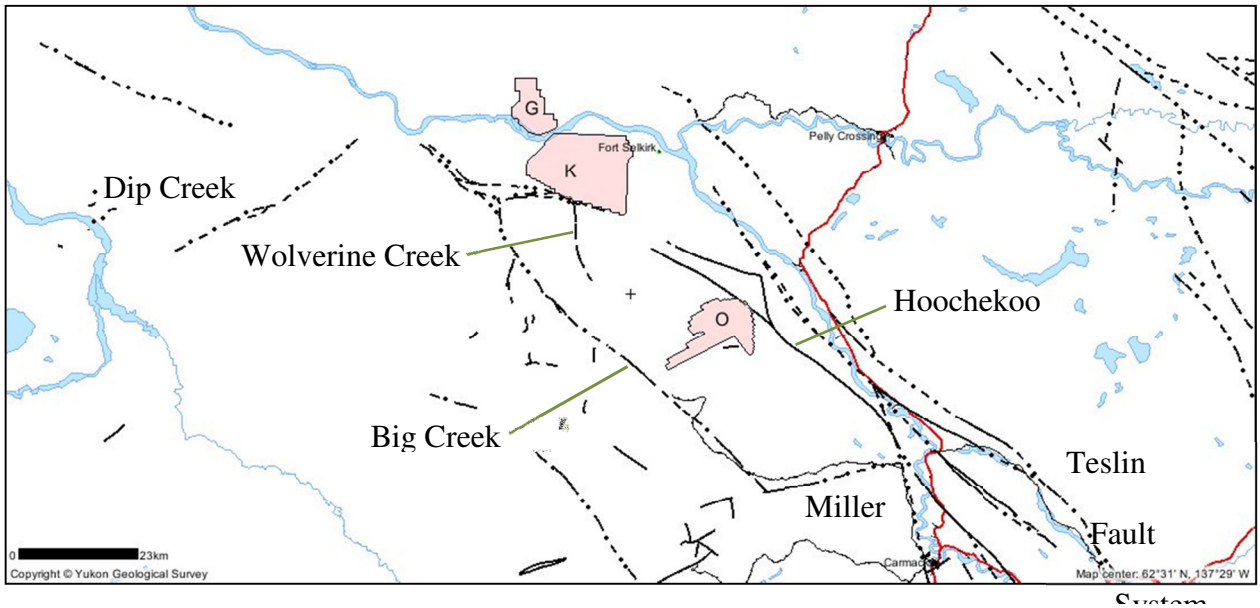

Figure 2: Major faults within the project area. The Dehua Properties (G, K, and O) are shown in pink.

Second-order north- and northeast-trending faults may also play an important role in controlling mineralization in the Dawson Range. Faults with such orientations are common in eastern Alaska where they are associated with mid-late Cretaceous mineralization, but they are poorly recognized in western Yukon. One known example in the Dawson Range is the Dip Creek Fault

southeast of the Casino deposit. Further work is required to resolve the timing and kinematics of these structures in this region.

2.1.2. Major Lithologies and Contacts

In general, magmatic products that have intruded the Yukon-Tanana and Stikinia terranes in this region can be divided into three temporally (and broadly spatially) distinct groups: 1) an early Jurassic belt located closest to the Tintina Fault in the east; 2) a mid-Cretaceous belt immediately west of the Jurassic belt; 3) a late-Cretaceous belt located along the western margin of the Dawson Range Mineral Belt (**Error! Reference source not found.**). The late-Triassic to early-Jurassic plutonic suites have also produced major Cu-Au-Mo deposits in British Columbia.

The Dehua properties are located within the early-Jurassic magmatic belt, specifically associated with intermediate to felsic intrusive and meta-intrusive rocks of the Granite Mountain Batholith. The batholith is predominantly composed of massive to very weakly foliated granodiorite and diorite/quartz diorite, but also includes zones of variably deformed intrusive rocks such as biotite-rich gneiss and quartzofeldspathic gneiss.

In general, the batholitic rocks are in fault and/or intrusive contact with Upper Triassic volcanic rocks of Stikinia to the east and Early Mississippian meta-plutonic rocks of Yukon-Tanana to the west. Portions of the batholith are also in fault contact with basalt of the Upper Cretaceous Carmacks Group, which unconformably overlies the batholith in some areas. Quaternary basalt flows cover the intrusion just north of the Minto Mine.

With respect to the nearby Dehua properties, the G Property is predominantly underlain by intrusive rocks of the Minto Pluton, part of the early-Jurassic Granite Mountain Batholith. An intrusive contact with Upper Triassic volcanic rocks (augite-phyric basalt flows) of Stikinia parallels the eastern boundary of the G Property. The K Property is also underlain by the Minto Pluton. Here the pluton has intrusive contacts with the augite-phyric basalts to the north, and with Early Mississippian meta-plutonic rocks (foliated tonalite, granodiorite, and granite) of Yukon-Tanana in the south. These meta-plutonic rocks comprise the southern half of the property, except for the south-eastern corner, which is covered by Quaternary basalt flows, and

the southwest border where there is a contact with Devonian-Mississippian graphitic quartzite and quartz muscovite schist. There are also isolated blocks of granodiorite belonging to the Minto Pluton that outcrop within the meta-plutonic rocks. The O Property is almost entirely underlain by the Granite Mountain Batholith; much of the northern border is defined by where the Upper Cretaceous Carmacks Group basalts unconformably overly the intrusion. The south-west portion of the property includes an intrusive contact with the older meta-plutonic rocks.

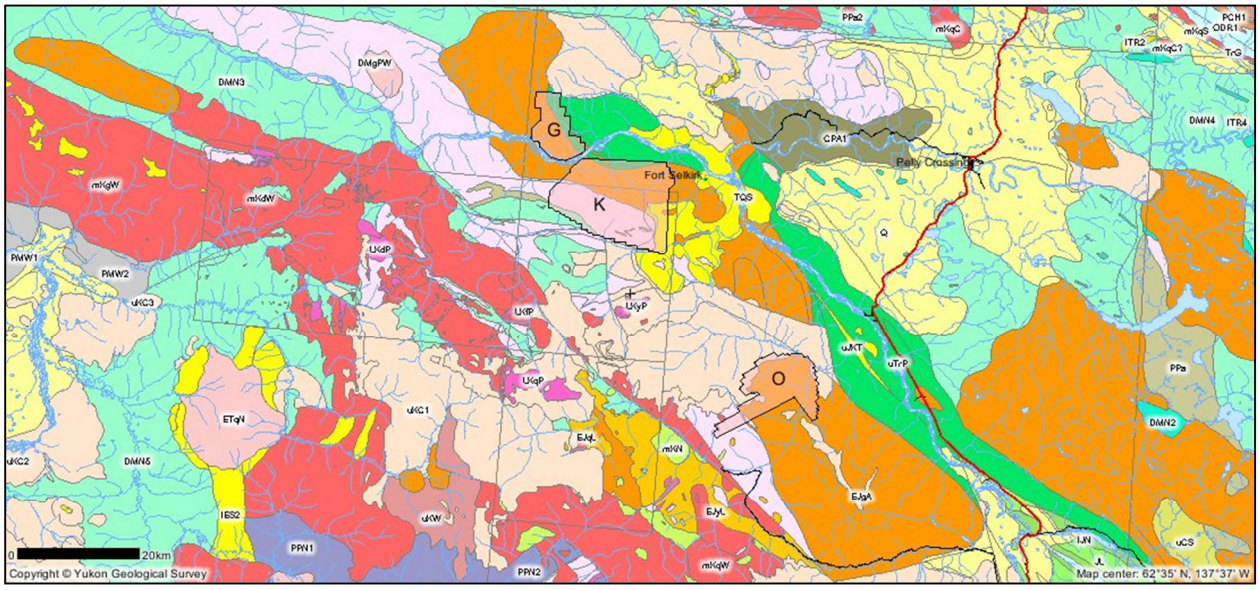

Figure 3: Bedrock geology map of west-central Yukon. The Dehua Properties (G, K, and O) are outlined in black. See text for discussion.

2.1.3. Alteration

A summary of the alteration mineralogy and assemblages observed at the nearby Minto and Carmacks Copper localities is provided (Tafti and Mortensen, 2004; Hood et al., 2009). Veining is typically characterized by thin (<0.5 cm) late-stage calcite, hematite, and gypsum veins, as well as epidote veins or stringers. Silicification, where quartz forms the majority of the rock matrix, overprints some lithologies and their alterations. Sericitization is most commonly observed as fine-grained saussuritization of plagioclase, with development of medium-grained white mica being less common at Minto and absent at Carmacks Copper. Biotite and hornblende

are replaced by epidote with chlorite ± magnetite within the alteration selvage. Hematite + chlorite ± K-feldspar is one of the most common alteration assemblages at Minto; fracture-controlled selvages of hematite "dusting" accompany the replacement of biotite and hornblende by chlorite, and feldspars by orthoclase. Development of biotite + magnetite occurs in a range of lithologies and mineral associations, though always within deformed units.

Thus, strong potassic alteration, characterized by the development of secondary biotite and lesser amounts of secondary K-feldspar, appears to have been well developed during formation of the hypogene mineralization. The absence of widespread pyrite and sericite suggests that hypogene phyllic and argillic alteration may not have been widely developed. Propylitic alteration may have been developed, but would be largely obscured by later deformation and supergene processes.

Supergene effects are represented by the presence of abundant secondary copper minerals including chalcocite, azurite and malachite, as well as by the local presence of abundant hematite and clay. Zones of supergene alteration are typically found near the surface, and are only locally observed at depth resulting from fault-controlled meteoric water penetration.

2.1.4. Regional Geochemistry

There is limited geochemical information since detailed soil sampling surveys have not yet been carried out on the properties. However, stream sediment analyses from the 2003 Yukon regional geochemical database (Yukon Geological Survey) are available and may provide some insight.

Relatively low Cu values (< 54 ppm) and Mo values (< 6 ppm) are found within the Dehua properties (Figures 3A and 3B). The highest Cu and Mo values in this region, located to the west of properties G and K, are associated with Western Copper's Casino project (Cu-Au-Mo porphyry). With respect to Au, some elevated values (20-82 ppb) are found within or near the Dehua properties (Figure 3C). One stream sediment sample from Block O returned an Au value of 475 ppb. Proximity to the drainage regions of streams with anomalous Au values will be a consideration during the targeting.

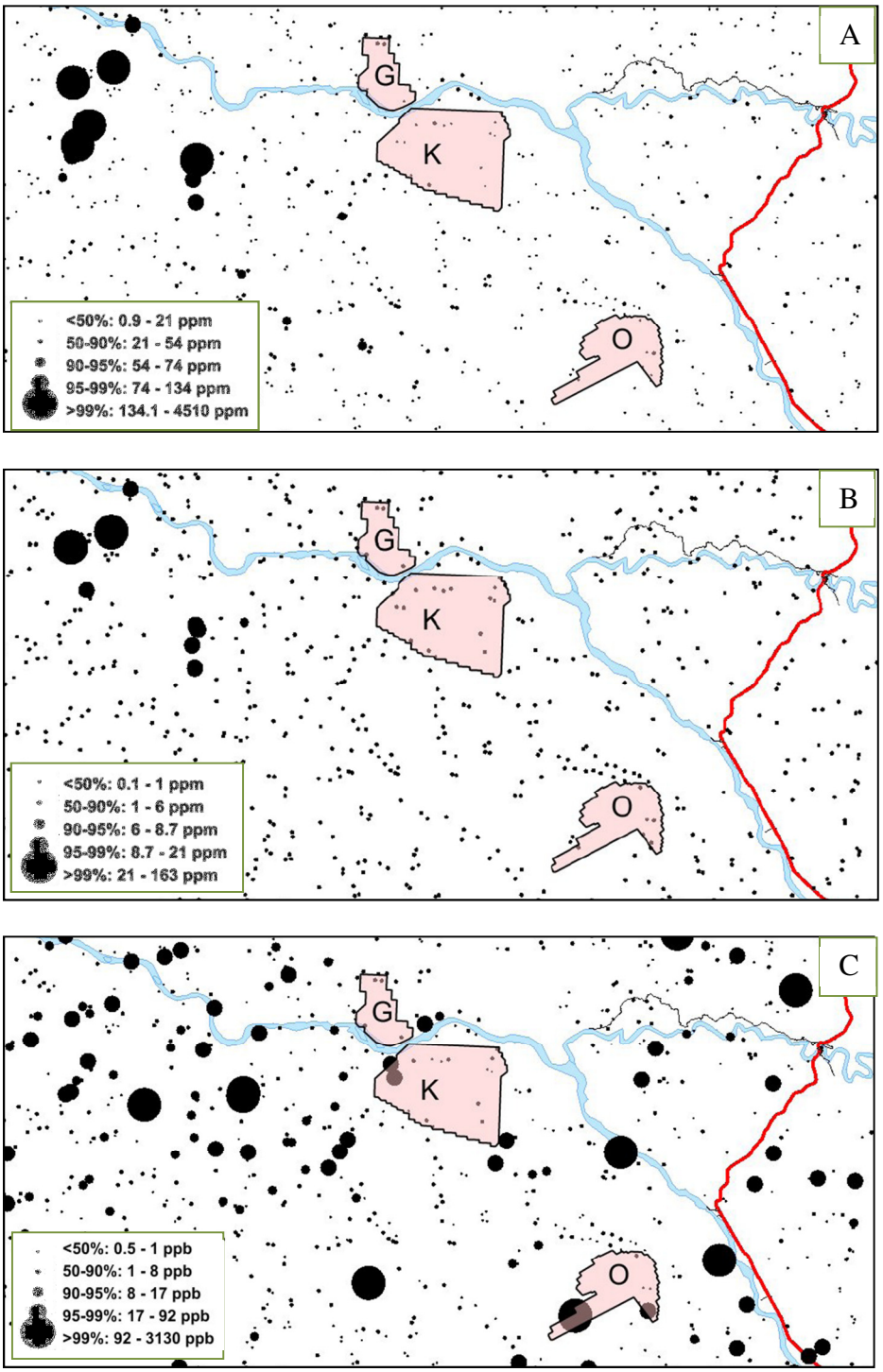

Figure 4: (A) Cu values (ppm), (B) Mo values (ppm), and (C) Au values (ppb) of stream sediments in the project area. The Dehua Properties (G, K, and O) are shown in pink.

2.2. Known Mineralization

2.2.1. Mineral Occurrences within the Dehua Properties

Within the Dehua properties, there are 3 known mineral occurrences listed in the Yukon Geological Survey MINFILE Database (Figure 5). MINFILE# 115I 081 (Status: Drilled Prospect), located within property G, was first staked in 1973 by Kerr Addison Mines, who drilled 6 holes and conducted airborne geophysical, IP, and ground magnetic surveys, as well as geological mapping, soil sampling, and hand pitting. Pyrite, chalcocite and molybdenite were disseminated and in fractures cutting chlorite schist and biotite granodiorite. The best mineralization was found in an (argillic/phyllic) altered zone in the intrusion beneath a cap of unmineralized volcanics. MINFILE# 115I 090 (Status: Anomaly), located within property K, was staked in 1974 by Canadian Superior Exploration, who carried out mapping, soil sampling, and bulldozer trenching. The claims are underlain by Devono-Mississippian hornblende-biotite schist and amphibolite. Trenching of a weak copper anomaly exposed unmineralized gneiss. MINFILE# 115I 028 (Status: Unknown), located just outside the northwestern boundary of property K, was staked as two copper claims, where old pits were found on an unmineralized quartz vein cutting granodiorite. MINFILE# 115I 014 (Status: Unknown), located within property O, has a long and complicated staking and work history. United Keno Mines reported that the area was primarily underlain by massive granodiorite containing pockets of foliated granodiorite, within which they located copper mineralization in the form of malachite (up to 6 m wide, with 100-2800 ppm Cu and trace Ag and Au). A small IP survey conducted over the area did not return any anomalies. Soil sampling on nearby claims outlined numerous spot Cu anomalies, but follow-up trenching did not uncover any substantial mineralization. Proximity to mineral showings will be a consideration during the targeting.

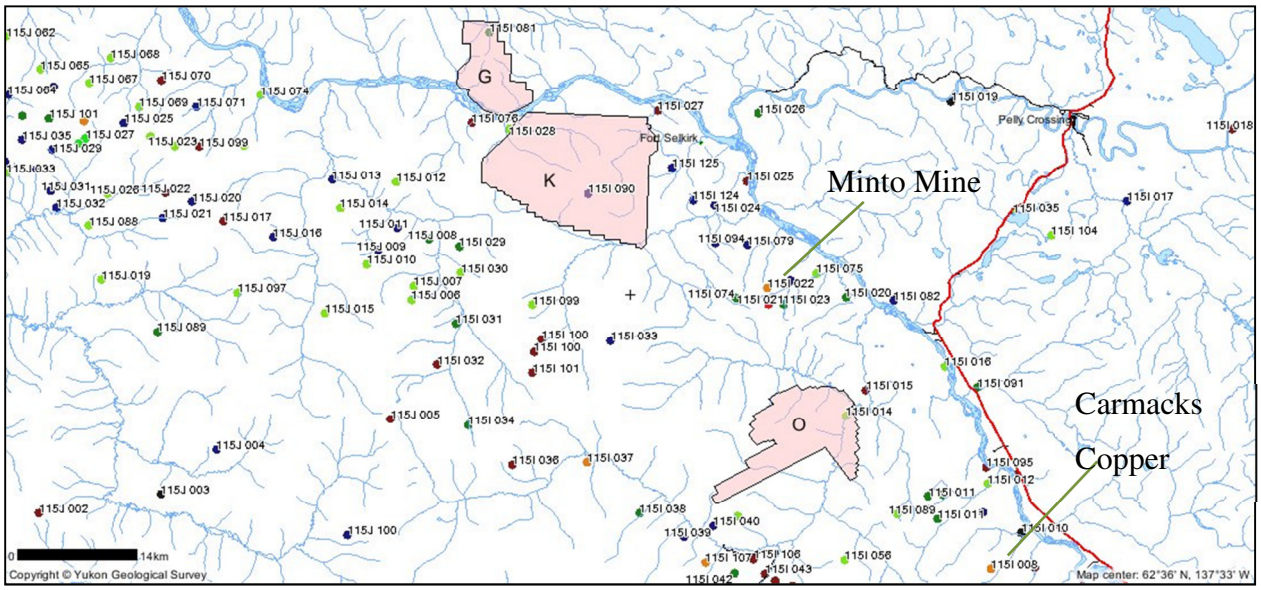

Figure 5: Yukon MINFILE mineral occurrences in the project area. The Dehua Properties (G, K, and O) are shown in pink.

2.2.2. Nearby Mineral Occurrences and Deposits

As mentioned above, the Dehua properties are located within the prospective Dawson Range Mineral Belt and as such, many mineral occurrences and deposits are located in the regions near the properties (Figure 5). Many of the occurrences are located slightly to the west along the Big Creek Fault, a known structural mineral corridor. Notable deposits along this fault include the Sonora Gulch property (Northern Tiger Resources) in the north, and the Freegold Mountain property (Northern Freegold Resources) in the south.

Other notable deposits in the area include the Mt. Nansen gold-silver deposit in the southeast, and the Casino (Western Copper) Cu-Au-Mo deposit in the northwest. Further to the northwest lies the newly recognized "White Gold District", where significant new gold discoveries have recently been made at the White Gold (Kinross Gold) and Coffee (Kaminak Gold) properties.

Other nearby deposits include the operating high-grade copper-gold Minto Mine (Capstone Mining) near Minto, and the Carmacks Copper deposit (Western Copper) near Carmacks, both of which are briefly discussed in more detail below.

2.2.3. The Carmacks Copper Belt

This section focuses on the Carmacks Copper and Minto deposits because they lie along the same northwest-trending belt (the informally named "Carmacks Copper Belt") as the 3 Dehua properties and are hosted by the same early Jurassic magmatic suite. Other deposits mentioned above are located further to the west and mineralization is associated with a younger (Cretaceous) phase of magmatism.

The Minto Deposit contains ~9 million tonnes with an average grade of 1.73% Cu, 0.48 g/t Au and 7.5 g/t Ag, while the Williams Creek deposit contains 15.5 million tonnes at 1.01% Cu (Deklerk, 2002). Mineralization at both properties is hosted by deformed and metamorphosed rafts and pendants of older intrusive rocks units contained within the Granite Mountain Batholith (Tafti and Mortensen, 2004). At Minto, mineralization is hosted mainly within foliated biotite and quartzofeldspathic orthogneiss, with a lesser amount within a banded, relatively quartz-rich rock, and at Williams Creek, the main host rock is dioritic to quartz dioritic orthogneiss, and in supracrustal rocks to a lesser extent. Mineralization in these deformed intrusive units occurred prior to the ductile deformation recorded by their host units. Sulphide minerals are mainly disseminated or occur as narrow, discontinuous, foliaform stringers. Chalcopyrite, bornite, and magnetite are the main hypogene minerals, with very minor pyrite and molybdenite. As mentioned above, strong potassic alteration is well developed, whereas there is little evidence for widespread phyllic, argillic, or propylitic alteration (Tafti and Mortensen, 2004).

Both deposits are interpreted to have involved 4 distinct events: 1) intrusion of early plutonic rocks into supracrustal rocks of the Yukon-Tanana Terrane at 198-197 Ma; 2) mineralization and alteration of these intrusives; 3) ductile deformation of the mineralized units; 4) intrusion of the main, massive, post-mineral phases of the Granite Batholith at ~197 Ma.

2.3. Mineralization Styles

Mineralization styles within the Dawson Range Mineral Belt include porphyries, epithermal veins and breccias, skarns, structurally-hosted veins and breccias, as well as placer gold deposits in numerous creeks draining the belt.

Many of the nearby deposits, especially those that lie along the Big Creek Fault, are porphyry-type deposits. For example, the Freegold Mountain project has identified at least 20 mineralized zones, including the Nucleus and Revenue deposits, which are believed to be part of a large porphyry gold-copper system. The Sonora Gulch Property is a large and strongly altered system hosting multiple styles of mineralization, and is currently being evaluated as a Cu-Au-Mo porphyry system. As well, the Casino property is recognized as a porphyry Cu-Au-Mo deposit. An important characteristic of metal concentration in these deposits is the superposition of intrusion-related mineralization upon pre-existing ores, such that early phase mineralization can be enriched and/or remobilised along active structural corridors to be subsequently deposited at structurally and chemically favourable sites (e.g. Mortensen et al., 2003; Bineli Betsi and Bennett, 2010).

As discussed above, the Minto and Carmacks Copper deposits appear to be the best examples of potential deposit types related to the Dehua properties. These deposits have been interpreted to represent a variety of deposit types including volcanogenic massive sulphide (VMS), redbed copper, porphyry copper, magnetite skarn, and iron oxide copper gold (IOCG) (e.g. Pearson, 1977; Sinclair, 1977; Pearson and Clark, 1979; Tafti and Mortensen, 2004; Quin and Mercer, 2008). However, the typical calc-silicate skarn mineral assemblage is absent, which would seem to preclude the skarn deposit type. Numerous factors also argue against these deposits representing a porphyry system. For example, the host rocks were emplaced at depths of >9 km (and possibly up to 18-20 km), which is greater than those that would permit formation of a porphyry-type deposit. As well, typical porphyry-type alteration zoning (such as widespread propylitic, phyllic, and argillic alteration and introduction of pyrite) and quartz stockwork, fracture, or vein mineralization is absent.

However, Tafti & Mortensen (2004) argue that these deposits represent an aborted or stalled porphyry system. The observed mineralization and alteration assemblages are consistent with the early stages of a typical porphyry system. They suggest that a hydrothermal system had begun to develop a typical porphyry deposit, but was shut off when the system was buried to depths of >9 km, thus preventing development of late stages of hypogene mineralization and

alteration. This burial event was followed by regional uplift at ~197 Ma. The absence of a significant quartz stockwork is similar to alkali copper-gold porphyry deposits of similar age in British Columbia (e.g. McMillan et al., 1995).

At the Minto Mine however, Capstone is working on the basis that this deposit is a variant of the IOCG class of deposits (Quin and Mercer, 2008). Though the company cannot unequivocally demonstrate that an IOCG origin is correct, this style of mineralization is thought to provide the most consistent model for the current level of understanding.

3. Targeting Strategy

With any exploration targeting project, computer-aided or not, the first step is to define the characteristics of the target. There may be several styles of mineralization, or targets, to be considered in one project area. Each target type will have a set of criteria that must be considered separately.

Establishment of exploration criteria can be carried out from standard ore deposit models, which provide general information, or derived from site-specific geological knowledge. Using those criteria that demonstrate meaningful statistical correlation to standard ore deposit models, a map of favourable mineral potential is constructed.

3.1. Methodology

The methods employed here are inspired by a history of successful application in 2D GIS systems in mineral exploration going back to the 1980's and 1990's (see for example Bonham-Carter, 1994 and 1997). We use a knowledge-driven weights targeting procedure. The general principle is to combine multiple data streams to target individual groupings of cells having high mineral potential for further investigation.

The exploration criteria are modelled as quantitative or classified properties in a 2D or 3D model encompassing the exploration volume. Exploration criteria are typically a mixture of interpreted rock properties such as lithology, geochemistry, and physical properties, and non-rock property target indicators such as proximity to faults or significant contacts. "Target" locations are identified, ranked, and classified by computing and analyzing a score at each cell of the model. The process is summarized graphically in Figure 6.

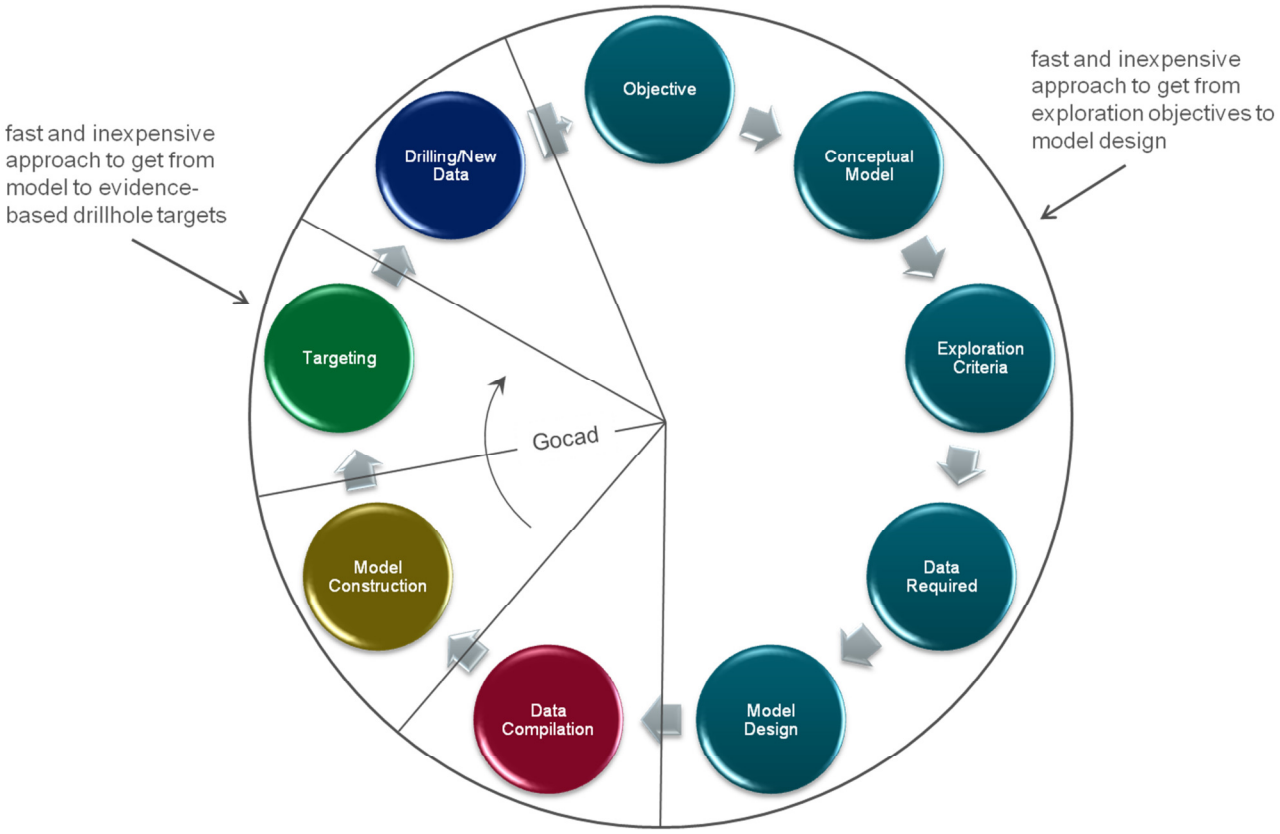

Figure 6: Target generation process displayed as a cycle of project actions.

Figure 6 shows the basic cyclical flow of project actions. In the first five steps of the project, the objectives were set, exploration criteria were defined, and the model designed. Data compilation and model construction followed, where model construction consisted of geophysical interpretation and geophysical inversion. The end-point of the model construction phase results in creation of the exploration block model in which each cell of the model is attributed with multiple geological, geochemical, geophysical, and spatial variables. The targeting phase of the project takes that exploration block model as input and creates, using the knowledge-based weights method, a new block model variable representing mineral potential for a given target type.

The remainder of this report provides a detailed description of the geophysical interpretation used to define the targeting criteria, model construction, some useful background on the knowledge-driven weights technique, and a description of its deployment on the G, K, and O Block properties in the generation of mineral prediction targeting models.

3.2. Exploration Model

Mineralization at the G, K, and O properties is likely to be intrusive-hosted and thus structurally-controlled. In this project we are considering only criteria that relate to intrusive porphyry-style deposits similar to the exploration model proposed by Hollister (1976).

The primary considerations in targeting potential mineralization at the G, K, and O properties will be 1) structures, 2) contacts, 3) magnetic anomalies, and 4) radiometric anomalies.

3.3. Exploration Criteria

Given the intrusive-hosted conceptual model as described in Section 3.2, the primary considerations for targeting potential mineralization at the G, K, and O Block properties are (see Figure 7):

- Proximity to favourable structure; near contact with intrusive rock, near faults and fault intersections, proximity to structural dilation zones,
- Favourable Lithology and Alteration; proximity to existing mines and/or known mineralization,
- Proximity to magnetic anomalies; magnetic highs,
- Proximity to radiometric anomalies; potassium anomaly.

Due to the very limited property-specific geologic information and lack of geochemical data, the majority of the targeting will rely on the geophysical modelling and interpretation, though this will be guided by the regional geologic context, as well as known nearby mineralization and deposit styles. Based on the magnetic data, structures will be delineated, particularly major faults, cross-cutting features, and dilational zones. The magnetic inversion will allow for identification of important contacts and magnetic highs related to variations in magnetite

abundance. The radiometric analysis allows better definition of the lithologies and anomalous areas, such as zones of potassic alteration.

The challenge is to quantitatively represent each of these criteria, and others as they arise, in a single block model representation encompassing the entire exploration volume. This is the model that will serve as input to the knowledge-based weights method of computing mineral potential. The construction of that model from geophysical data is described in the following sections.

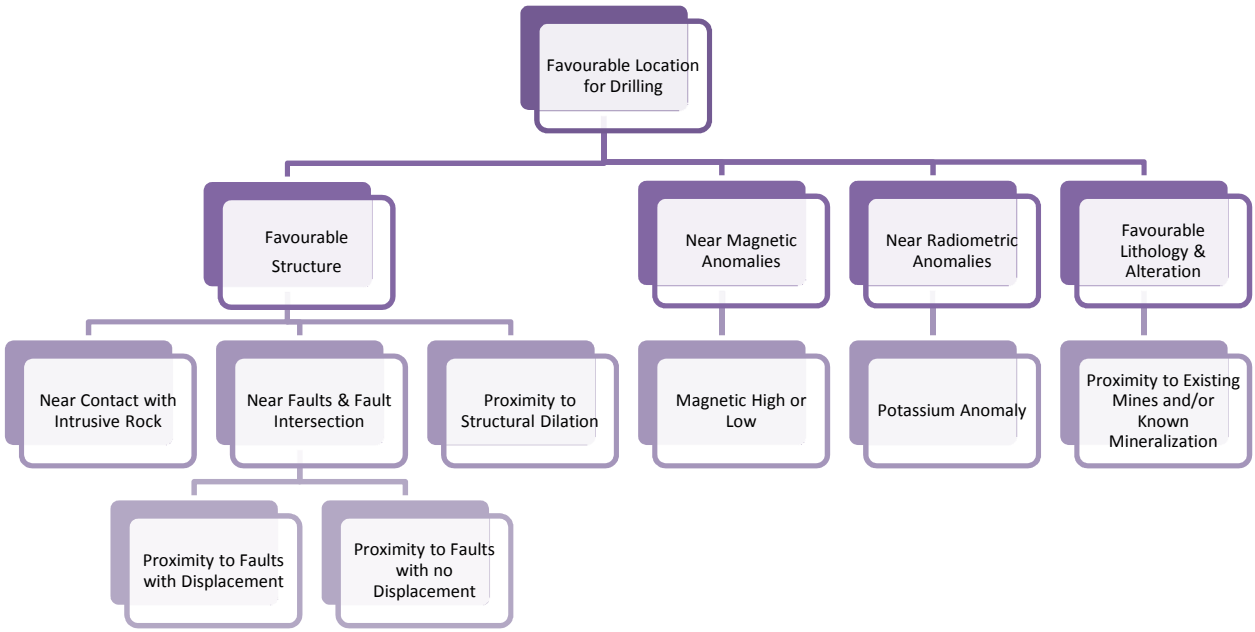

Figure 7: Criteria considered for targeting mineral potential at the G, K, and O block properties.

4. Data Processing and Interpretation Results

4.1. Magnetic Data and Processing

4.1.1. Magnetic and Radiometric Data

Magnetic and radiometric data were acquired by Precision Geosurveys Inc. for Canadian Dehua International Mines Group Inc. over three survey areas, the G, K, and O Blocks. The G Block area of interest is approximately 10.8 km by 8.8 km, the K Block is approximately 15.2 km by 20.3 km, and the O Block is approximately 14.1 km by 16.8 km. Survey specifications are listed in Table 1. The data were provided in digital Geosoft GDB format. A separate database was provided for the magnetic and radiometric data. The magnetic data included the total field data. The radiometric data included Potassium, Thorium, Uranium, and the total count. Figure 8, Figure 9, and Figure 10 show the total field magnetic data for each survey area.

Table 1: Survey specifications

Survey acquisition	August 2010, by Precision Geosurveys Inc.
Data format	Geosoft GDB, ASCII
Flight Height	Radar altimeter, GPS (nominal flight height of 30m)
Coordinates	GPS Easting and Northing
Flight line spacing	100 meters traverse, 1000 tie lines
Line direction	045°/225° at G and K Blocks, 060°/240° at O Block
Data spacing	Approximately every 2 meters along flight track
Line kilometres	G Block = 604km, K Block = 2,472km, O Block = 1,168km
Data projection	WGS84 UTM zone 8N

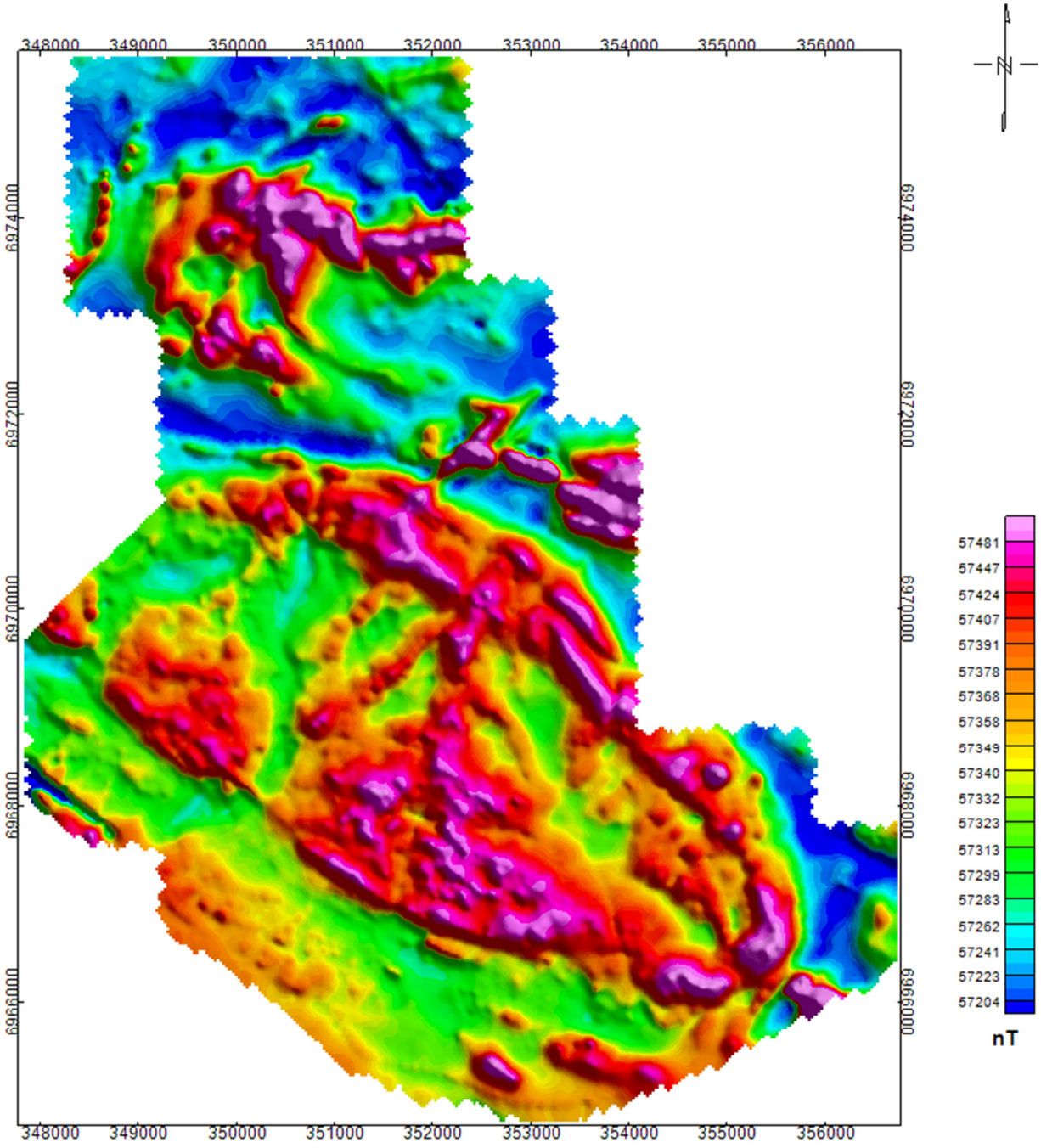

Figure 8: Total Magnetic Intensity data for the G Block

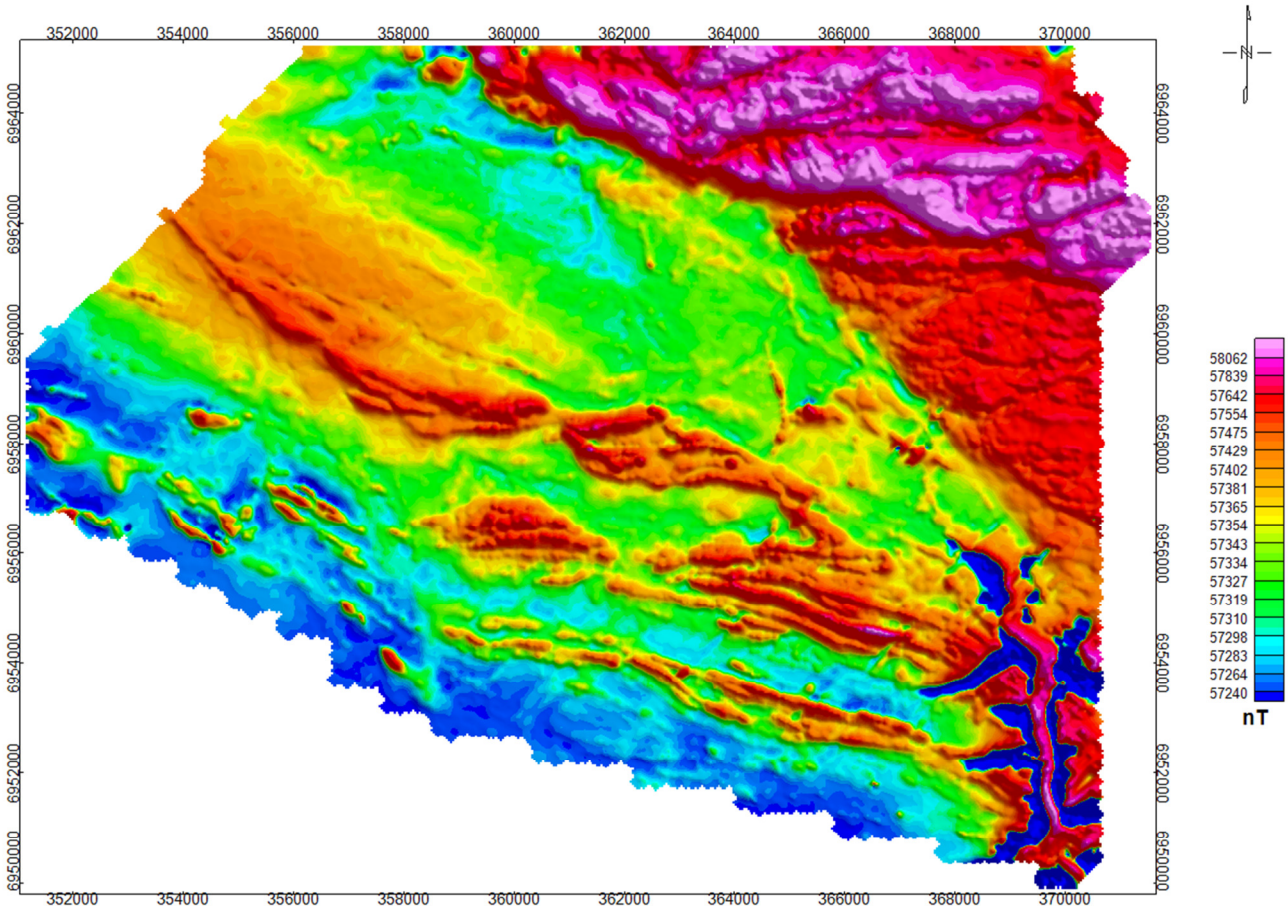

Figure 9: Total Magnetic Intensity data for the K Block

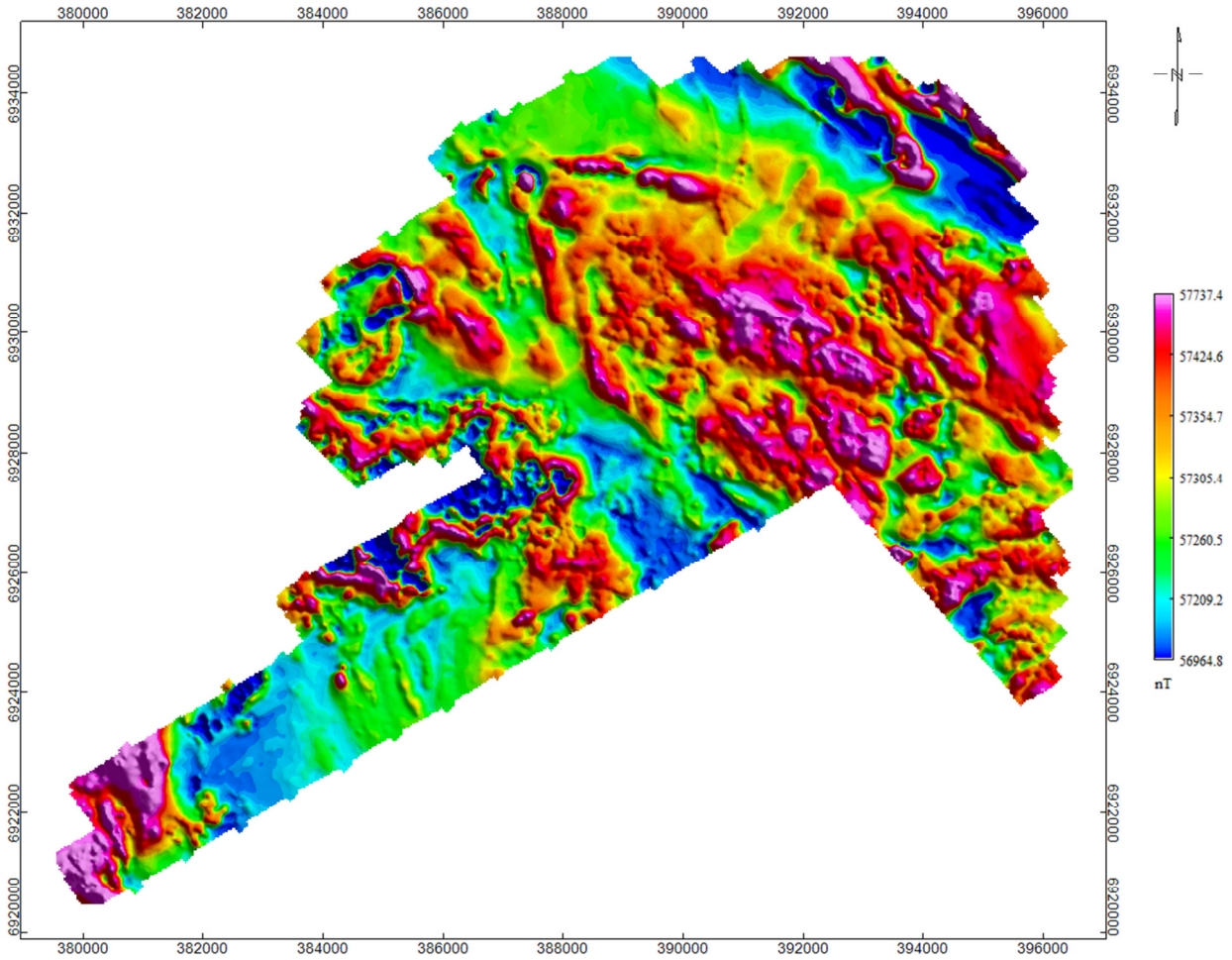

Figure 10: Total Magnetic Intensity data for the O Block

4.2. Magnetic Data Post-Processing

Additional processing was performed on the magnetic data to aid in the interpretation of faults and contacts within the survey areas. A combination of filtering techniques were used, including Reduction-to-the-Pole (RTP), analytic signal, regional-residual separation, first vertical derivative (1VD), and tilt derivative.

The shape of any magnetic anomaly depends on the inclination and declination of the main magnetic field of the earth. Thus the same magnetic body will produce an anomaly of different

shape depending on where it happens to be and its orientation. The RTP filter reconstructs the magnetic field of a dataset as if it were at the magnetic pole. This means that the data can be viewed in map form with a vertical magnetic field inclination and a declination of zero. In this way the interpretation of the data is made easier as vertical bodies will produce magnetic anomalies that are centered on the body symmetrically. RTP requires the assumption of induced magnetization with the result that anomalies from remanently- and anisotropically- magnetized bodies can be severely distorted. Nonetheless, it is a useful tool to aid structural interpretation.

A method that is less sensitive to magnetization direction is the amplitude of the 3-D analytic signal of the total magnetic field. It produces maxima over magnetic contacts regardless of the direction of magnetization. Although the amplitude of the analytic signal is dependent on magnetization strength and the direction of geologic strike with respect to the magnetization vector, this dependency is easier to deal with in the interpretation of analytic signal amplitude than in the original total field data or pole reduced magnetic field. The analytic signal is therefore useful for identifying regional structure and edges of magnetic bodies, particularly when magnetic remanence is present.

Additional filtering techniques were used to enhance near-surface and subtle magnetic features. The regional-residual separation technique subtracts the regional, long wavelength, magnetic signal from the Total Magnetic Intensity (TMI) to produce a dataset that enhances near-surface, short wavelength features (Li and Oldenburg, 1998). The 1VD of the TMI is commonly applied to total magnetic field data to enhance shallow geological sources in the data and edges of magnetic bodies, contacts, and linear features. It is also useful for discriminating textural changes that may characterize different lithologies. The tilt derivative is useful for mapping shallow basement structures and identifying contacts (Verduzco et al., 2004). Both the 1VD and tilt angle derivatives define maxima centred over source edges and contacts.

4.3. Structural Interpretation

As part of the targeting criteria, structures and contacts were identified based on interpretation of the magnetic data. Both gridded data and profile data were used to identify structural features. Post-processing techniques as described in Section 4.2 were used to aid the interpretation.

Faults and contacts were first interpreted visually from the RTP and residual TMI grids by identifying linear features and breaks and/or discontinuities in magnetic anomalies. Interpreted geologic units were traced to determine offsets and changes in structure along strike. Faults were digitized based on displacement or offsets observed in dikes or magnetic units. The strike of each fault was interpreted based on the nature of displacement or offset between magnetic anomalies. In areas where dikes were not present, filtered grids and sun shading were used to highlight linear features. Contacts were mapped in the same manner, but included the radiometric data to aid with interpretation.

Contacts were interpreted by identifying edges of magnetic sources and by identifying textural changes in magnetization across a given survey area from the 1VD and tilt derivative grids. Maxima on these filtered grids highlight contacts and edges of magnetic bodies. Textural changes can be identified by magnetically quiet areas compared to more magnetically active or "noisy" areas. Sun shading was helpful for highlighting linear features in the data. The inclination and declination of the sun angle was interactively manipulated to help identify subtle features, particularly when combined with a greyscale colour scheme. The analytic signal was useful for identifying areas where remanence might be present, notably the volcanic rocks along the edges of the surveys. Identification of contacts and lithologies were challenging in areas of variable magnetization. In these areas, the lithology could be broadly classed as granodiorite, however localized zones of enriched magnetite may be present. Since the interpretation is based predominantly on the magnetics, these enriched magnetite zones have been identified as a different lithology, however it may simply be variable magnetite content within the same unit. The magnetic inversion results were useful for identifying contacts as magnetic susceptibility isosurfaces form bodies around units of similar magnetite content (refer to Section 4.7).

The following figures show the structural interpretation for each survey area. These layers were compared with the 3D magnetic inversion model (refer to Section 4.7) to confirm their location. Plan sections were extracted from the inversion model and the 2D structural interpretation was validated by the 3D modelling. It should be noted that the inversion code does not account for magnetic remanence or self-demagnetization. In these areas, structural interpretation is based on limited geologic knowledge of the area.

Layers were digitized for geologic contacts, dikes, and faults, to be included as separate layers in the targeting process. Further interpretation was done to create additional layers. These layers show where faults intersect and where geologic contacts, dikes, and faults change strike. These structural changes are referred to as "jogs" or "bends" for simplicity. It refers to a change in strike that may indicate that the geologic unit or fault has been disrupted by an event, structural or possibly related to an intrusion or alteration that could suggest the presence of mineralization. As such, these locations are considered favourable for mineral potential.

4.3.1. Magnetic Structural Interpretation Results

The G Block survey data shows that the geology is quite magnetic. The area is characterized by several N-S and NW-SE trending cross-cutting faults. These faults do not cause significant offset of the geologic units but do cause a noticeable breaks in the units. The magnetic unit in the centre of the survey may be part of a fold structure, or the unit could be intruded and ovoid shaped, as the unit appears to trend roughly NW-SW then pinch out in the south-east part of the survey. The magnetic body is surrounded by a magnetic low suggesting a contact with a different unit. This is most likely the contact with the basalt unit. The low may suggest the presence of magnetic remanence in the basalt unit. The contacts appear to be fairly conformable with few changes in strike along the main lithologic contact. Within each unit, the contacts are not well defined and more ragged. This is a reflection of variable magnetic mineral content within the unit. There are a few small dikes in the area. There does not appear to be a common trend among the dikes, but several are oriented N-S and NE-SW.

The K Block survey data has the most well defined contacts. Along the northern and eastern edge of the survey are strongly magnetic basalts. The south-eastern portion of the survey suggests the presence of an ancient stream bed where magnetic minerals drained into the valley. These minerals were subject to changing magnetic fields of the earth as they were deposited over time and are likely associated with detrital remanence. Exploration using the magnetic data will be difficult in these areas, as remanence will be a problem for magnetic interpretation. The contact along the basalt and granodiorite is clearly defined and has numerous jogs which are of interest for porphyry exploration. The contact between the granodiorite and foliated granite/granodiorite gneiss is also well defined as the foliation is magnetic and easily mapped. Because of this magnetic foliation, faults and their resultant displacement are clearly visible. Most of the major faults trend roughly N-S and some have significant displacement. There are also numerous small faults trending NW-SE between the units. In the basalt unit, there are several E-W trending faults that have caused a significant break. It is difficult to tell the nature of the offset because the unit is strongly magnetic. The foliation also shows some deformation and it appears as though the unit folds in the eastern part of the survey. A shear zone mapped to the south by the Yukon Geological Survey could be controlling the structure and deformation observed in the K Block. There are some small N-S and NW-SE trending dikes that have numerous jogs. Based on the number of faults cross-cutting the survey and the displacement caused by them, there are numerous dilational zones which are prospective for mineralization.

The O Block survey data shows that the geology is magnetically noisy. The western edge of the survey outlines a highly magnetic unit that is likely the quaternary basalt flow. This unit appears to have significant remanence. The contact between the basalt and granodiorite is well defined along the western edge of the survey but is less defined in the north-east. The granodiorite is fairly magnetic and shows numerous breaks where faults cross-cut the unit. The faults trend in multiple directions. There are large regional faults that trend ENE-WSW and show a clear break in the geologic unit. Displacement is difficult to interpret as the unit is variably magnetic but there does appear to be a significant offset. A series of smaller faults, trending roughly N-S, also define breaks in the unit. There are several dikes present that tend to follow the structure

observed by the faults. Several dikes show a N-S trend while others trend NW-SE. Based on the number of faults cross-cutting the survey, there are numerous dilational zones which are prospective for mineralization.

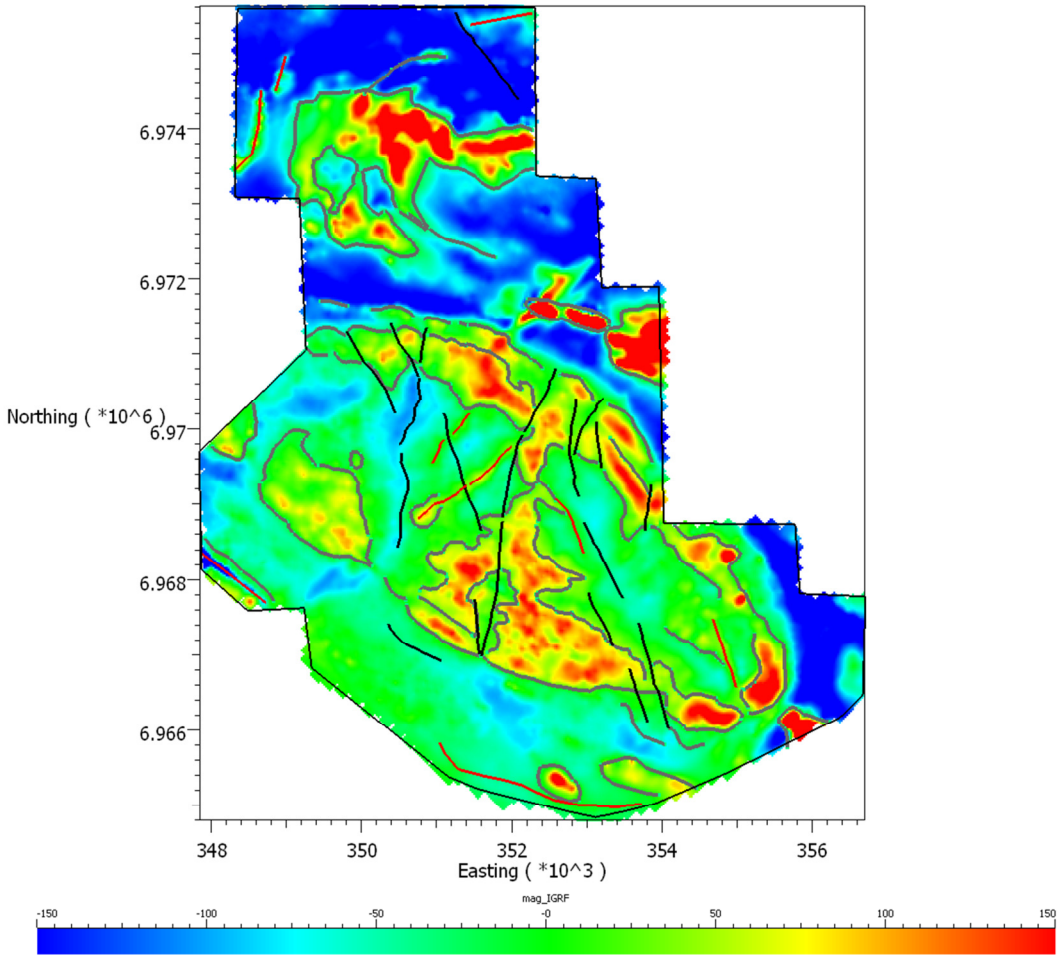

Figure 11: Digitized layers of structural interpretation for the G Block. Black shows faults, grey outlines geologic contacts, red shows dikes. Background shows the IGRF corrected magnetics.

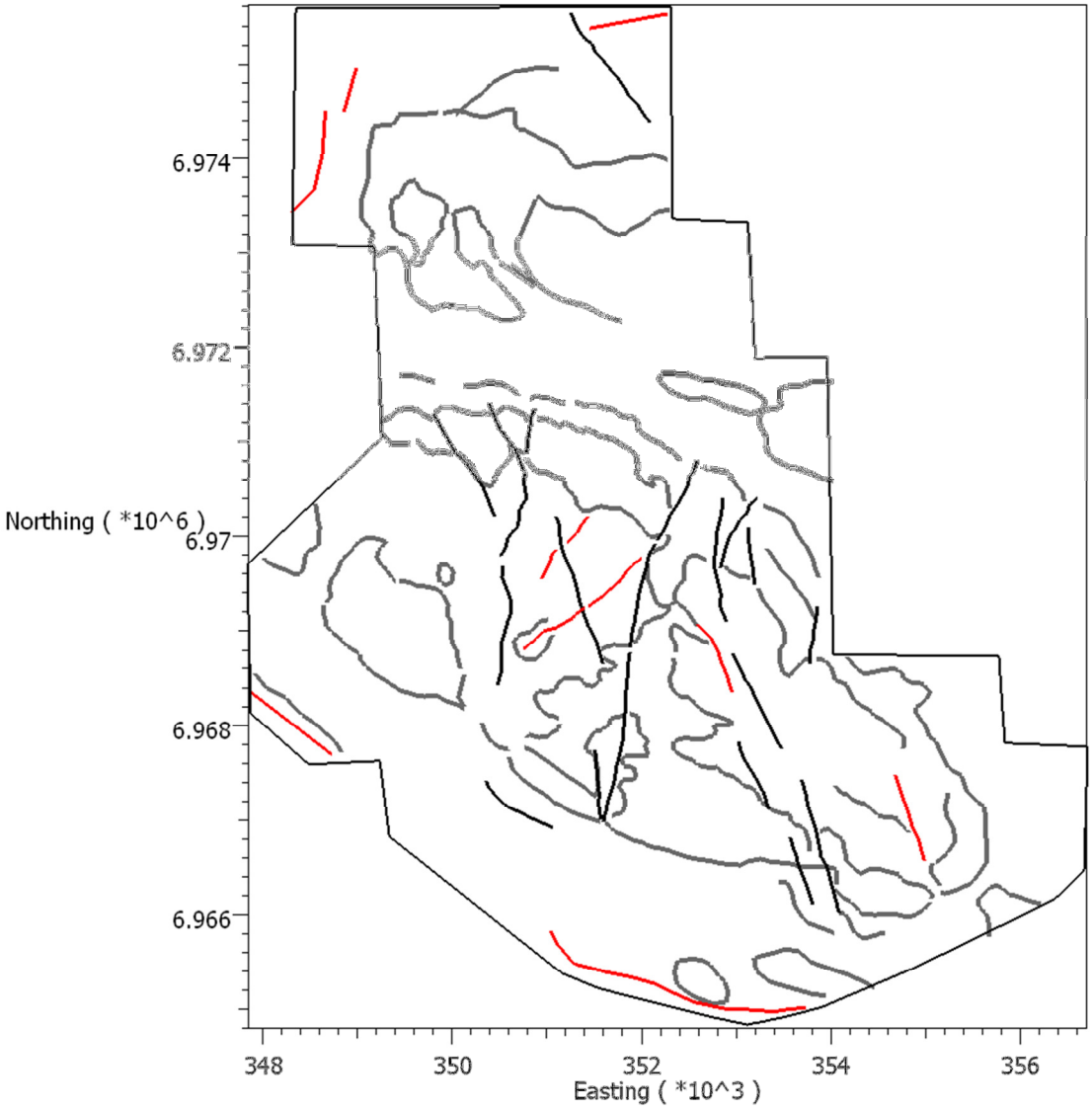

Figure 12: Digitized layers of structural interpretation for the G Block. Black shows faults, grey outlines geologic contacts, red shows dikes.

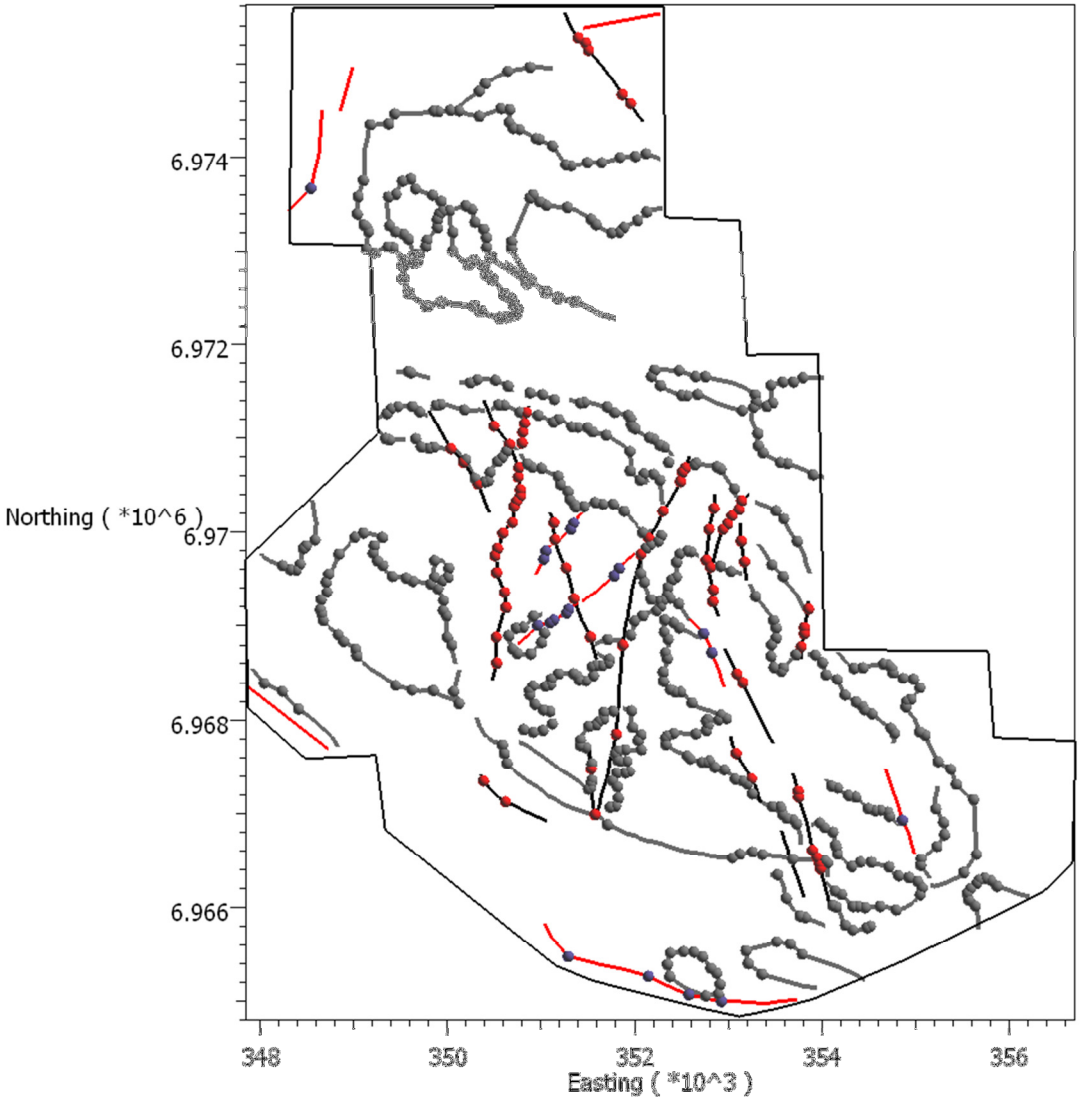

Figure 13: Digitized layers of structural interpretation for the G Block. Black shows faults, grey outlines geologic contacts, red shows dikes. Dots show changes in strike of contacts (grey), faults and fault intersections (red), and dikes (purple).

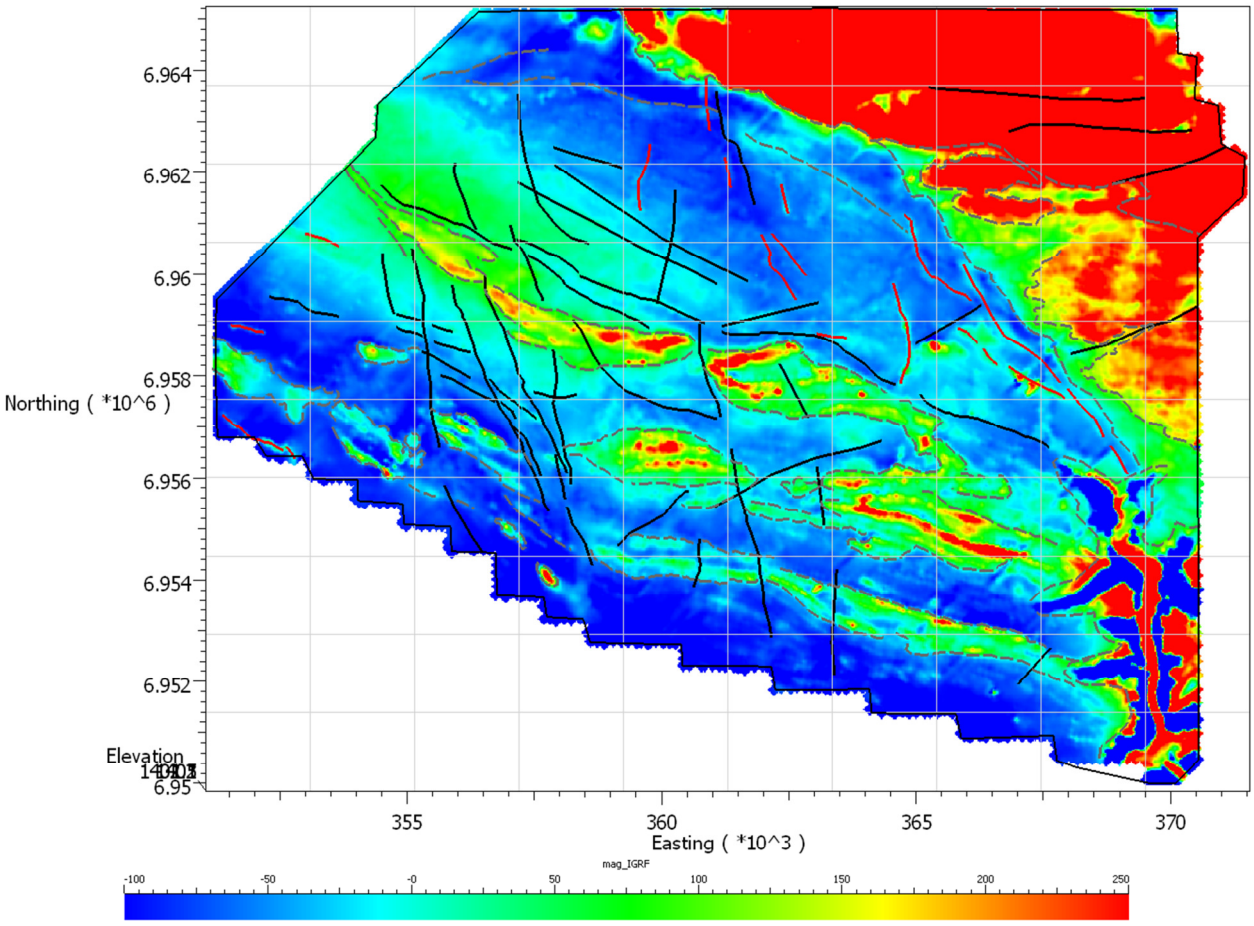

Figure 14: Digitized layers of structural interpretation for the K Block. Black shows faults, dashed grey outlines geologic contacts, red shows dikes. Background shows the IGRF corrected magnetics.

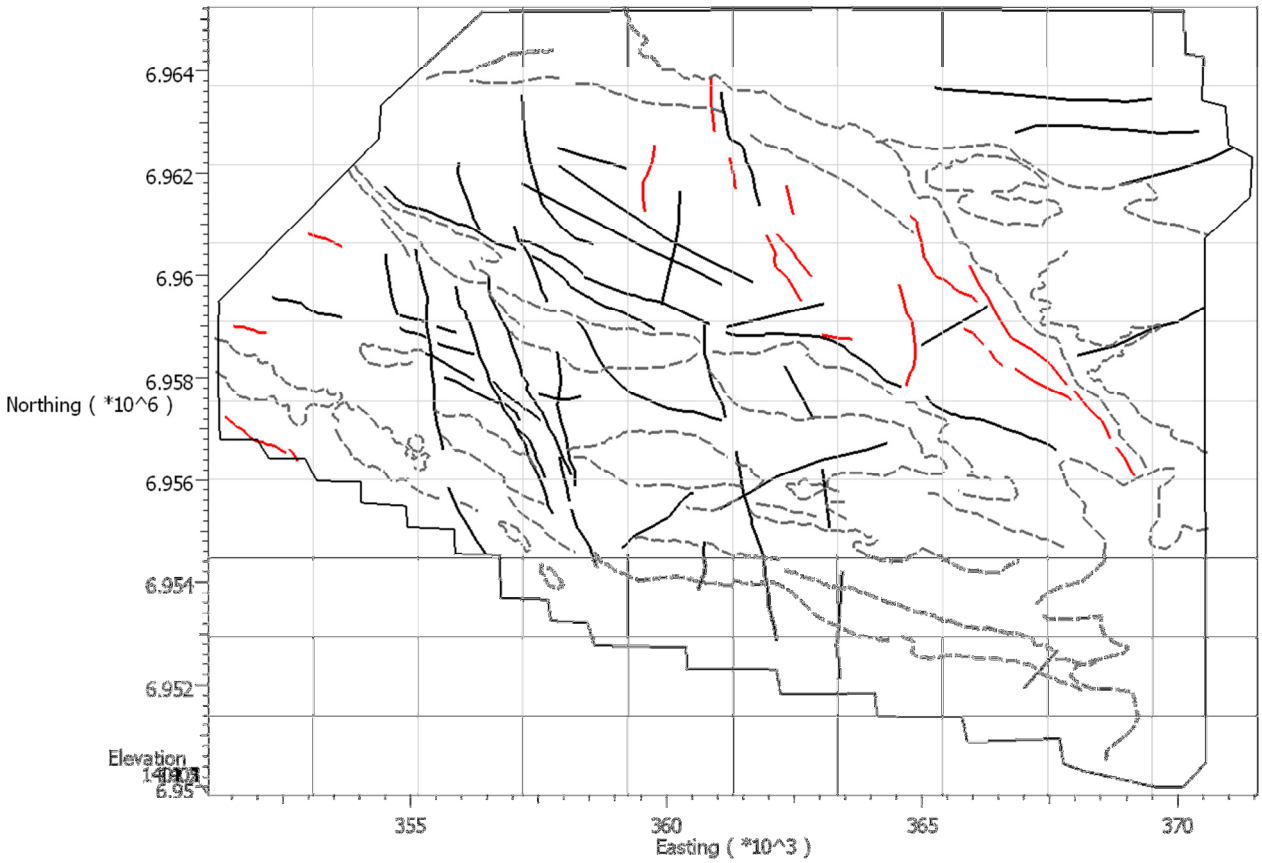

Figure 15: Digitized layers of structural interpretation for the K Block. Black shows faults, dashed grey outlines geologic contacts, red shows dikes.

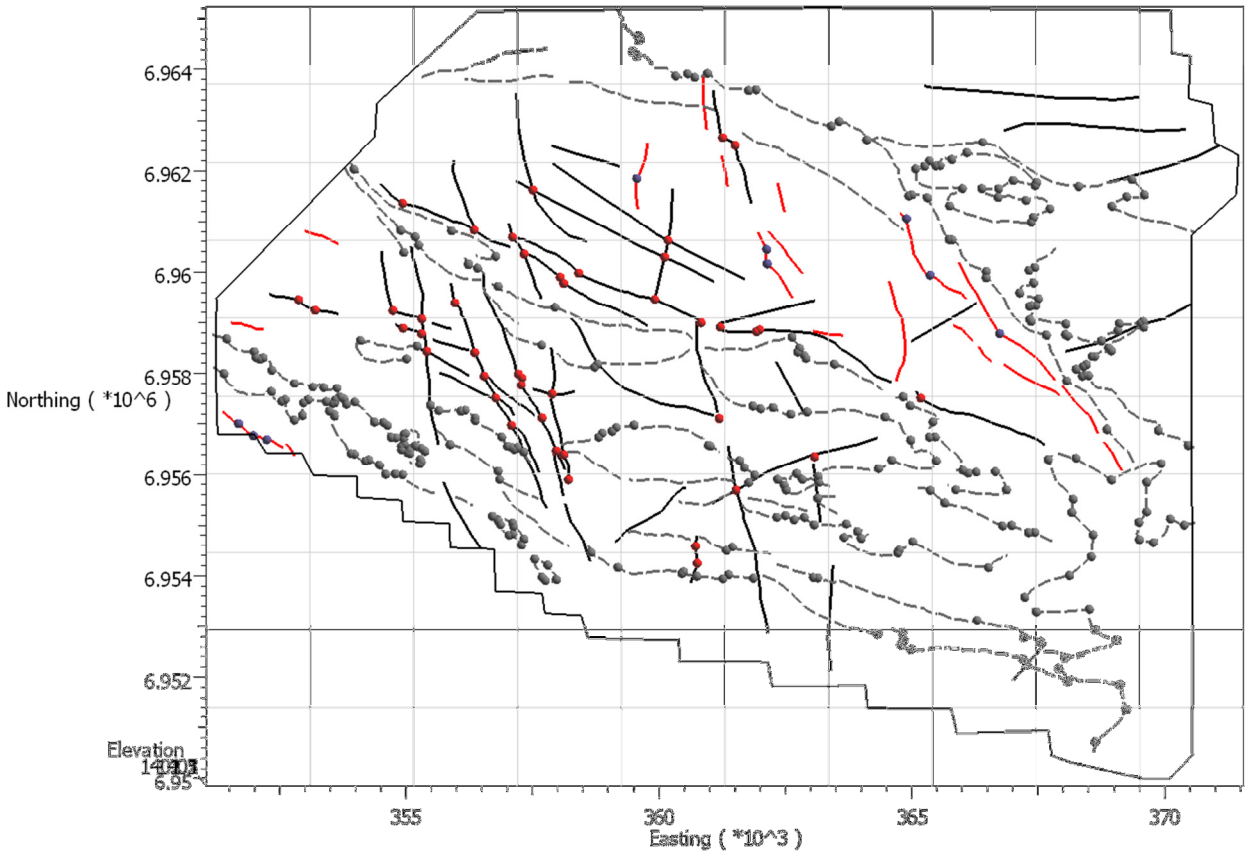

Figure 16: Digitized layers of structural interpretation for the K Block. Black shows faults, dashed grey outlines geologic contacts, red shows dikes. Dots show changes in strike of contacts (grey), faults and fault intersections (red), and dikes (purple).

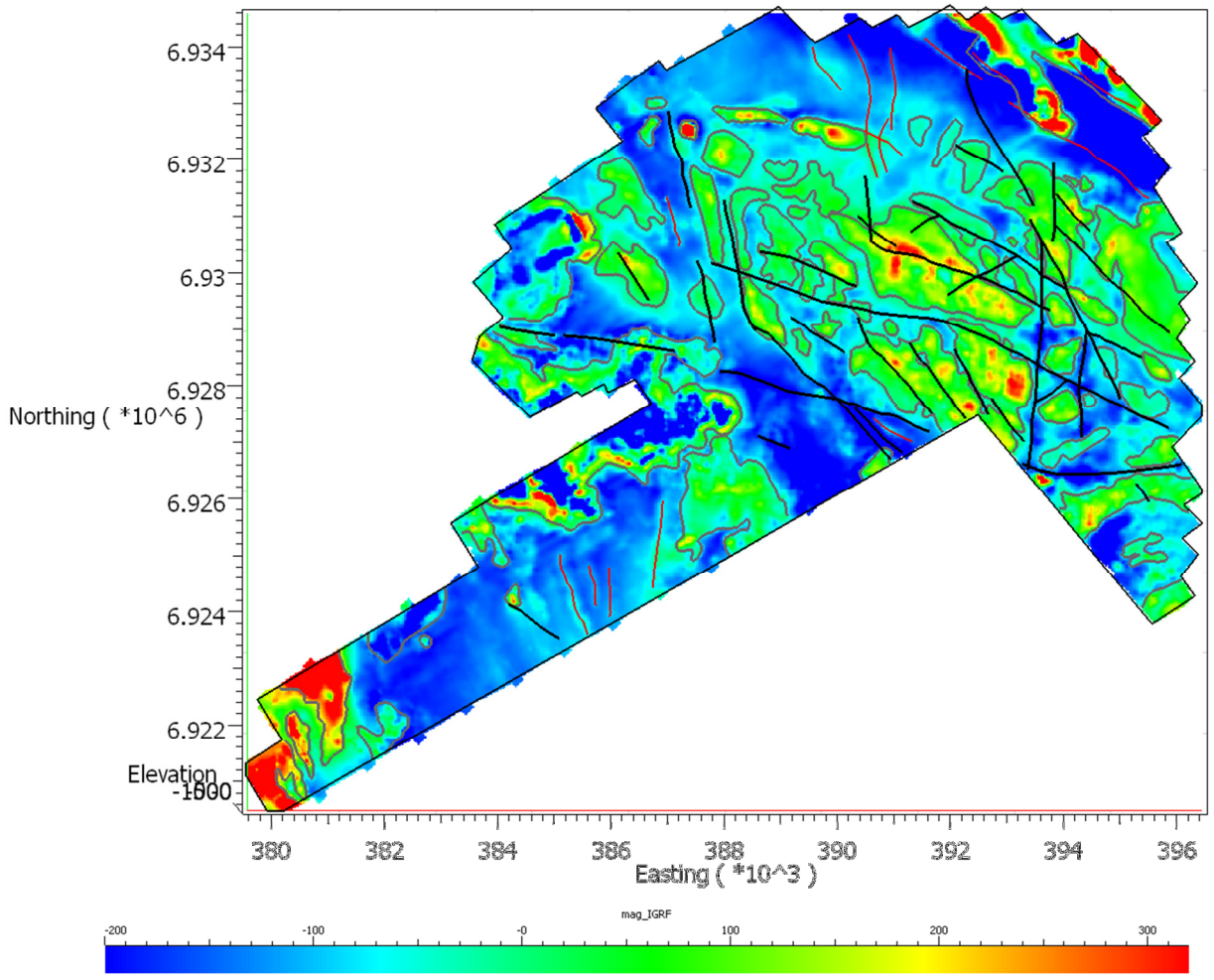

Figure 17: Digitized layers of structural interpretation for the O Block. Black shows faults, grey outlines geologic contacts, red shows dikes. Background shows the IGRF corrected magnetics.

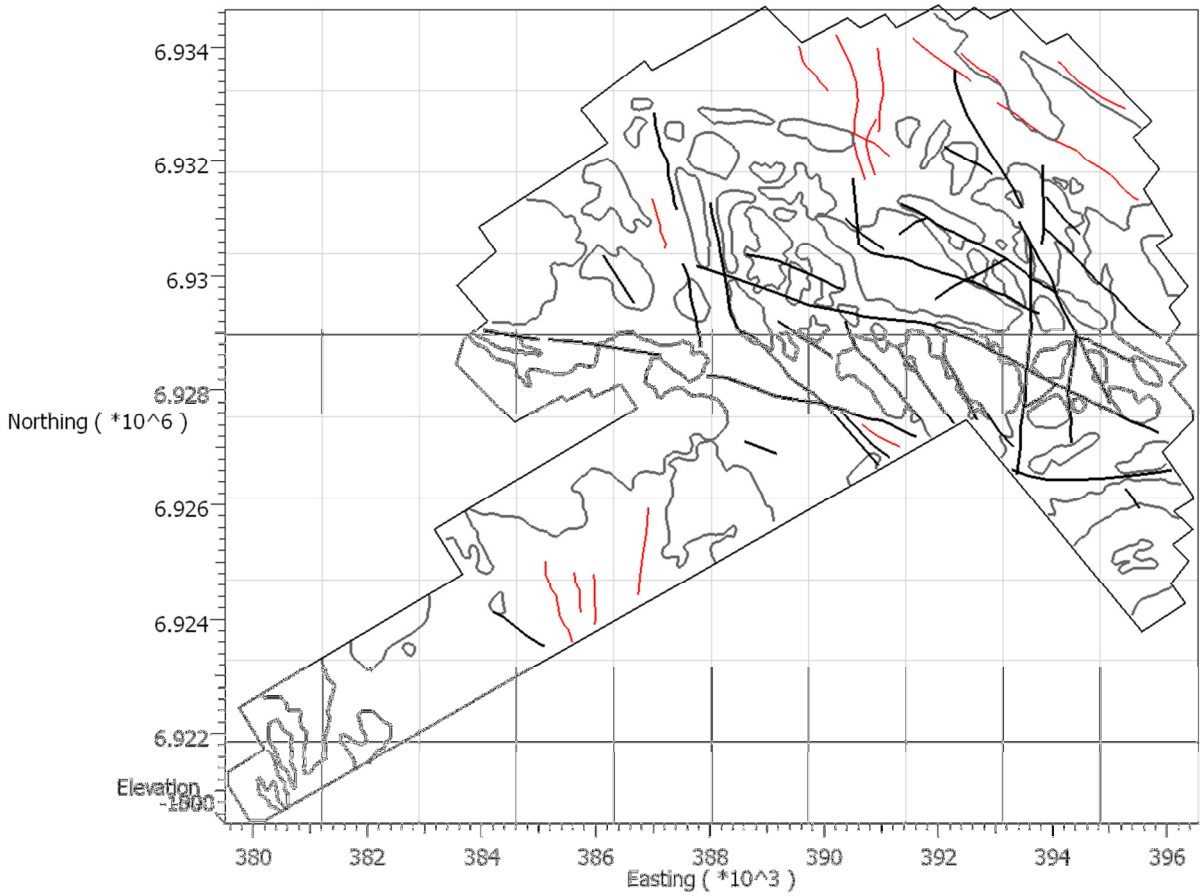

Figure 18: Digitized layers of structural interpretation for the O Block. Black shows faults, grey outlines geologic contacts, red shows dikes.

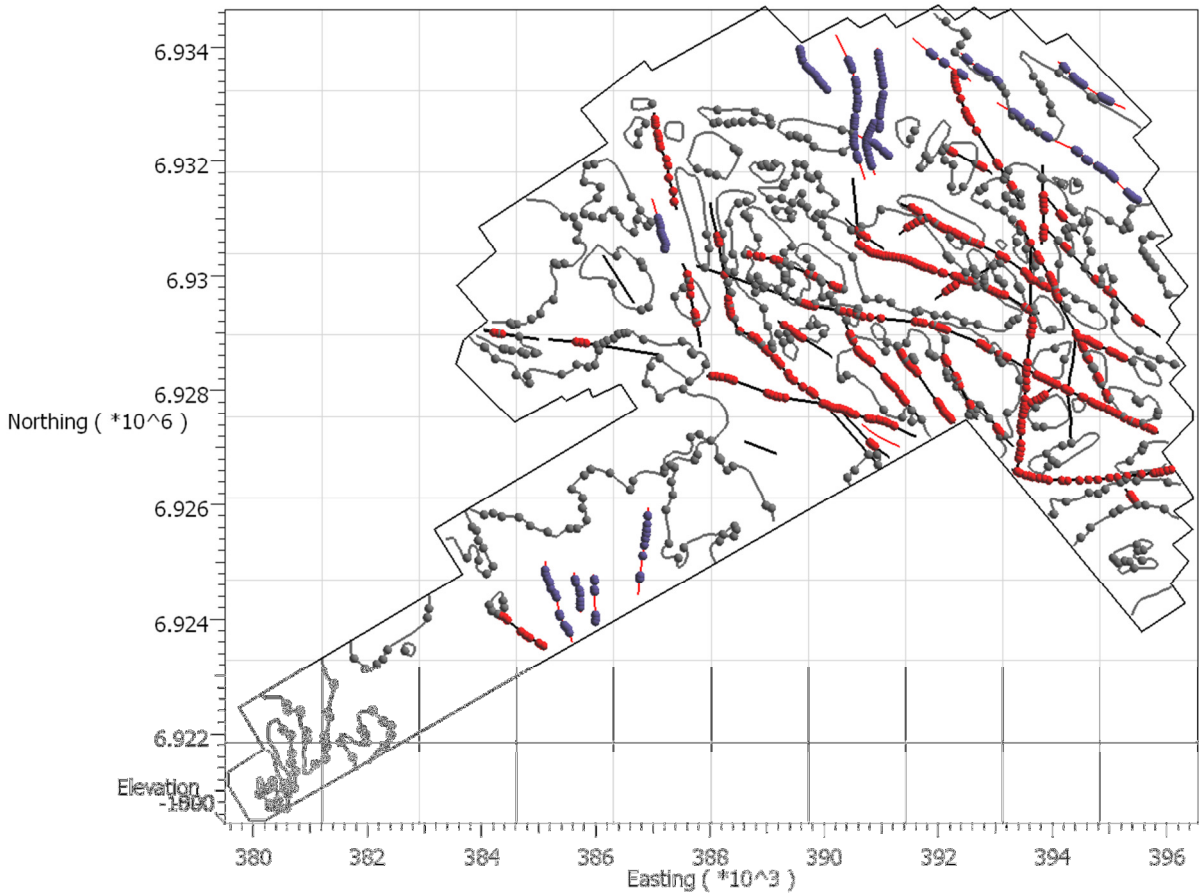

Figure 19: Digitized layers of structural interpretation for the O Block. Black shows faults, grey outlines geologic contacts, red shows dikes. Dots show changes in strike of contacts (grey), faults and fault intersections (red), and dikes (purple).

4.4. Radiometric Analysis

Radiometric data analysis is a useful tool to help discriminate different lithologies within a survey area. In addition, porphyry copper deposits are often associated with potassic alteration. Thus, potassium anomalies are often a good indicator of the presence of alteration, which may consequently be an indicator of Cu mineralization. Post-processing was performed on the radiometric data collected at the G, K, and O Blocks to identify anomalous zones of potassium.

An effective way to look at the proportions of the radioelements in an image is to use a Ternary diagram. Hue is related to the ratios of the three elements (U, K, Th) and intensity is proportional to the Total Count. A ternary diagram shows the hues, and hence the ratios. The use of a ratio removes the effect of varying count rates due to varying amounts of ground cover or the effect of wet soils, which otherwise change the overall averages of the counts, and so make recognizing potassium anomalies difficult.

The data was gridded using a nearest neighbour algorithm and large cell size (200m x 200m) for each survey, to increase the number of counts in each cell. As radiometric counts are random, the errors are related to square root N. The potassium channel has contributions from the Uranium and Thorium channel due to Compton Scattering. These contributions can mask potassium anomalies at low count rates. The equivalent concentration processing applied by the survey provider helps reduce noise and using bigger gridding cells and averaging more readings into them also helps reduce this problem.

A ternary image of the K-U-Th data field was produced after gridding the data with 200m cells. In order to smooth the data but retain the statistical advantage of the large 200m cells, the data was interpolated to 50m cells after the nearest neighbour gridding done at 200m. Note that this is not the equivalent of gridding using 50m cells; the grid is controlled by the 200m grid nodes of the parent 200m nearest neighbour grid. This was compared with the K:Th ratio - highs in the K:Th ratio corresponded with areas of interest seen in the K-U-Th RGB ternary image.

K:Th ratios were calculated for each survey block to highlight areas of high potassium. The K:Th ratio helps suppress the response from intrusives, which tend to have high thorium counts, while showing areas within the intrusive that are anomalous in potassium. Statistics were run on the element grid and the maximum value in the linear colour range was set to the mean plus two standard deviations (mean + 2 sigma) and the minimum value was set to zero.

When looking at K:Th anomalies, it is useful to look at the ternary image combined with the topography. This is important in that radiometric surveys only provide insight into the upper 1 m to 1.5 m of material, and therefore is a considered a surficial method. Interpretation and rock

type identification can be difficult or erroneous in areas of severe weathering of the geologic strata, particularly if there has been movement of the weathering products by aeolian or fluvial transport. Overlaying (or draping) the radiometric data onto a topographic surface can aid in identifying the source areas from which the weathering products may have derived.

Anomalies were identified as 1 standard deviation and 2 standard deviations from the average of the K:Th image grid. The K:Th ratio dataset has a near normal histogram. Highs in the K:Th ratio corresponded with areas of interest seen in the K-U-Th RGB ternary image (Figure 20, Figure 21, Figure 22).

The following parameters were used to create the sigma 1 and 2 anomaly maps for each of the G, K, and O Blocks.

G Block - 1 standard deviation is 0.255, with an image average of 0.21. The evidence space is built with the following values:

- NULL when K:Th <0.255
- 1 when 0.255 <= K:Th < 0.3
- 2 when K:Th >= 0.30

K Block - 1 standard deviation is 0.0715, with an image average of 0.22. The evidence space is built with the following values:

- NULL when K:Th <0.29
- 1 when 0.29 <= K:Th < 0.36
- 2 when K:Th >= 0.36

O Block - 1 standard deviation is 0.15, with an image average of 0.31. The evidence space is built with the following values:

- NULL when K:Th <0.40
- 1 when 0.40 <= K:Th < 0.50
- 2 when K:Th >= 0.50

Note that in this case, using 1 and 2 sigma anomaly levels produced a very spotty map, so these were relaxed to 0.66 and 1.3 sigma anomaly levels.

The sigma 1 and 2 contours of the K:Th ratio are used as layers in the targeting process since potassium anomalies are often an indication of the presence of potassic alteration with may be an indication of Cu mineralization.

4.4.1. Radiometric Interpretation Results

The G Block highlights a potassium anomaly in the middle of the survey area in the granodiorite unit near the contact with the basalt. Based on the structural magnetic interpretation, there are several faults that cross-cut the unit in that region. These faults may have provided conduits for fluid flow and subsequent potassic alteration of the rocks.

The K Block highlights the granodiorite unit which may have an increased potassium anomaly likely due to the presence of K-Feldspar. What is interesting to note is that when compared with the magnetic interpretation, the radiometric anomaly also highlights a geologic unit that is associated with a strong magnetic anomaly, interpreted as basalts. This indicates differentiation of the basalts, it is normal in ophiolitic volcanic sequences, and the highly potassic unit in the basalts is prospective for Kuroko type base metal mineralization.

The O Block highlights potassium anomalies in the granodiorite unit which may have an increased potassium anomaly likely due to the presence of K-Feldspar. Based on the structural magnetic interpretation, there are numerous faults that cross-cut the unit in that region. These faults may have provided conduits for fluid flow and subsequent potassic alteration of the rocks.

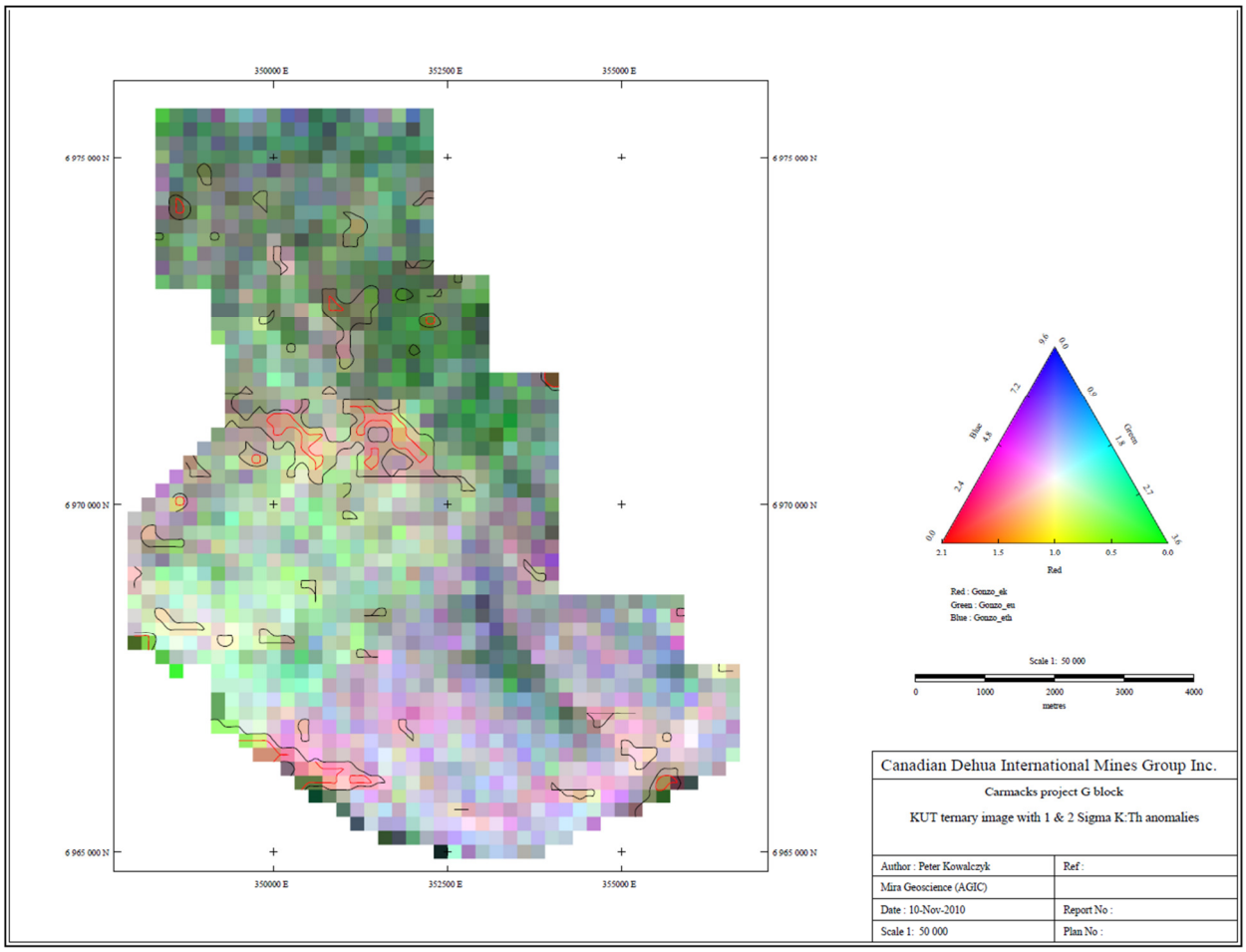

Figure 20: KUT ternary diagram for G Block showing sigma 1 and 2 contours from the K:Th ratio image. Note that data collected on different days has a different response (i.e., the large purplish area in the SE is a data collection artefact). The use of ratios reduces the effects of these artifacts.

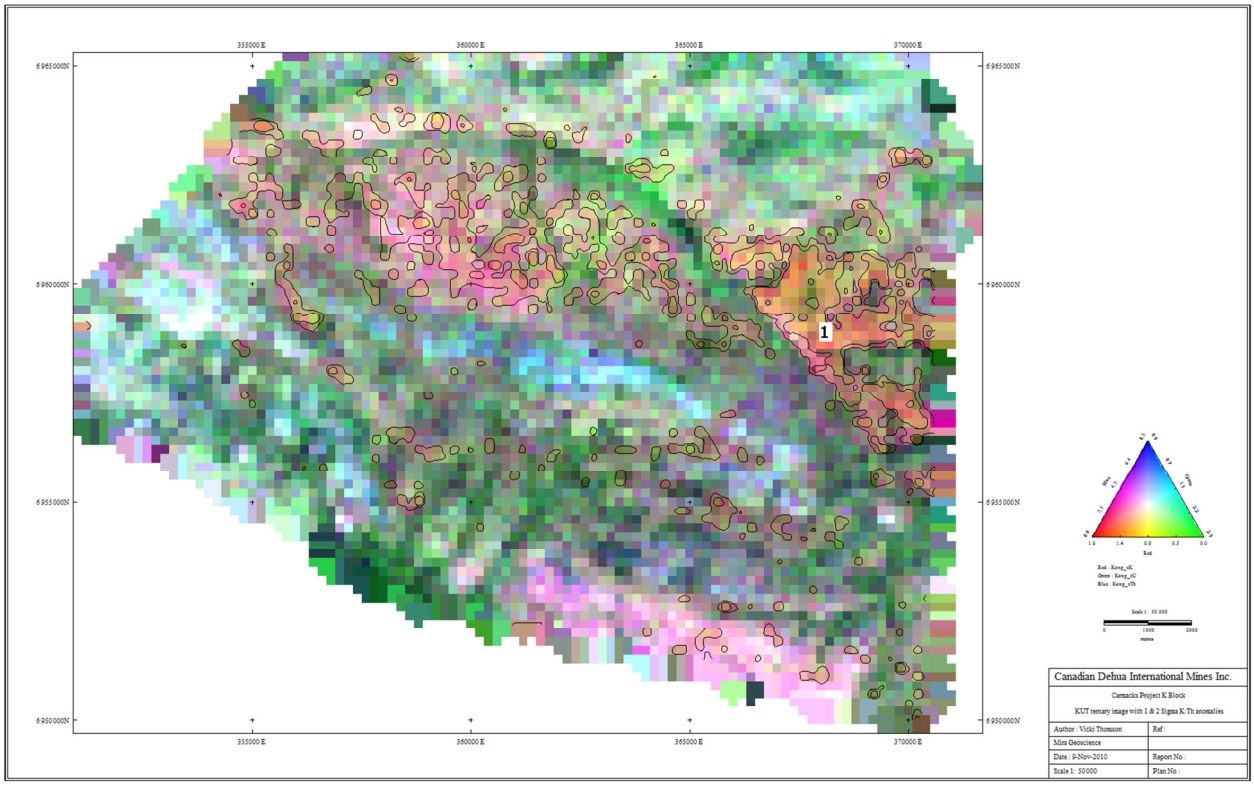

Figure 21: KUT ternary diagram for K Block showing sigma 1 and 2 contours from the K:Th ratio image. Note region marked 1 which maps region of high potassium basalts.

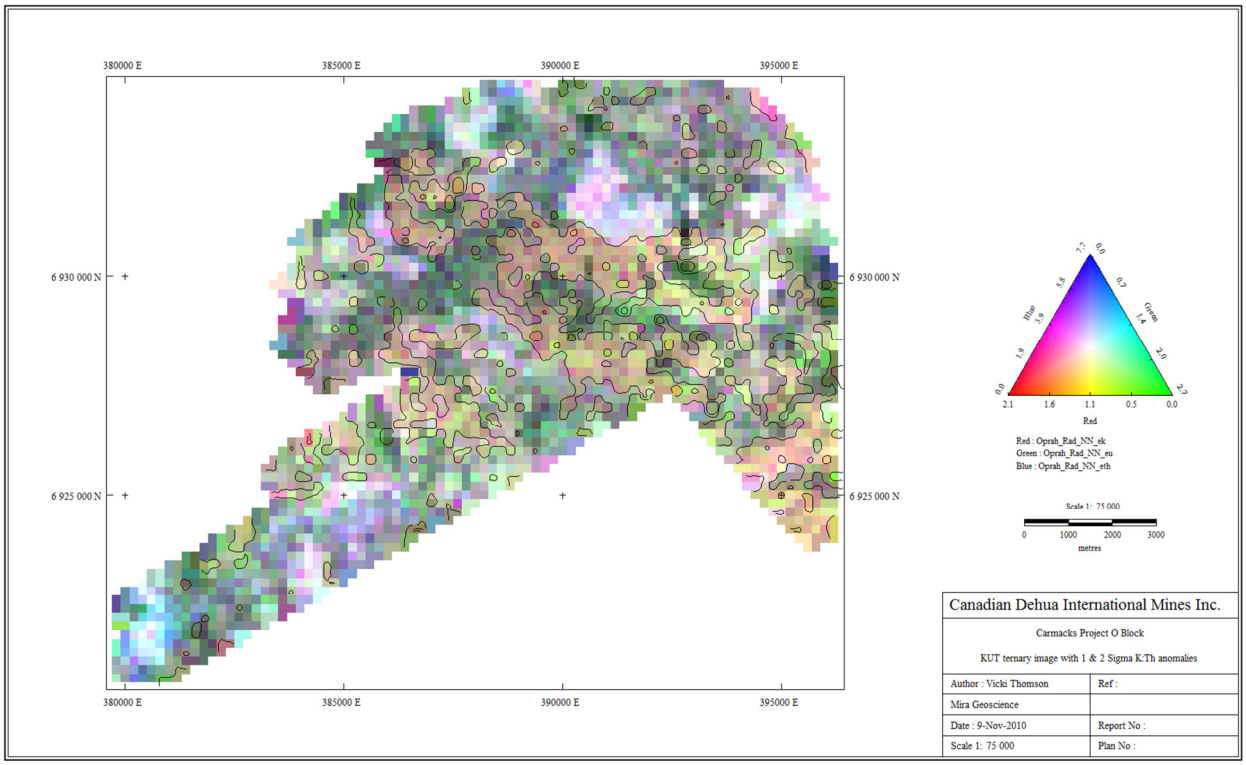

Figure 22: KUT ternary diagram for O Block showing sigma 1 and 2 contours from the K:Th ratio image

4.5. Topographic Data

A digital terrain model (DTM) was provided with the geophysical data for the G, K and O Blocks. The DTM supplied by the client was used to define the topography for the inversion for each dataset (Figure 23, Figure 24, Figure 25). Due to the irregular shape of the surveys, the DTM was merged with Shuttle Radar Topography Mission (SRTM) data for each survey block to extend the topography to cover the extents of the inversion model. The best publicly available topography is considerably coarser than the DTM acquired from the survey and as such there is an offset between the two datasets. This decrease in resolution does not have a significant impact on the inversion as most of the lower quality topography data is outside to core mesh of the inversion.

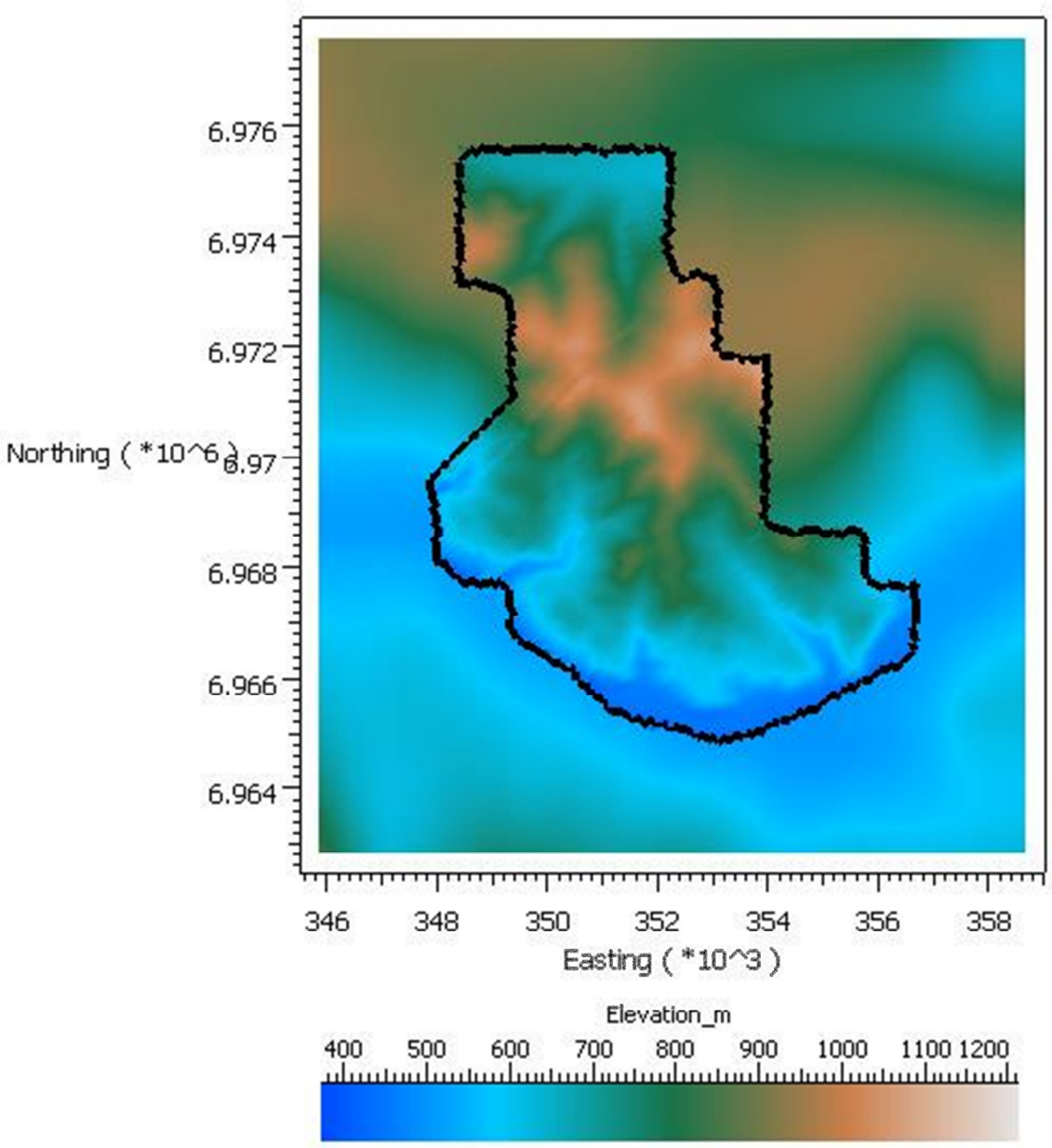

Figure 23: Survey area topography in metres for the G block. Survey boundary shown in black.

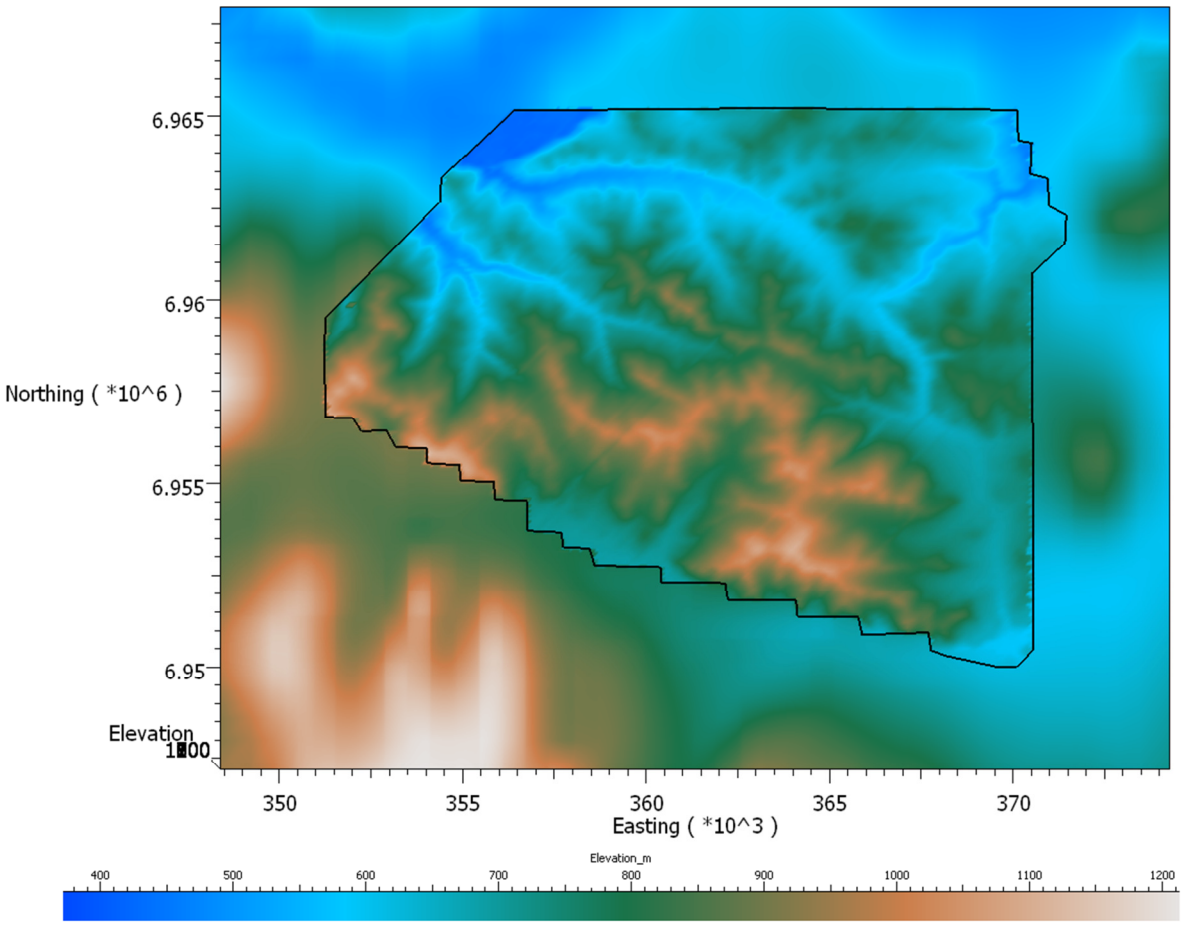

Figure 24: Survey area topography in metres for the K block. Survey boundary shown in black.

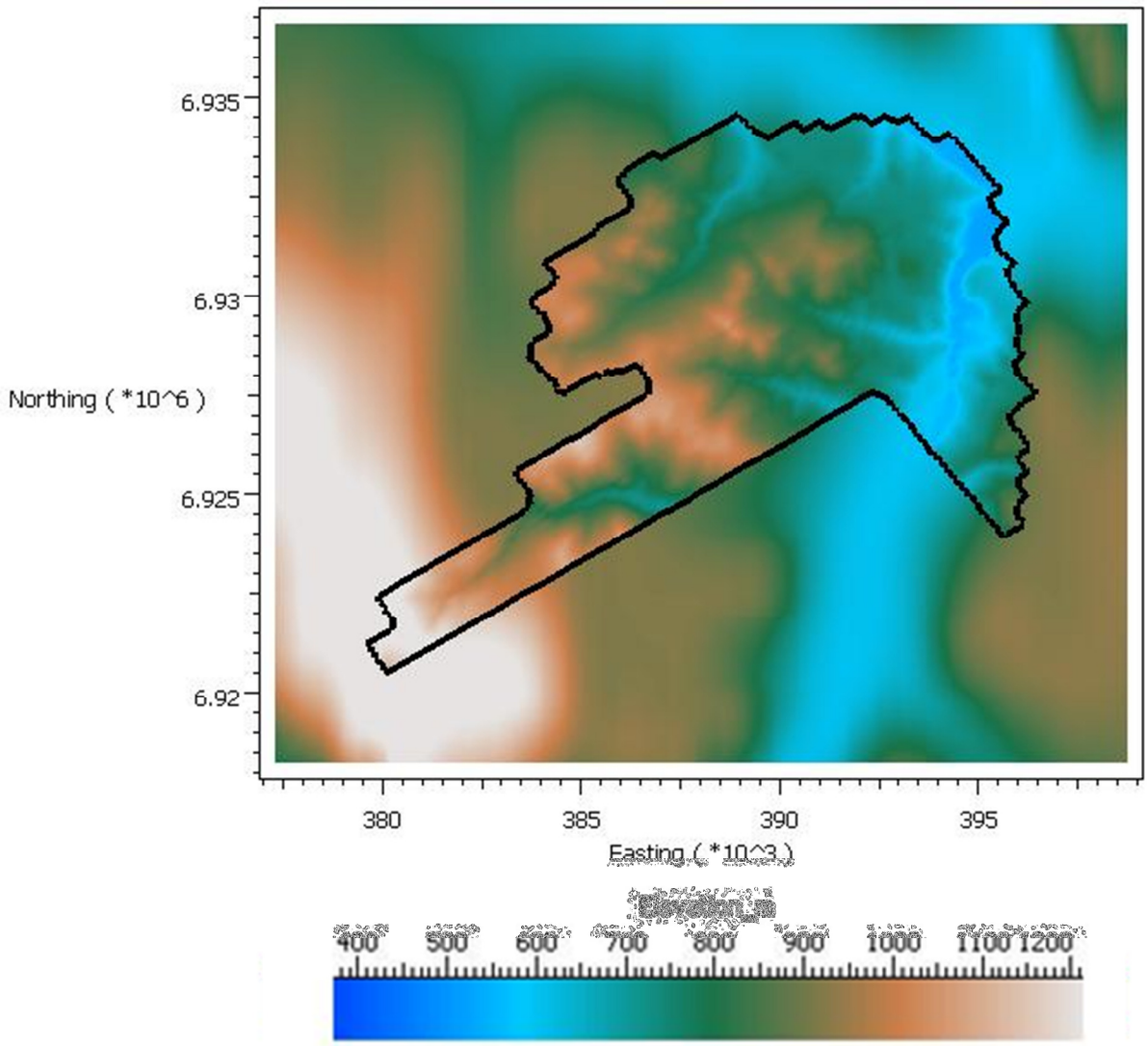

Figure 25: Survey area topography in metres for the O block. Survey boundary shown in black.

4.6. Unconstrained Magnetic Inversion

Magnetic susceptibility inversion models for each survey area were produced to aid the structural interpretation and targeting phase, providing information about the local geology and mineralization. Magnetic susceptibility is one of the criteria to be attributed to the exploration model. Porphyry copper deposits are often associated with intrusive rocks or batholiths that contain magnetite, a magnetic mineral, and thus produce a magnetic anomaly. The objective of the magnetic inversion modelling is to produce a 3D susceptibility distribution for a volume of interest represented by the extents of the airborne survey area to aid interpretation of the local geology.

The inversion modelling process creates a 3D representation of the earth using a discretization with many small cells each of constant magnetic susceptibility. The resulting model will predict the observed data to within a predetermined tolerance and will be optimized to produce robust, simple magnetic susceptibility features in the model that represent major geologic features when no additional geologic information is provided (unconstrained by geology). Topography is included in the modelling process. Total Field Magnetic data are inverted for a 3D susceptibility model of the earth using the UBC-GIF MAG3D inversion code. Magnetic anomalies are assumed to result from the inducing field only. Remanence or self-demagnetization is not considered. Appendix 3. MAG3D Modelling Software" summarizes the modeling software used.

4.6.1. Magnetic Data Processing

The data were prepared for inversion by reviewing the positioning and amplitude of the data, and were determined to be of good quality and appropriate for inversion modelling. The entire magnetic dataset was modeled for each survey. It is presumed that all appropriate diurnal corrections and control-line leveling were applied to the data. The data were down-sampled in order to make the inversion modelling process tractable. The resultant data separation distance of approximately 25 m, 35 m and 30 m for the G, K and O blocks respectively is consistent with the scale of modelling being undertaken.

Prior to inversion, the IGRF value (International Geomagnetic Reference Field) was removed from the data. The values for magnetic field inclination, declination and IGRF are shown in Table Table 2: Inducing Magnetic Field Parameters. The merged survey DTM and SRTM data was used to define the topography for each inversion, due to the irregular shape of the surveys. The modelling was carried out in the same coordinate system as that in which the data were provided; WGS84, UTM Zone 8N.

Table 2: Inducing Magnetic Field Parameters

	G-Block	K-Block	O-Block
Latitude (degrees N)	62.8271	62.7309	62.4741
Longitude (degrees E)	-137.977	-137.696	-137..144
Mean Elevation (m)	772.958	789.449	865.935
Survey Date	Aug 13 – 15, 2010	Jul 27 – Aug 04, 2010	Aug 11 – 13, 2010
Magnetic Field Inclination (degrees)	77.317	77.300	77.217
Magnetic Field Declination (degrees)	22.800	22.817	22.800
Magnetic Field Magnitude (nT)	57370.2	57378.1	57376.7

A standard deviation was assigned to the data for inversion modelling purposes. The standard deviation represents an estimate of all possible sources of data uncertainty including: sensor sensitivity and noise, GPS location uncertainty, modelling uncertainties (topographic representation in the model and small magnetic sources that cannot be accounted for in the

discretization). The value is an estimate and the actual level of data misfit is determined during inversion. The uncertainties assigned to the data in the inversions were 2% of the magnitude of the data range for all points except those in the area outside of the black curve in Figure 27, which represent a suspected area of remnant magnetization in the K block data. These data were assigned a standard deviation value greater than the data range. This was done to minimize the contributions from these data as the MAG3D code is not designed to deal with magnetic remanence. If the errors were not increased, the areas containing remanence would dominate the inversion and skew the model results.

In order to enhance near surface features, regional inversion modelling was performed to separate the near surface features from the deeper sources. Coarser-scale inversions are used to remove the regional signal from the datasets prior to the detailed inversions. This helps separate signal in the data that is from magnetic sources external to the volume and depths of interest. For this project the regional removal was done using the same detail as subsequent inversions. The resulting residuals (total field magnetics with regional removed) are shown in Figure 26, Figure 27, and Figure 28, for the G, K and O blocks respectively. The residual data reveals more detail with the large-scale regional trends removed. The inversion-based regional signals can be found in

Appendix 5. Magnetic Inversion – Regional models removed. The inversion parameters are listed in Table 3.

Table 3: Inversion Parameters

Inversion Modelling Parameters	Inversion Modelling Parameter Value
Convergence Criteria	Fixed Target Misfit (Chi factor = 0.15)
3D Mesh	G= 50x50x25m cells with increasing vertical depth thicknesses on a scale of 1.4 K = 70x70x30m cells with increasing vertical depth thicknesses on a scale of 1.4 O= 60x60x30m cells with increasing vertical depth thicknesses on a scale of 1.4
Number of cells in mesh	G = 3178140 K= 4702080 O= 5085300
Length Scales	G = 150,150,75 K= 210,210,90 O= 180,180,90 (Le, Ln, Lz)
Number of data inverted	G = 24992 K= 78305 O= 33550
Achieved Data Misfit	G = 3.915258E+03 K= 4.992441E+03 O= 4.293908E+03
Data errors	2% magnitude of the data was applied to the data

The predicted TMI data generated by the model and the observed TMI data agree very well for the G, K, and O Block models. Most of the features of the magnetic signal are reproduced and ~95% of the difference between the observed and predicted data is within 1 standard deviations. There is some correlated signal seen in the difference plots suggesting that some of the high amplitude magnetic signal has not been fully recovered. The inability of the linear magnetic inversion process to recover all the signal features may have been caused by the presence of self-demagnetization and/or remanence from highly magnetic material or remanent magnetism. Appendix 2. Magnetization and Modelling describes remanent magnetization and self-

demagnetization and the implications of using modelling methods that do not consider these phenomena.

All 3 Blocks were affected by remanence to varying degrees. The most severe was the K block, followed by O and G. Work has been done to suppress these remanence artefacts. The K block was edited to remove data affected by remanence and errors increased. Figure 27 shows the outline of where data was edited. The non-positivity model was used for the O Block as it maintained the detail of the magnetic anomalies without needing to crop out the affected data. The remanence is primarily present in the volcanic units, specifically the basalts that surround the edges of the surveys. Some examples of the inversion models are shown in Figure 29 and Figure 30.

It should be noted that the data will only be able to provide useful definition at depths equal to the distance from the edge of coverage. That is the model will be well defined near the surface for all the data coverage, and in order for the model to be well defined at a depth of 1000m, the data coverage must extent in all directions at least 1000m.

4.6.2. Magnetic Inversion Interpretation Results

Interpretation of the magnetic susceptibility models was done in 4 stages. First was a comparison of the 2D structural interpretation to make sure that the contacts and faults were located in the correct position. The second was to digitize the outlines of the magnetic bodies based on the magnetic susceptibility isosurfaces ranging from 0.002 SI to 0.05 SI (example Figure 31). The third was to digitize the centre of those magnetic bodies (localized magnetic highs) and to identify areas of structural change by locating the edges of the magnetic anomalies that change strike or shape in a way that may indicate structural controls caused the change (examples Figure 32 and Figure 33). These structural changes are referred to as “bends”, or “pinch outs” for simplicity. It refers to a change in strike that may indicate that the geologic unit or fault has been disrupted by an event, possibly related to a structural event, intrusion, or alteration that could suggest the presence of mineralization. The fourth stage was limited to the K and G Blocks only. The magnetic susceptibility models for both blocks suggest the presence

of a batholith beneath the survey area. Based on the deposit styles of nearby operating mines Minto and Carmacks, mineralization appears to be related to the Battle Mountain Batholith and Minto Pluton. Therefore, the suggestion of a batholith present beneath the surveys is considered to be favourable as exploration criteria. The outline of the batholith was digitized in the same manner as stage 2. All of these layers, localized magnetic highs, areas where magnetic anomalies bend or pinch out, and batholith outlines, are used in the targeting process.

4.7. Magnetic Inversion Modelling Results

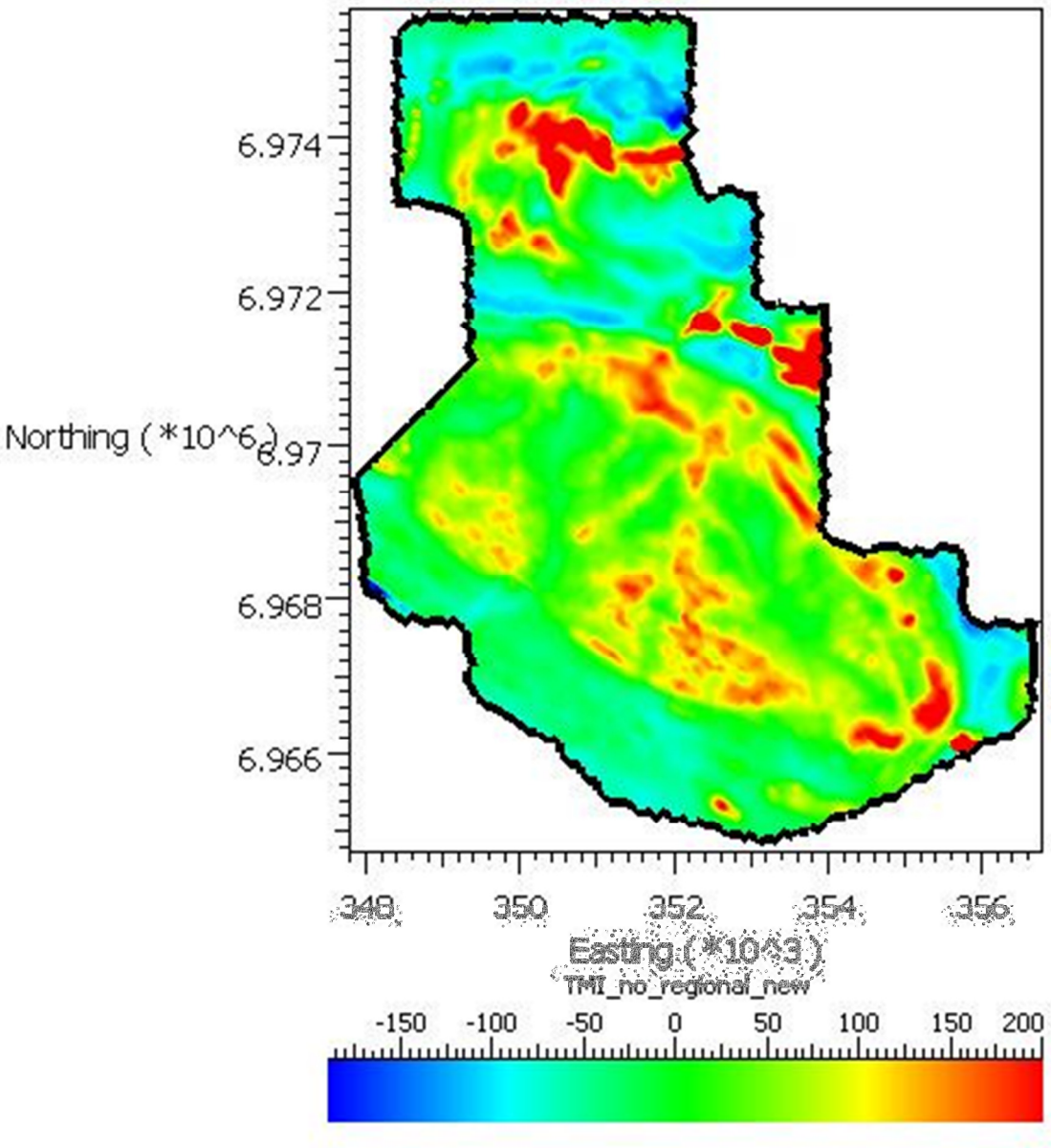

Figure 26: Residual magnetic data (nT) for G-Block survey area used in the magnetic inversion.

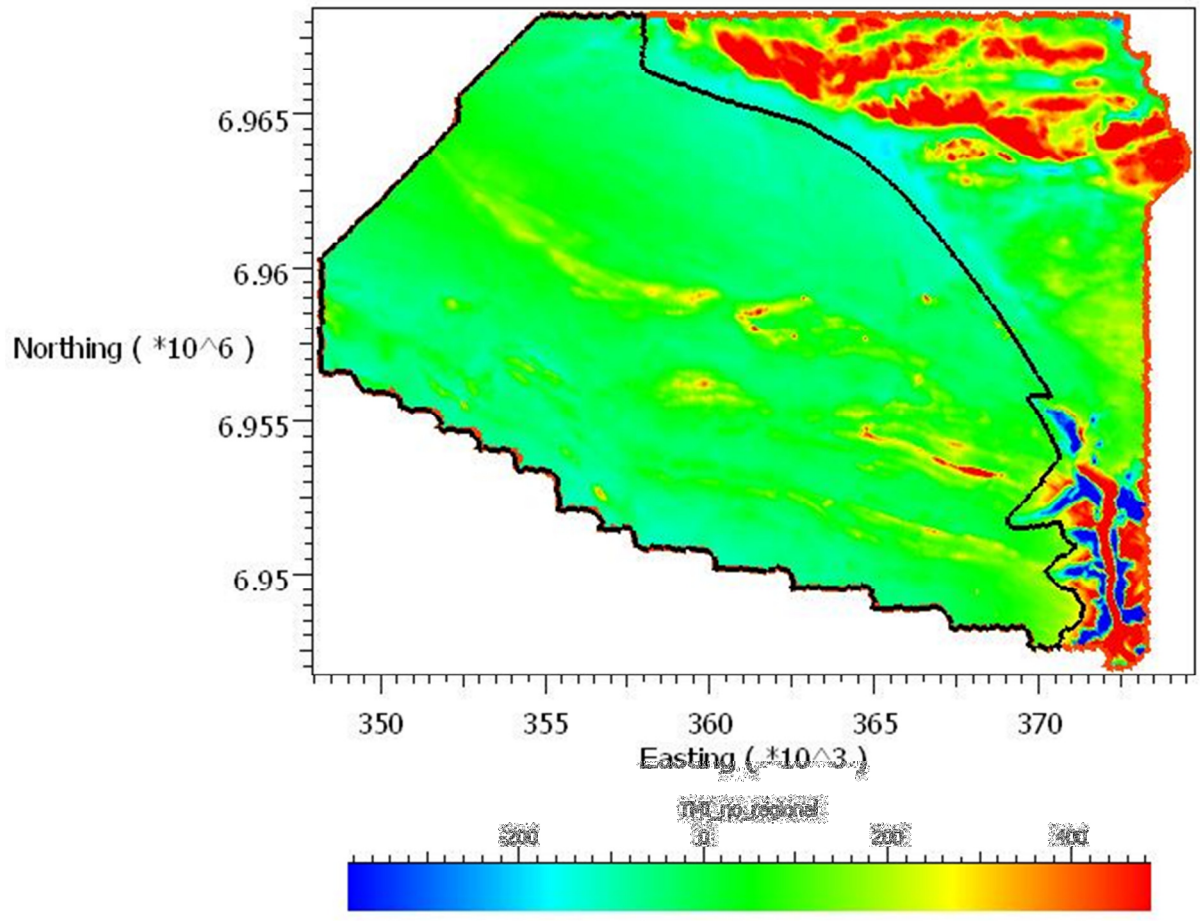

Figure 27: Residual magnetic data (nT) for K-Block survey area used in the magnetic inversion. Boundary of area least influenced by remanent magnetization outlined in black.

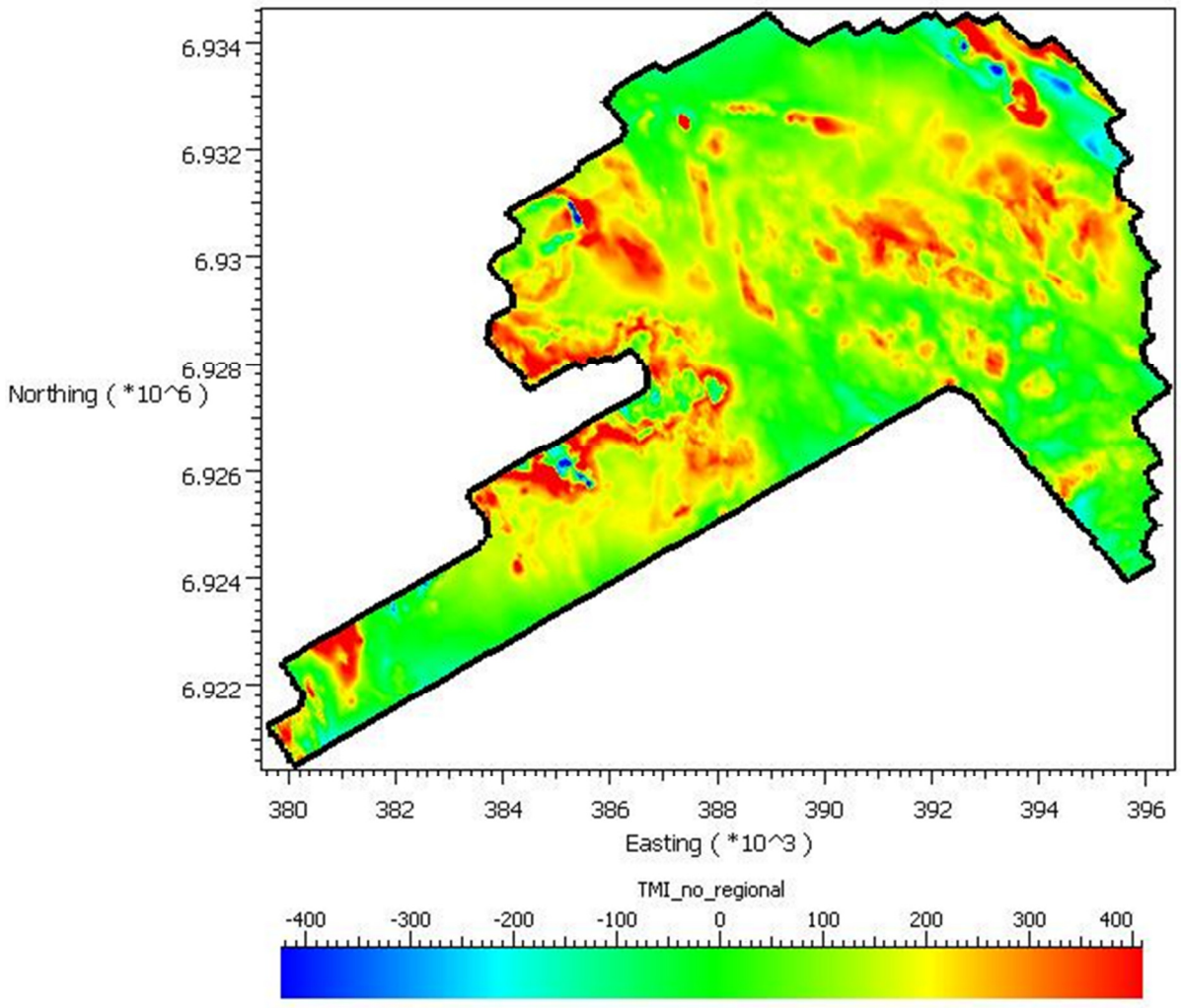

Figure 28: Residual magnetic data (nT) for O-Block survey area (bounded in black).

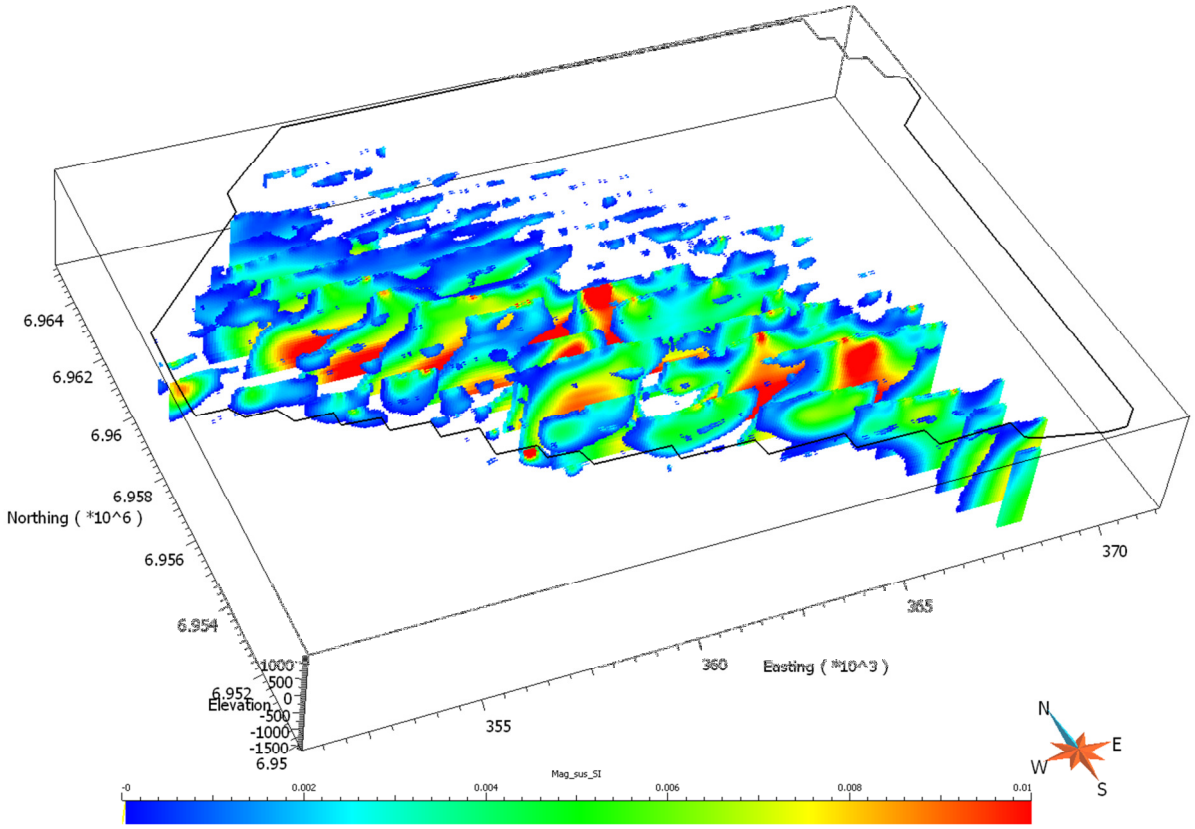

Figure 29: A 3D perspective view of the K Block showing E-W sections through the magnetic susceptibility inversion model.

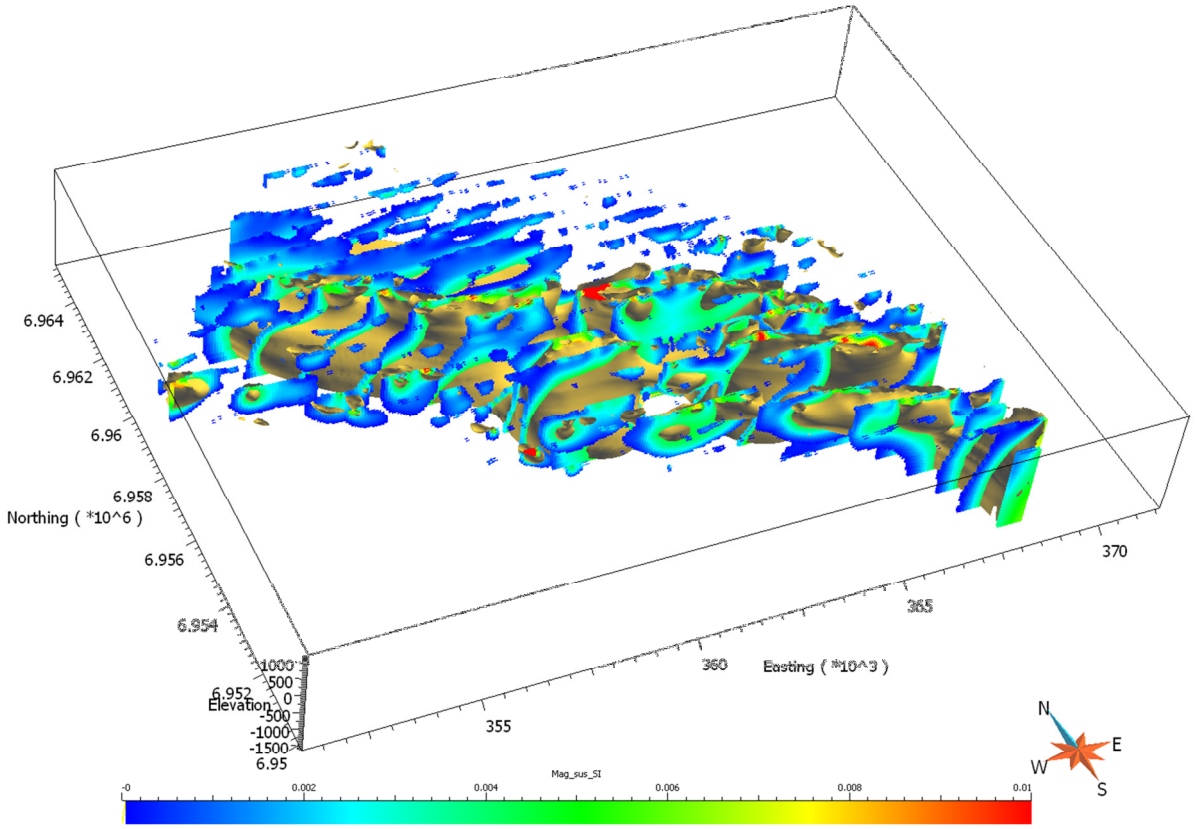

Figure 30: A 3D perspective view of the K Block showing E-W sections through the inversion model and a magnetic susceptibility isosurface of 0.004 SI.

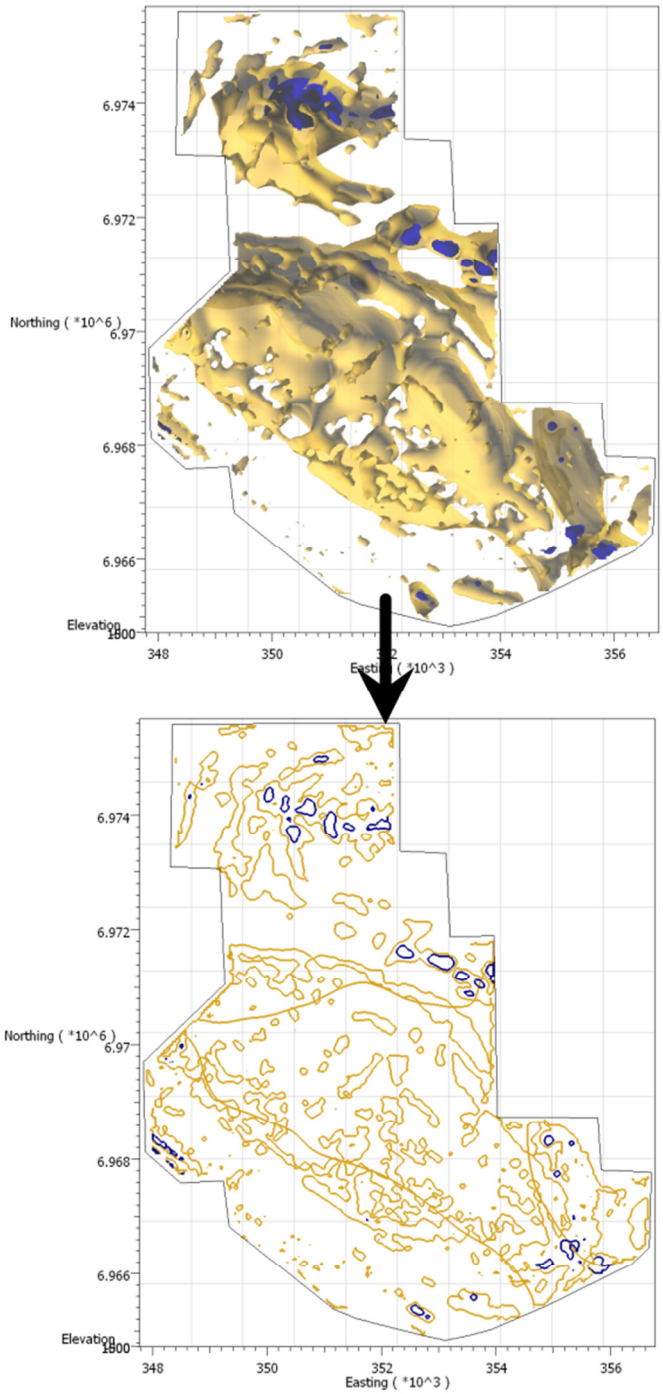

Figure 31: Magnetic susceptibility isosurfaces showing 0.003 SI (gold) and 0.015 SI (blue) and the digitized outlines of the isosurfaces for G Block.

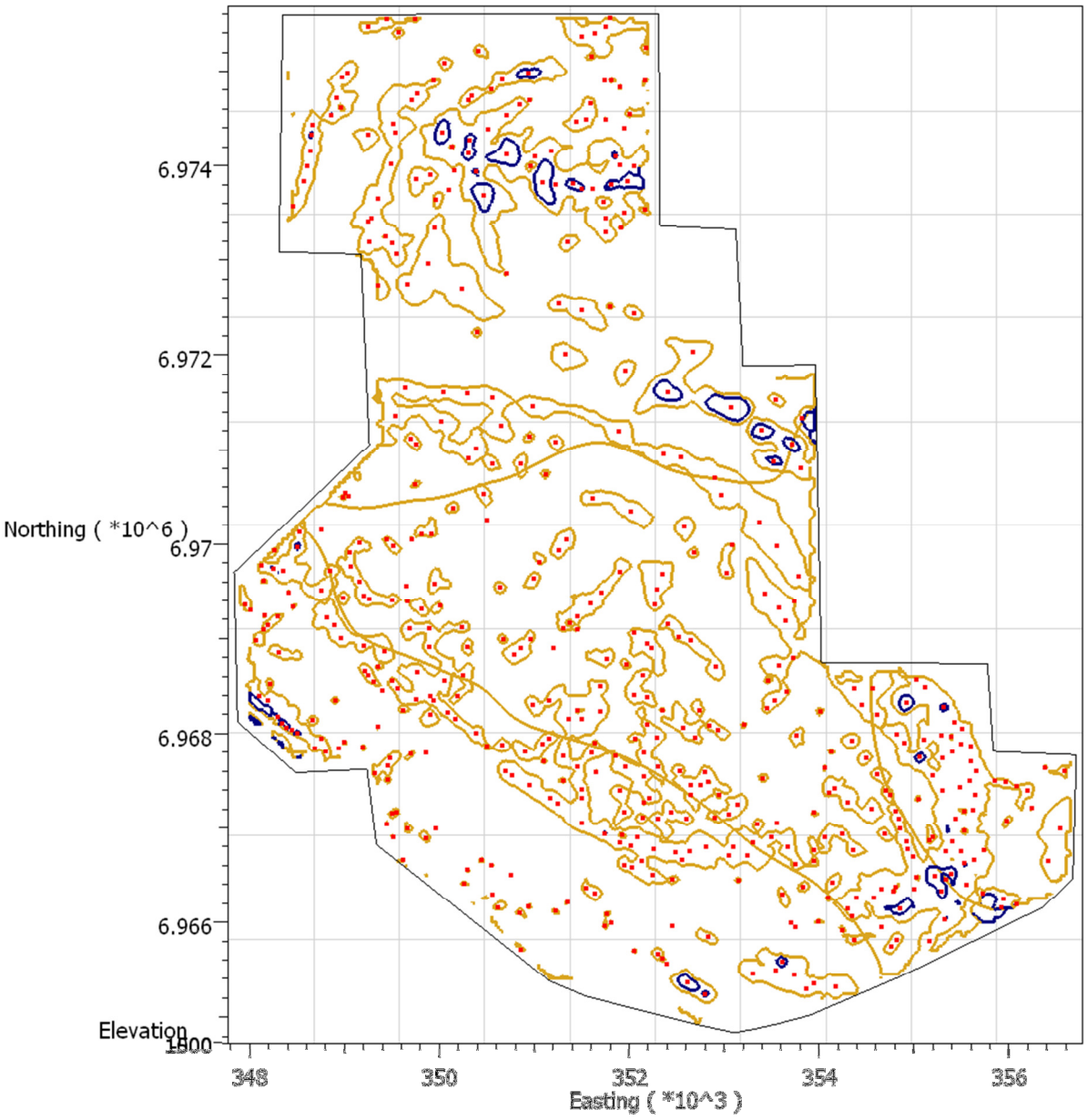

Figure 32: Digitized outlines of the magnetic susceptibility isosurfaces for 0.003 SI (gold) and 0.015 SI (blue) with digitized local magnetic highs based on the isosurfaces (red dots) for G Block.

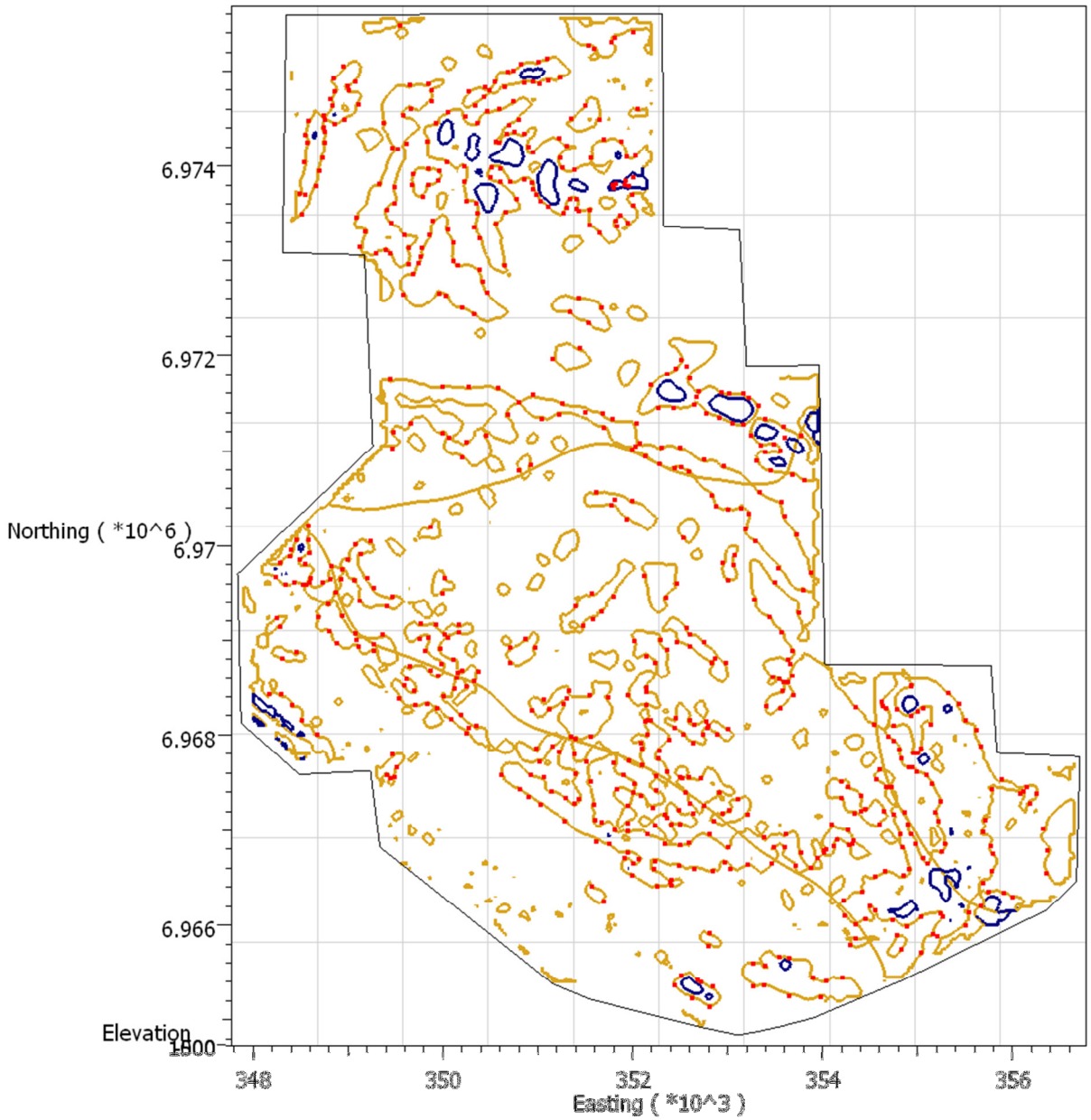

Figure 33: Digitized outlines of the magnetic susceptibility isosurfaces for 0.003SI (gold) and 0.015SI (blue) with digitized magnetic anomaly changes in shape based on the isosurfaces, representing structural controls for G Block.

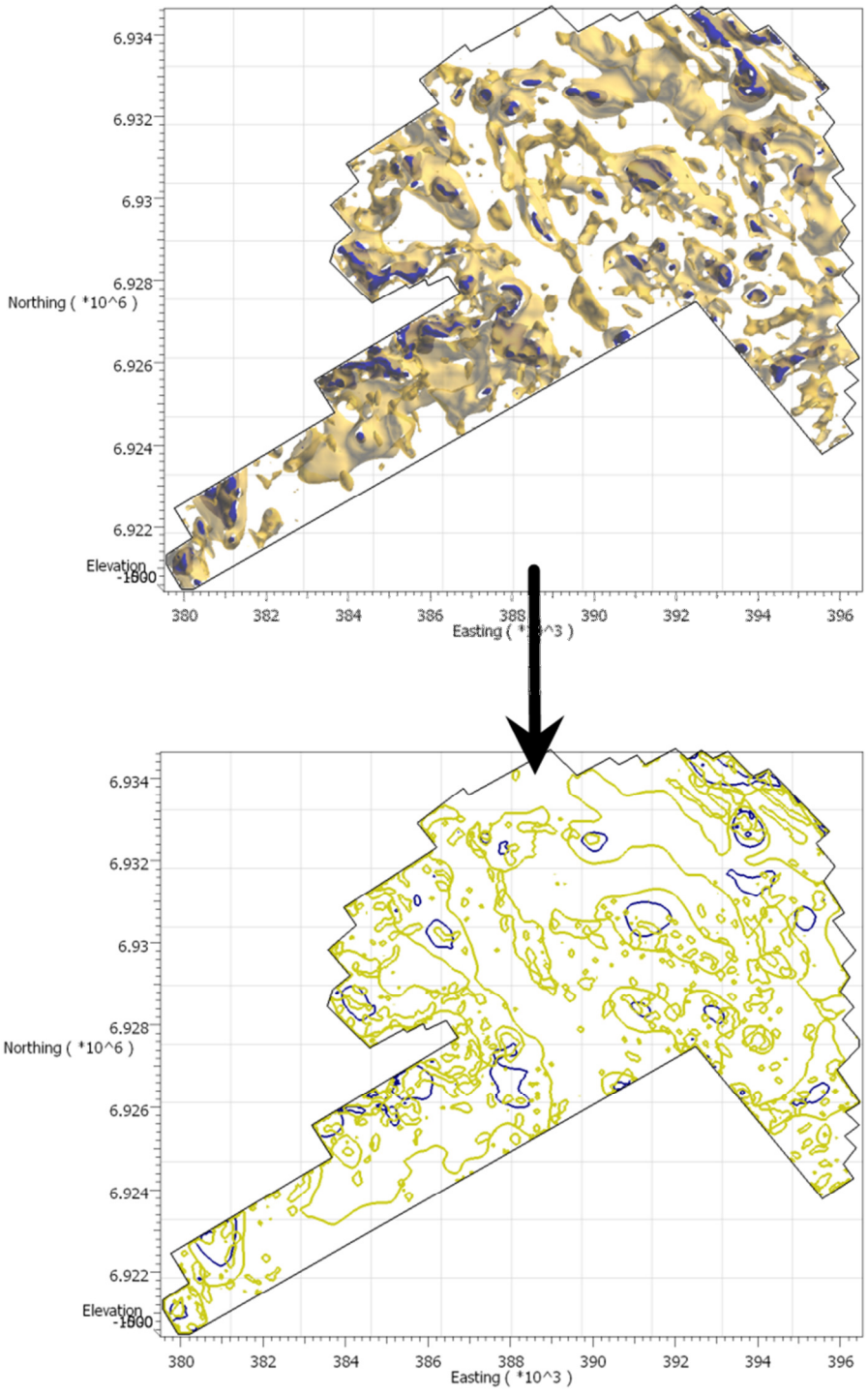

Figure 34: Magnetic susceptibility isosurfaces showing 0.002SI (gold) and 0.015SI (blue) and the digitized outlines of the isosurfaces for O Block.

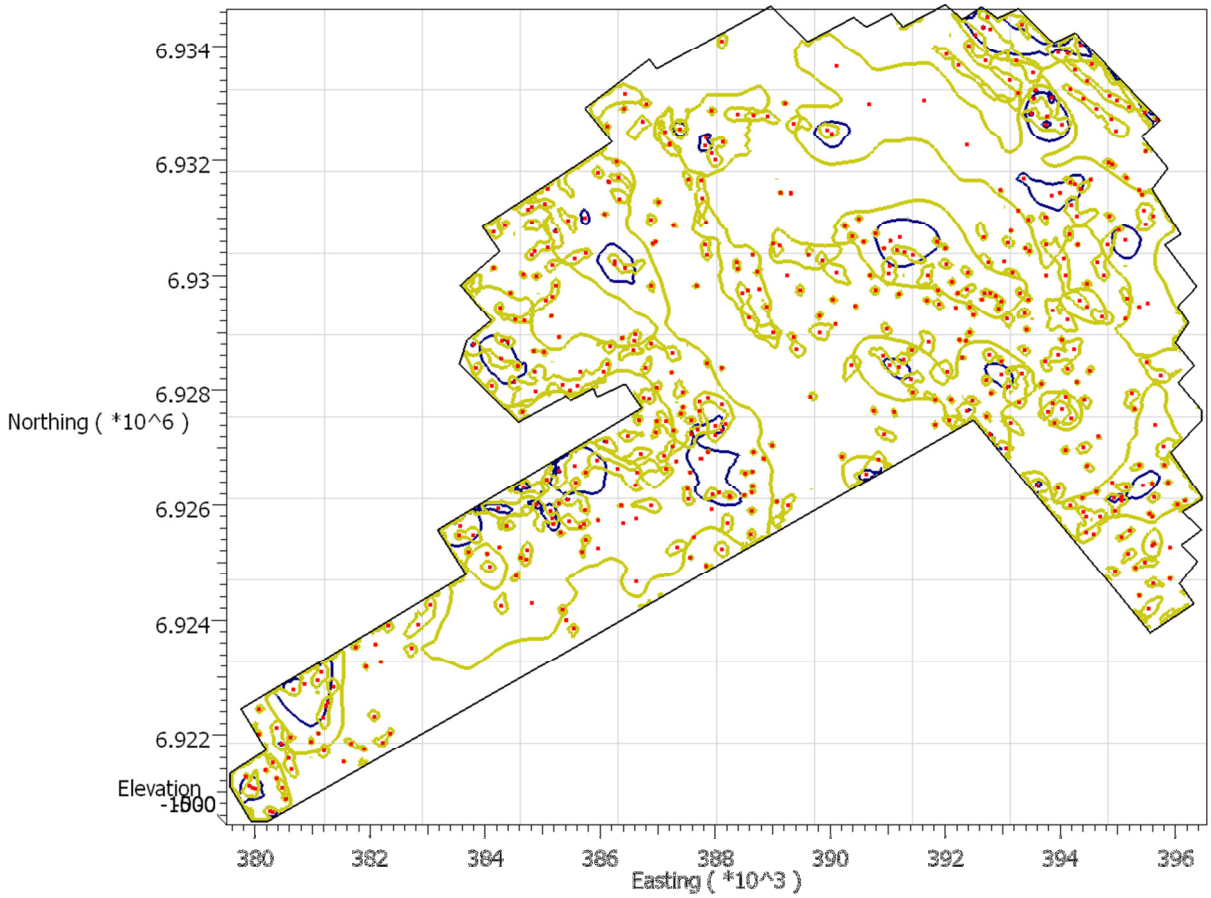

Figure 35: Digitized outlines of the magnetic susceptibility isosurfaces for 0.002SI (gold) and 0.015SI (blue) with digitized local magnetic highs based on the isosurfaces (red dots) for O Block.

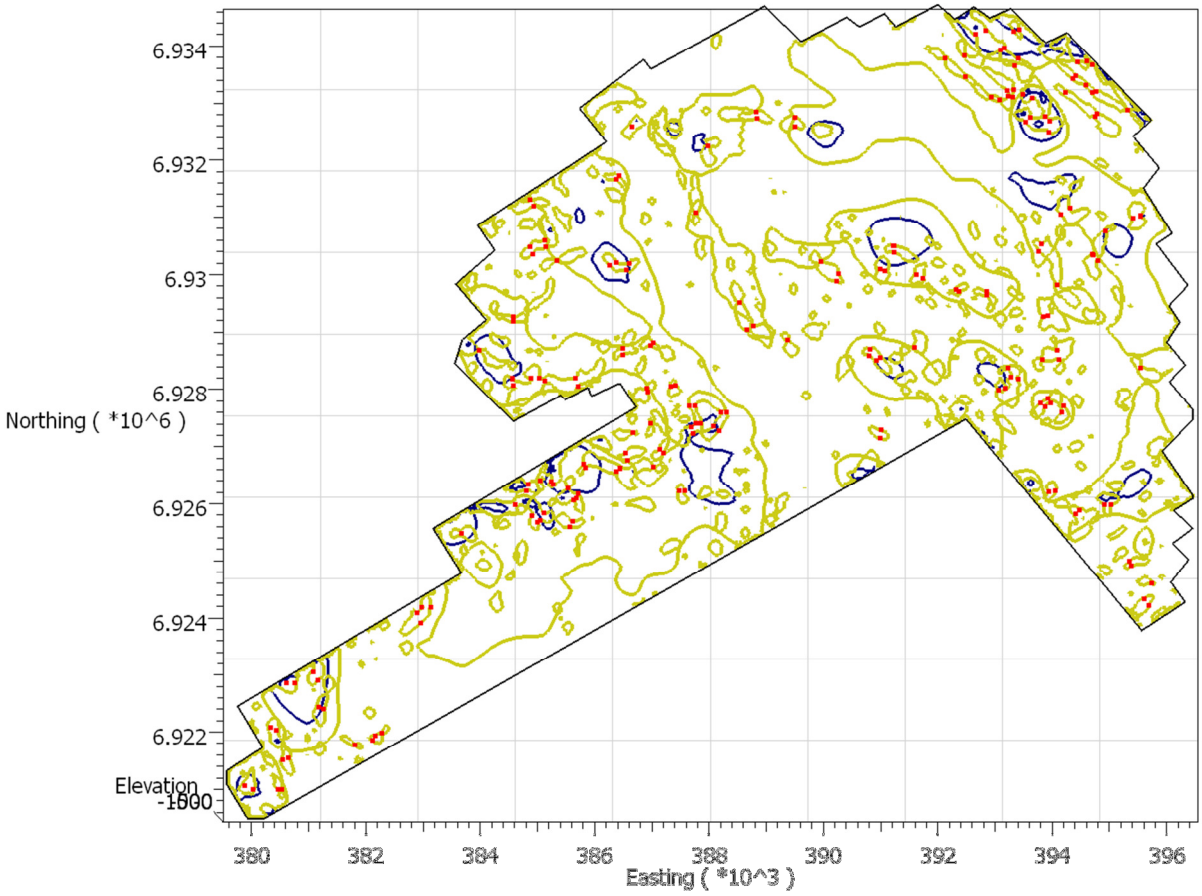

Figure 36: Digitized outlines of the magnetic susceptibility isosurfaces for 0.002SI (gold) and 0.015SI (blue) with digitized magnetic anomaly changes in shape based on the isosurfaces, representing structural controls.

5. Exploration Targeting using Knowledge-Driven Weights

The objective of the exploration targeting process is creation of a new property throughout the model that represents a relative potential for mineralization. The ultimate goal is to target individual groupings of cells having high mineral potential for further investigation.

We are using a knowledge-driven approach in this project because very little is known about the mineralization in the survey areas. The knowledge-driven approach produces subjective empirical models that are based on the experience of domain experts.

Binary Index Overlay involves a combination of weighted binary properties using a simple intersection algorithm where the binary classes (1 or 0) of each property are multiplied by a single weight factor, summed over all properties being combined and normalized by the sum of all weights following the equation:

$$S = \frac{\sum_{i}^{n} W_i \, class(MAP_i)}{\sum_{i}^{n} W_i}$$

Weights are defined by the expert and are based on the significance of the evidential property to the exploration model. The result is a weighted score defining favourability of mineral potential. This method allows for a simple ranking of the contributing evidences as a whole.

5.1. Application of Knowledge-Driven Weights

The knowledge-driven algorithm has been built into a Gocad workflow plug-in: the Targeting Workflow. The workflow is implemented as a series of sequential panels where the user is required to select data objects and other required input before proceeding to the next step. Software workflows in general are beneficial in that they allow practitioners to execute complex quantitative processes yielding robust, consistent and repeatable results. This ensures the

domain-expert thought process is captured and followed by the workflow user which in turn ensures rigorous application of the statistical methods.

To perform the knowledge-driven analysis, a model containing the exploration criteria represented as evidential properties is required. This was performed after the magnetic and radiometric interpretation was completed. Each of the grid cells contains an array of evidential property values. This section summarizes the data inputs, analysis, and mineral potential results for each of the survey Blocks.

5.2. Evidence Layers

Exploration criteria are geospatial variables that may be related to mineralization at the G, K, and O Block properties. These criteria were defined based on the intrusive porphyry deposit style proposed by Holister (1976). The magnetic and radiometric data were interpreted according to the exploration criteria discussed in Section 3.3. The interpretation of the geophysical datasets was converted to evidence layers for use in the targeting workflow.

The evidence layers are:

- distance to geologic contacts and bends in contacts
- distance to faults, bends in faults, and fault intersections
- distance to dikes and bends in dikes
- distance to Au stream drainage (Yukon Geological Survey geochemistry)
- distance to MINFILE mineral occurrences (Yukon Geological Survey reports)
- distance to magnetic anomalies and changes in the shape of the anomalies (pinch outs)
- distance to radiometric anomalies; potassium anomalies from K:Th ratio
- distance to intrusion (batholith)

5.3. Evidential Property Binary Reclassification

Continuous and discrete evidential properties are converted to binary properties for implementation of the knowledge-driven technique (binary index overlay). Each evidential property is divided into two classes based upon a threshold or cut-off value that best represents the conceptual exploration model, separating areas of high potential from areas of low potential. In Binary Index Overlay models, each evidential property is assigned a weight factor determined by its relative importance to the exploration model.

Based on the conceptual exploration model, proximity to geologic contacts, dikes, faults, mineral occurrences, and geophysical anomalies will be used to define the targeting criteria. The evidential properties were assigned a distance cut-off in which the properties inside that cut-off are considered favourable and beyond that are considered unfavourable. A distance of 210m was chosen as an appropriate cut-off for contacts and faults. This was based on interpretation of the data and cell size of the models. The distances and cut-offs are listed in Table 4.. The weights assigned to each property are relative and based on Holisters's (1976) ore deposit model and our own expertise of the geophysical data. Evidential properties were then assigned to cells in the model Figure 37.

Examples of binary classification for a few evidential properties are shown in Figure 38. The complete classifications for each survey block are shown in Appendices 6-8.

Proximity to known mineralization and stream sediment samples were given the highest weighting of the evidential properties, followed by proximity to potassium anomalies, and proximity to faults and batholiths. The rest of the evidential properties were weighted equally. Weights are listed in Table 4.

.

Table 4: Cut-off values and weights for each of the evidential properties used to compute the mineral potential model

Evidential Properties	Distance/Cut-off	Weighting
Distance_to_MINFILE_showings	1000 m	1.5
Au_Stream_Drainage_	From watershed map	1.5
Distance_to_KTh_rad_anomalies_sigma2	2 σ	1.3
Distance_to_Faults	210 m	1.2
Distance_to_Intrusion_(batholith)	1000 m	1.2
Distance_to_KTh_rad anomalies_sigma1	1 σ	1.15
Distance_to_Contacts	210 m	1.1
Distance_to_Dikes	210 m	1.1
Distance_to_Contact jogs	210 m	1.1
Distance_to_Dike_jogs	210 m	1.1
Distance_to_Fault_jogs	210 m	1.1
Distance_to_Fault_intersections	210 m	1.1
Distance_to_Magnetic_anomalies	210 m	1.1
Distance_to_Mag_anomaly_pinch_outs	210 m	1.1

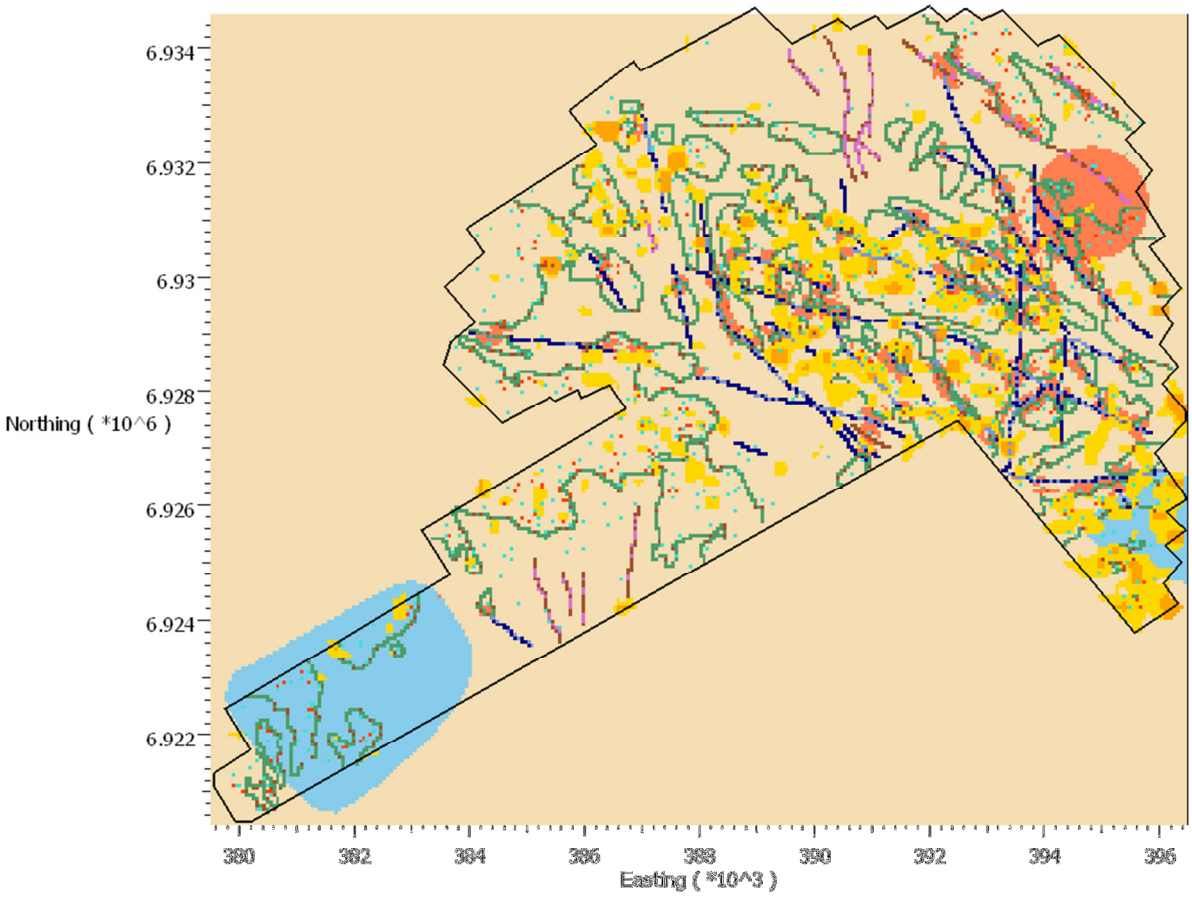

Figure 37: An example of evidential properties displayed as cells in the model for O Block.

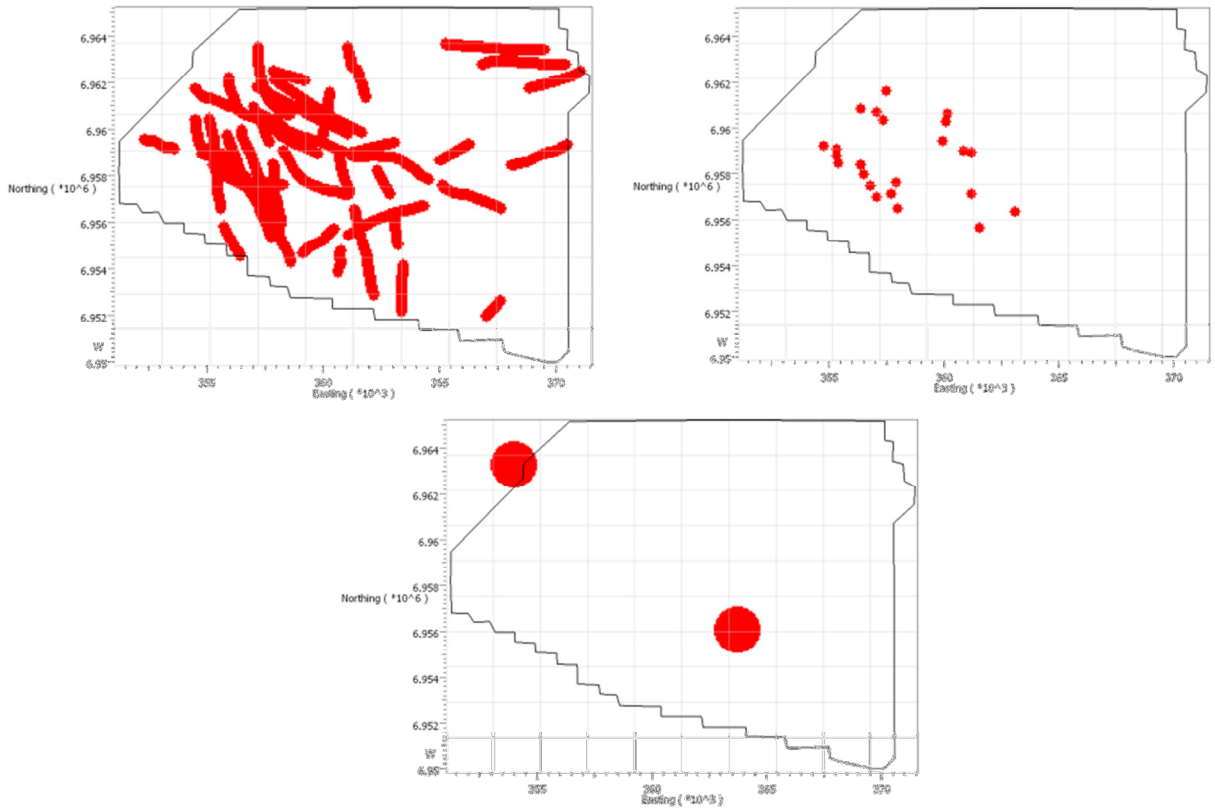

Figure 38: Evidential properties displayed as binary properties in the model for K Block. Red is assigned a binary index of 1, elsewhere is 0. A binary index rating of 1 is favourable for mineral potential.

5.4. Model Results

Once the evidential properties have been converted to binary classification and weights have been assigned, the knowledge-driven data combination algorithm is executed on the selected evidential properties, taking into account weights, to generate the prediction model. Multiple prediction models can be generated at this step by selecting various combinations of evidential properties, or changing the assigned weights. The cells in the model are assigned a score. The cells with the highest scores have the most layers of evidence met with the highest weighting value. Top scoring cells are selected as targets.

A target value cut-off is applied to show only the top percentage of the target result, in this case a 98% cut-off was chosen. From these top targets, clusters of values are generated using adjoining cell corners for connectivity and ranked based on size. The targeting results are shown in the following figures, displayed by score, with a 98% cut-off applied.

At the request of Canadian Dehua International Mines, a target list was generated from the target clusters for each survey Block. In order to create a single target value for the region, the centroid of the region is calculated. The centroid is the centre point of the region and its location depends entirely on the shape of the region. For example, if the region is shaped like a "C" the centroid will plot in the centre of the "C" and thus be located outside the actual target region. The target lists should not be used to spot drillhole locations, but rather as a guide when used in combination with the full targeting results and interpreted geophysical data. The targets have been ranked by mean score, and then further ranked by number of adjoining cells. A ranked list was generated for each block and can be found in

Table 5, Table 6, and Table 7. Figures showing the ranked targets are shown in Figure 45, Figure 52, and Figure 59. A complete list of targets for each cell in the model is provided in the final deliverables.

The G Block returned 30 target clusters, mainly in the centre of the survey area near the contact with the granodiorite and basalt. The mean target scores for the G Block are higher than to the K and O Blocks, suggesting that more targeting criteria was satisfied in this area. These targets are favourable for mineralization because they are near to an intrusive contact, in close proximity to faults, and coincide with both magnetic and radiometric anomalies.

The K Block returned 120 target clusters focused predominantly within the granodiorite and foliated granite/granodiorite gneiss. The highest scoring targets are found where the deformation is more pronounced and where a number of faults cross-cut the geology. Mean target scores are slightly lower overall, compared to the G and O Blocks. This is likely dependent on the magnetic interpretation. The basalts are strongly magnetic and interpretation in these units is very difficult, therefore less targeting criteria have been selected in these units. The granodiorite unit is magnetically quiet except for the distinct magnetic units present in the foliated granodiorite/gneiss unit. As such, less magnetic highs were selected for the targeting criteria in this area also. The radiometric anomalies do not coincide with the magnetic anomalies except in the eastern part of the Block. Therefore fewer criteria were satisfied in each model cell resulting in a lower score. This does not mean that the K Block is less prospective than the G or O Block, just that less targeting criteria were satisfied. It may mean that more evidence is needed to refine the targeting or that the exploration criteria may need to be modified. Refer to Section 6 for recommendations.

The O Block returned 87 target clusters, mainly concentrated in the middle of the survey area within the granodiorite, with some targets in the south-east part of the survey near the contact with the basalt. The O Block scores were higher than the K Block but lower than the G block. The targets in the south-east part of the survey area result from close proximity to a Yukon Geological Survey stream sediment sample with the presence of Au and along a geologic

contact. The targets concentrated in the middle of the survey satisfy a number of criteria; close proximity to faults and contacts, magnetic highs, and radiometric anomalies.

The targeting results for all three blocks suggest that there are a number of areas with high potential for mineralization on each survey property. These results are extremely encouraging and enable Canadian Dehua International Mines Inc. to focus future field work programs in areas where mineralization potential is highest.

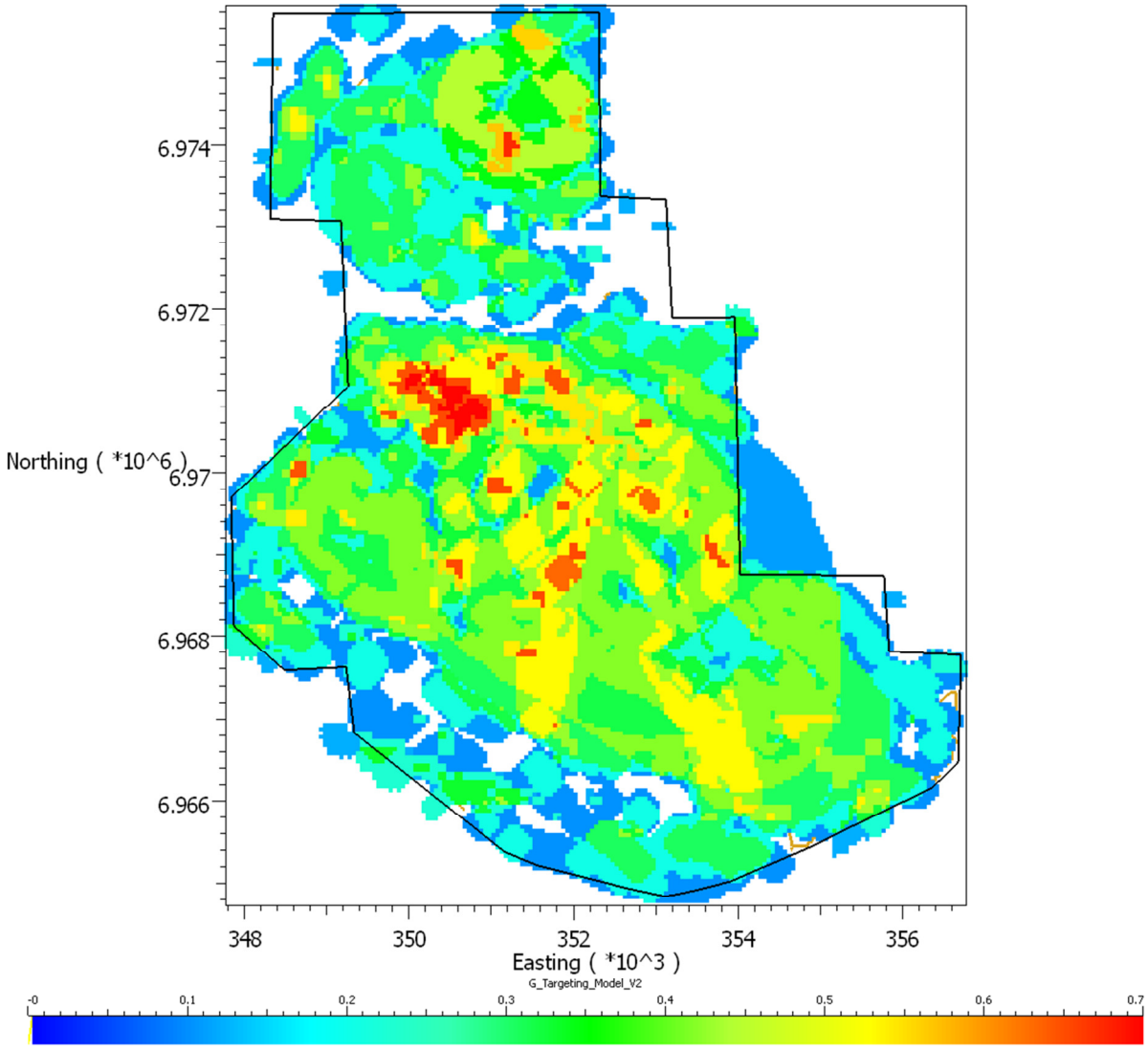

Figure 39: Targeting result for the G Block showing model cells coloured by score.

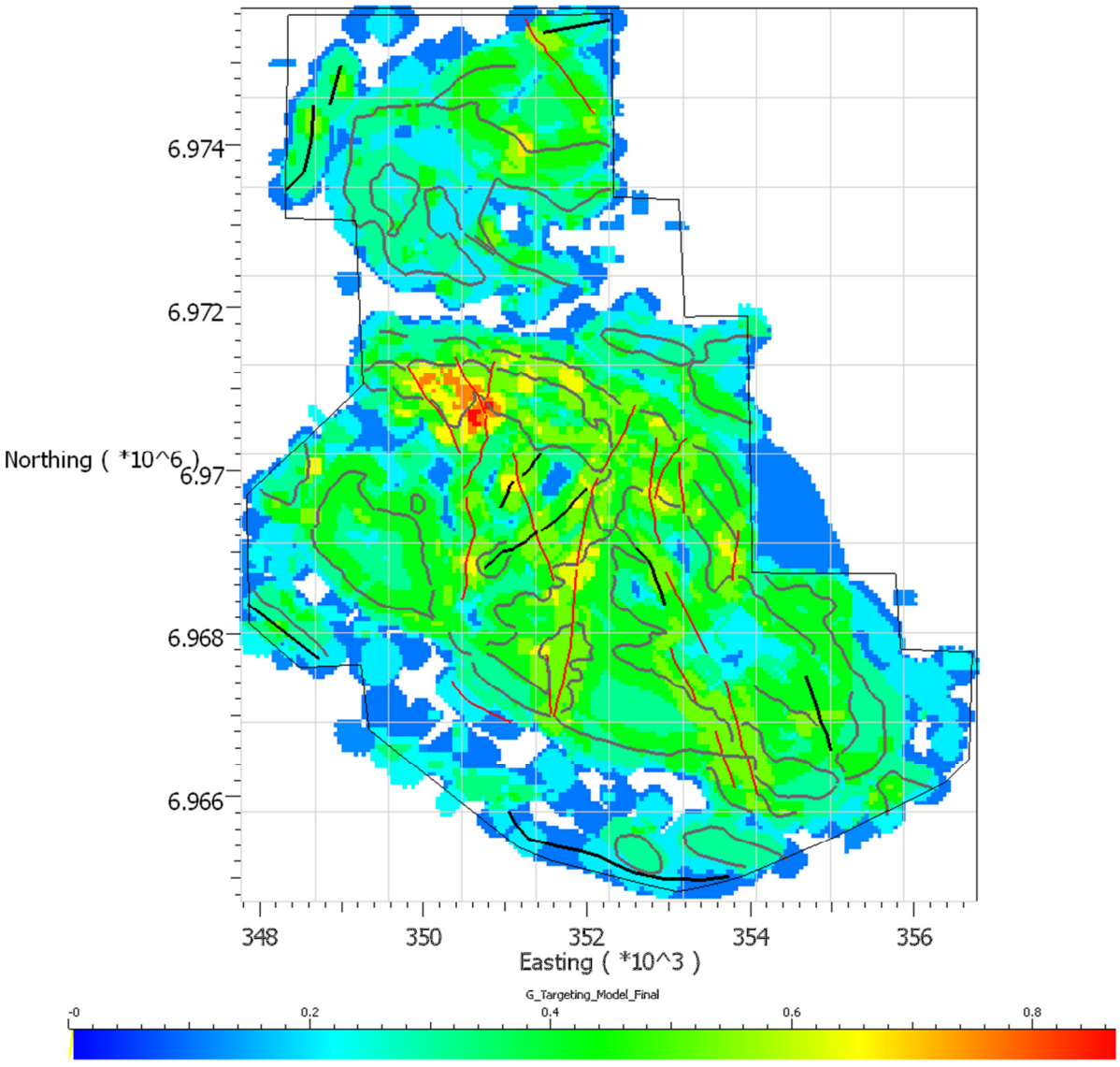

Figure 40: Targeting result for the G Block showing model cells coloured by score with structural interpretation shown.

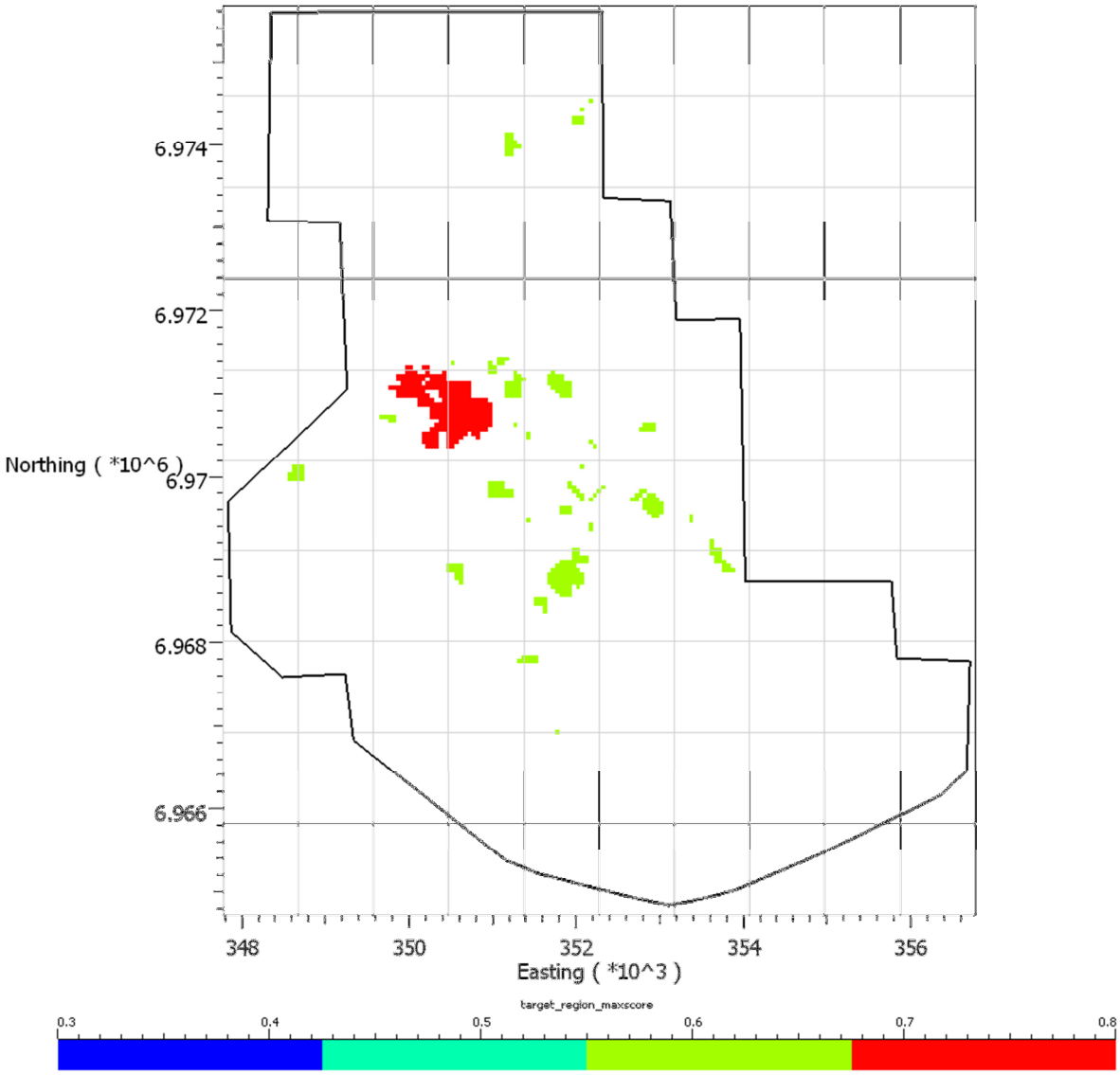

Figure 41: Targeting result for the G Block showing the 98% cut-off. Targets are coloured by score.

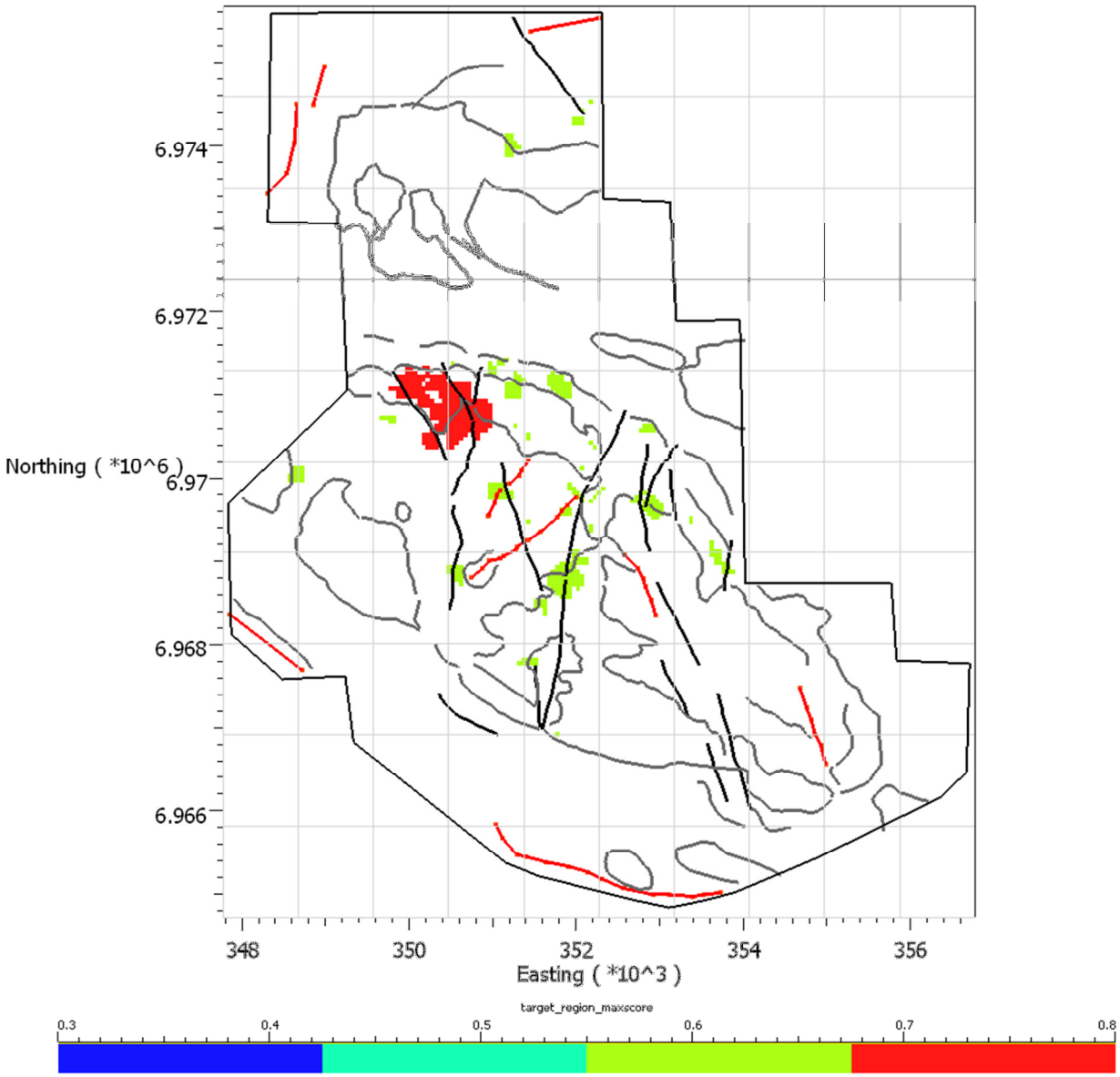

Figure 42: Targeting result for the G Block showing the 98% cut-off with structural interpretation shown.

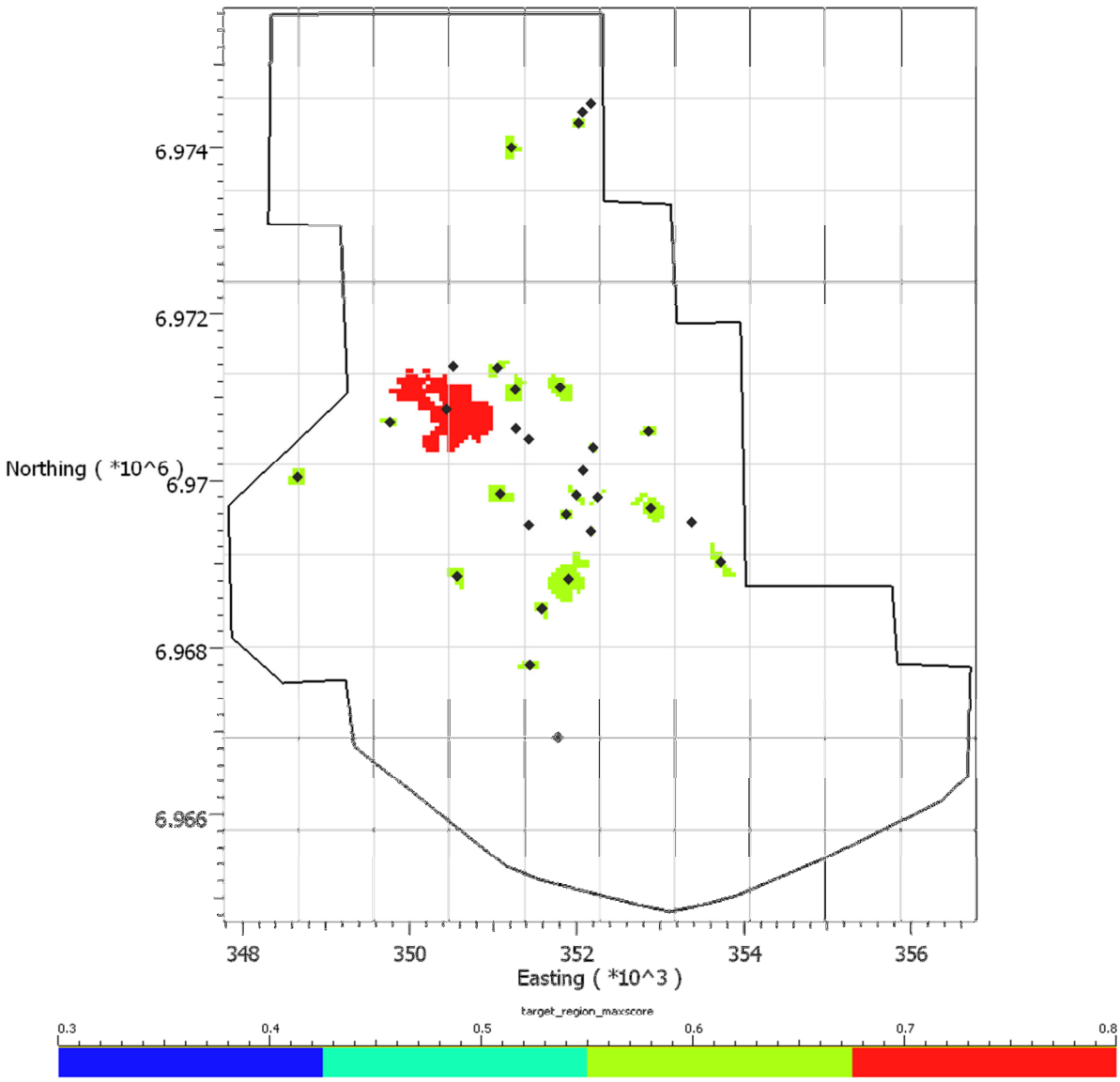

Figure 43: Targeting result for the G Block showing the 98% cut-off with the target centroid locations displayed as black diamonds.

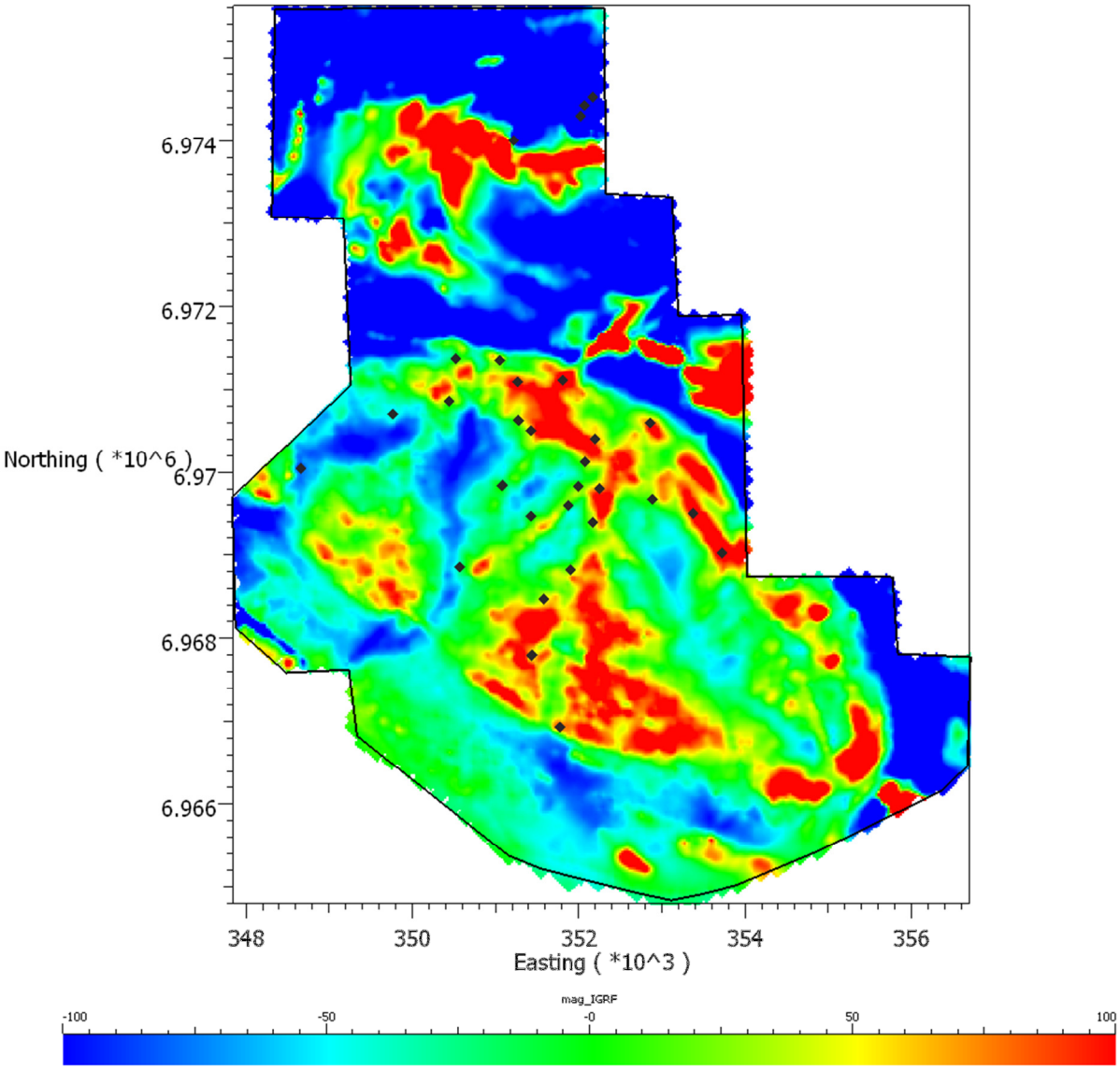

Figure 44: G Block IGRF corrected magnetic data with the target centroid locations displayed as black diamonds.

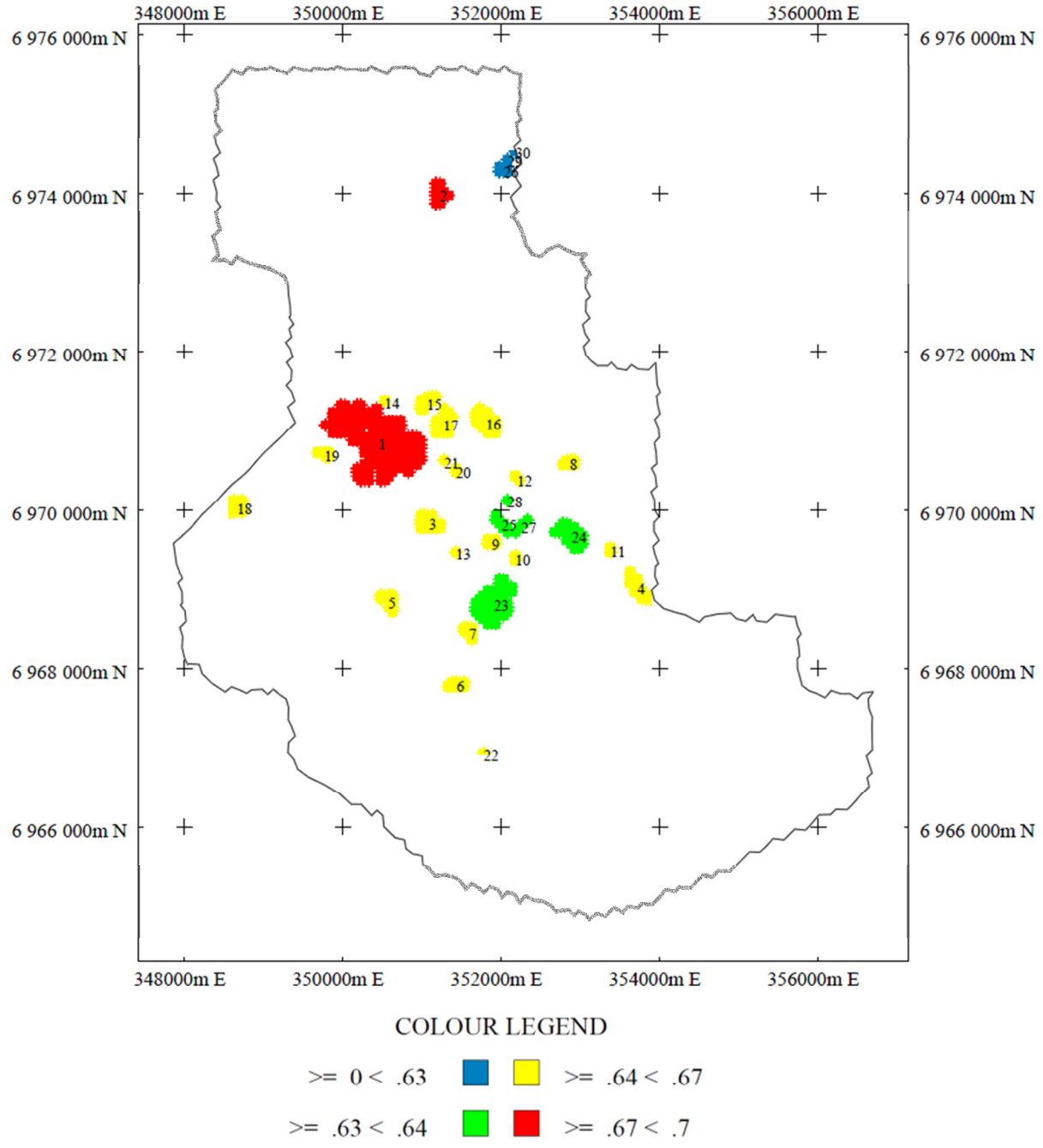

Figure 45: Targeting result for the G Block showing the 98% cut-off with the target centroid locations ranked by mean score then size.

Table 5: G Block target centroids ranked by mean score and number of cells.

Rank (based on Mean then size)	X	Y	Z	Target_Mean_Score	Number of cells in region
1	350443	6970859	963	0.698474	250
2	351218	6973999	743	0.674419	15
3	351080	6969840	829	0.651163	20
4	353719	6969025	864	0.651163	18
5	350571	6968856	618	0.651163	13
6	351436	6967797	819	0.651163	9
7	351588	6968475	782	0.651163	8
8	352861	6970597	905	0.651163	7
9	351875	6969600	895	0.651163	6
10	352175	6969400	915	0.651163	2
11	353375	6969500	868	0.651163	2
12	352200	6970400	1010	0.651163	2
13	351425	6969475	803	0.651163	1
14	350525	6971375	1001	0.651163	1
15	351055	6971360	1010	0.648837	10
16	351803	6971112	1045	0.646512	27
17	351266	6971093	1023	0.646512	22
18	348661	6970043	597	0.646512	14
19	349767	6970709	873	0.646512	6
20	351425	6970500	978	0.646512	2
21	351275	6970625	958	0.646512	1
22	351775	6966925	638	0.64186	1
23	351900	6968825	818	0.63589	67
24	352888	6969677	863	0.632558	28
25	352000	6969825	944	0.632558	8
26	352025	6974300	722	0.576744	6
27	352250	6969800	995	0.632558	4
28	352075	6970125	959	0.632558	1
29	352075	6974425	716	0.576744	1
30	352175	6974525	870	0.576744	1

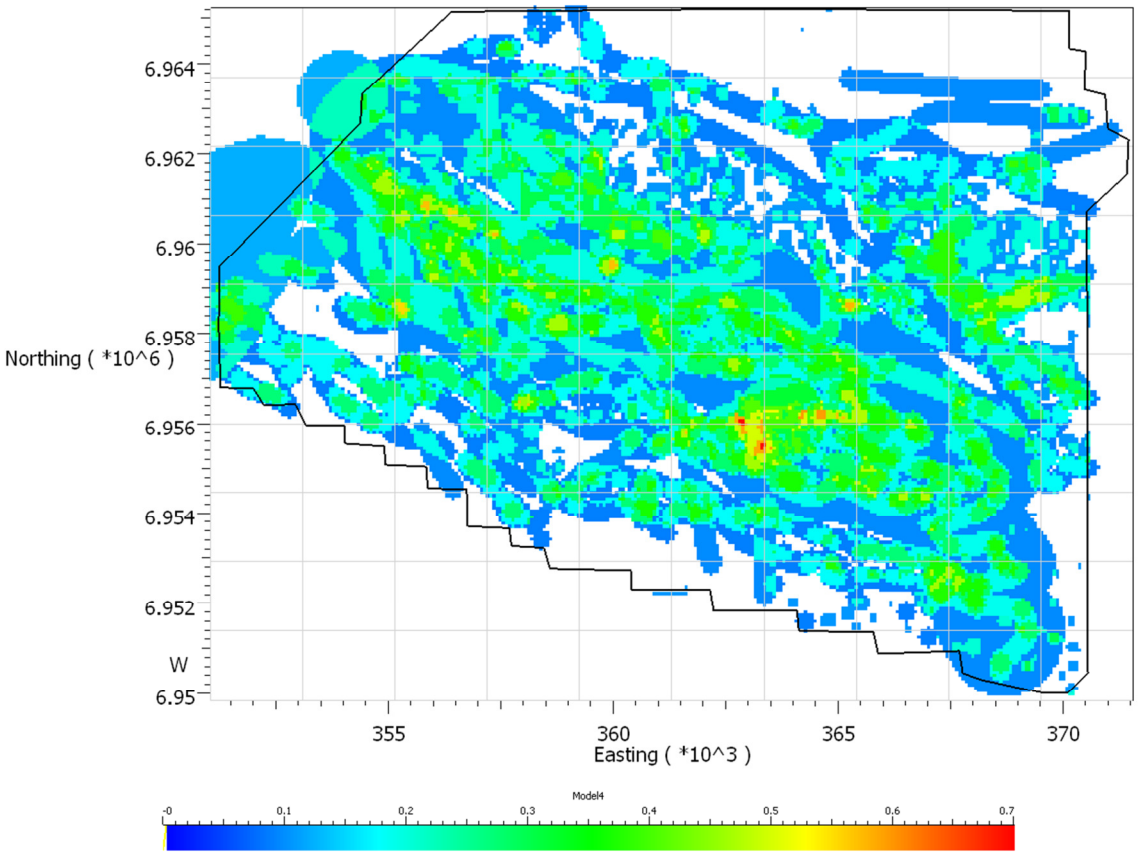

Figure 46: Targeting result for the K Block showing model cells coloured by score.

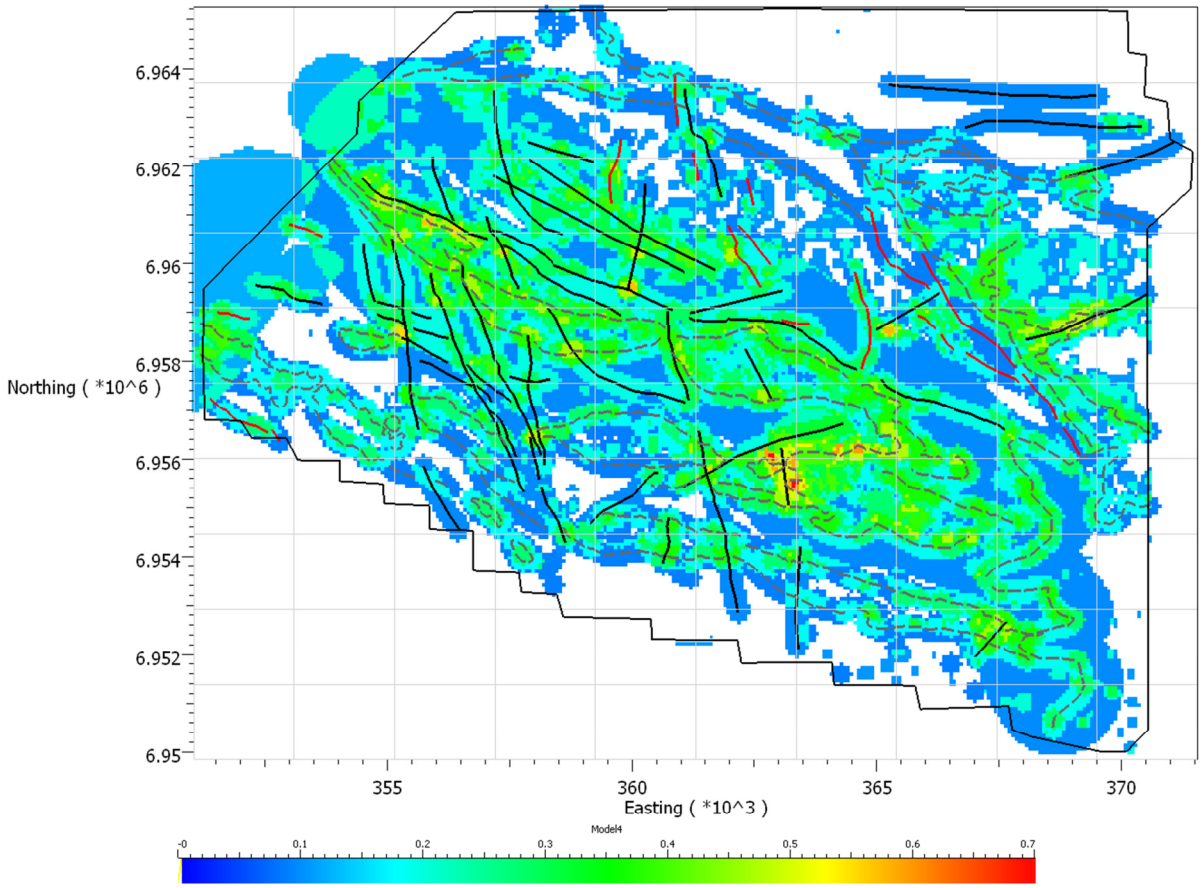

Figure 47: Targeting result for the K Block showing model cells coloured by score showing the structural interpretation layers.

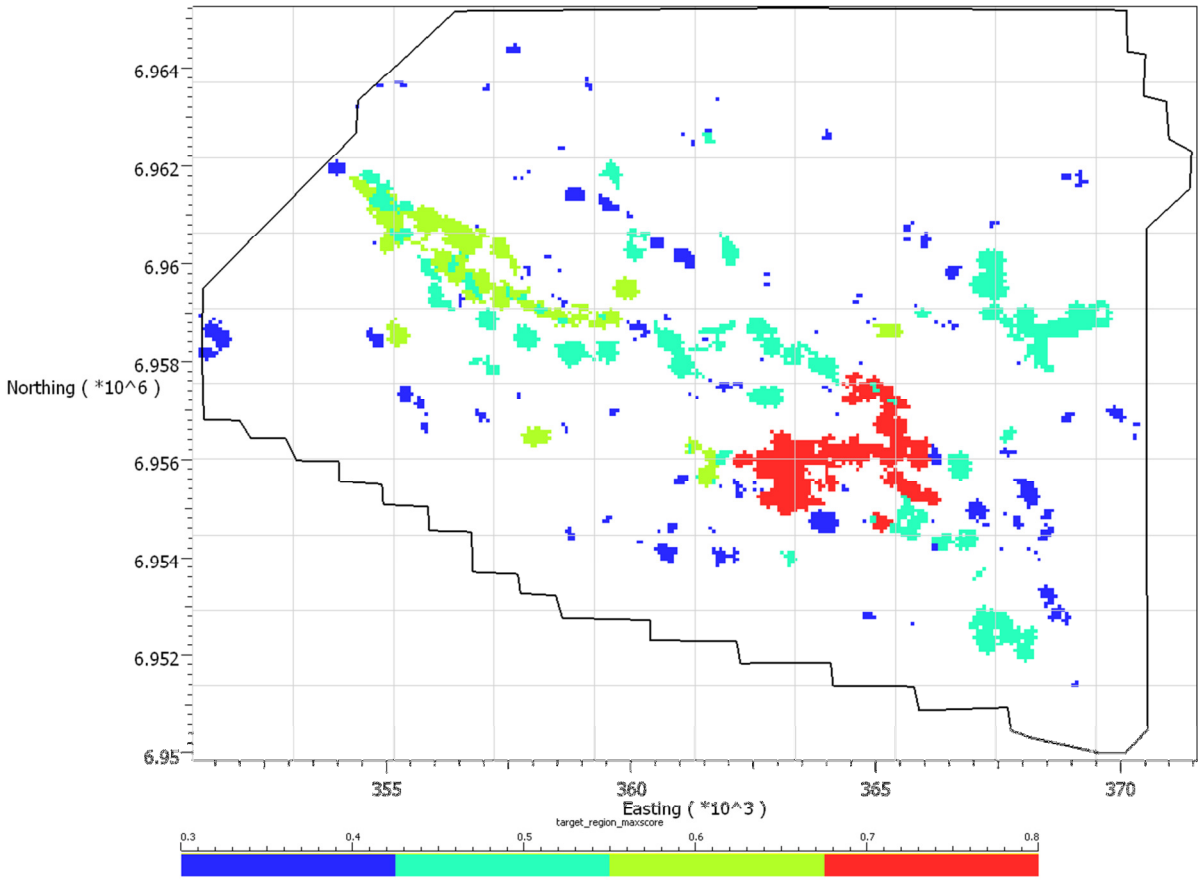

Figure 48: Targeting result for the K Block showing the 98% cut-off. Targets are coloured by score.

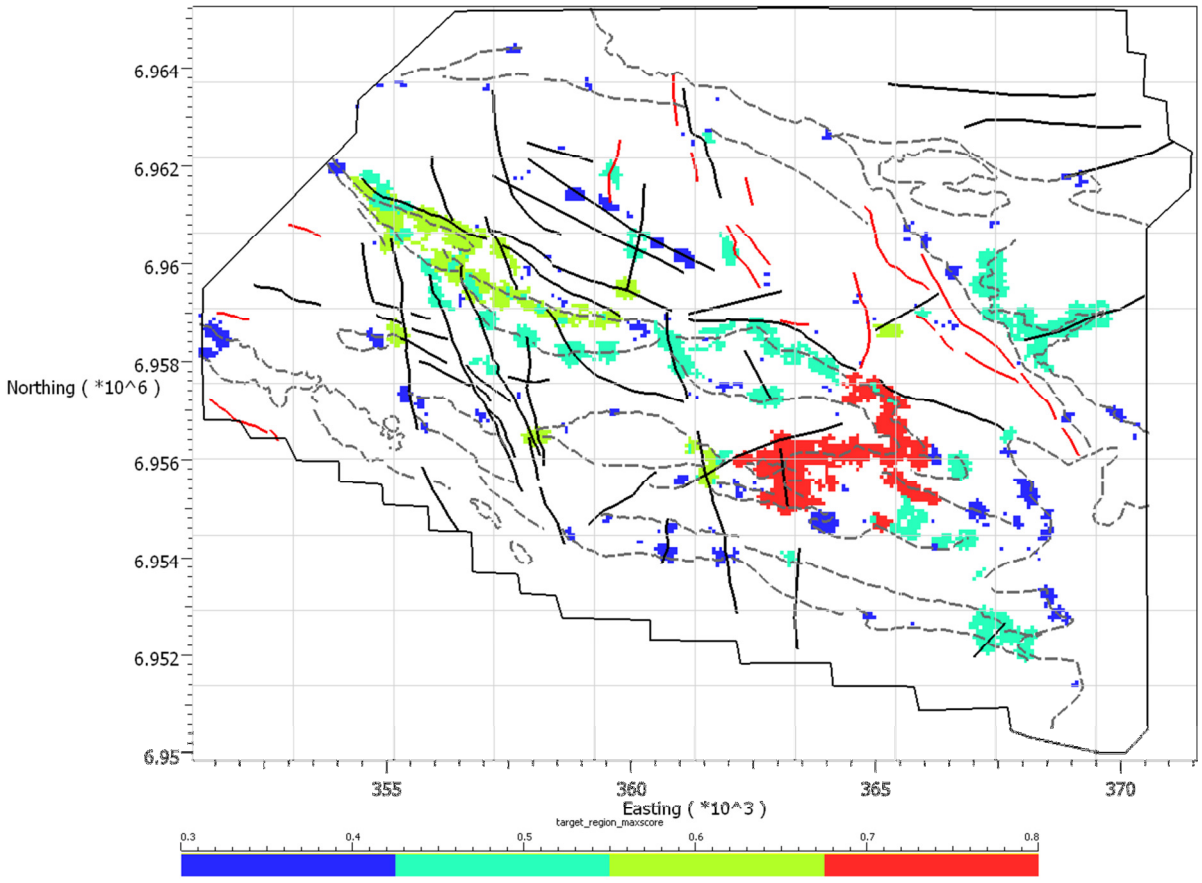

Figure 49: Targeting result for the K Block showing the 98% cut-off with structural interpretation layers.

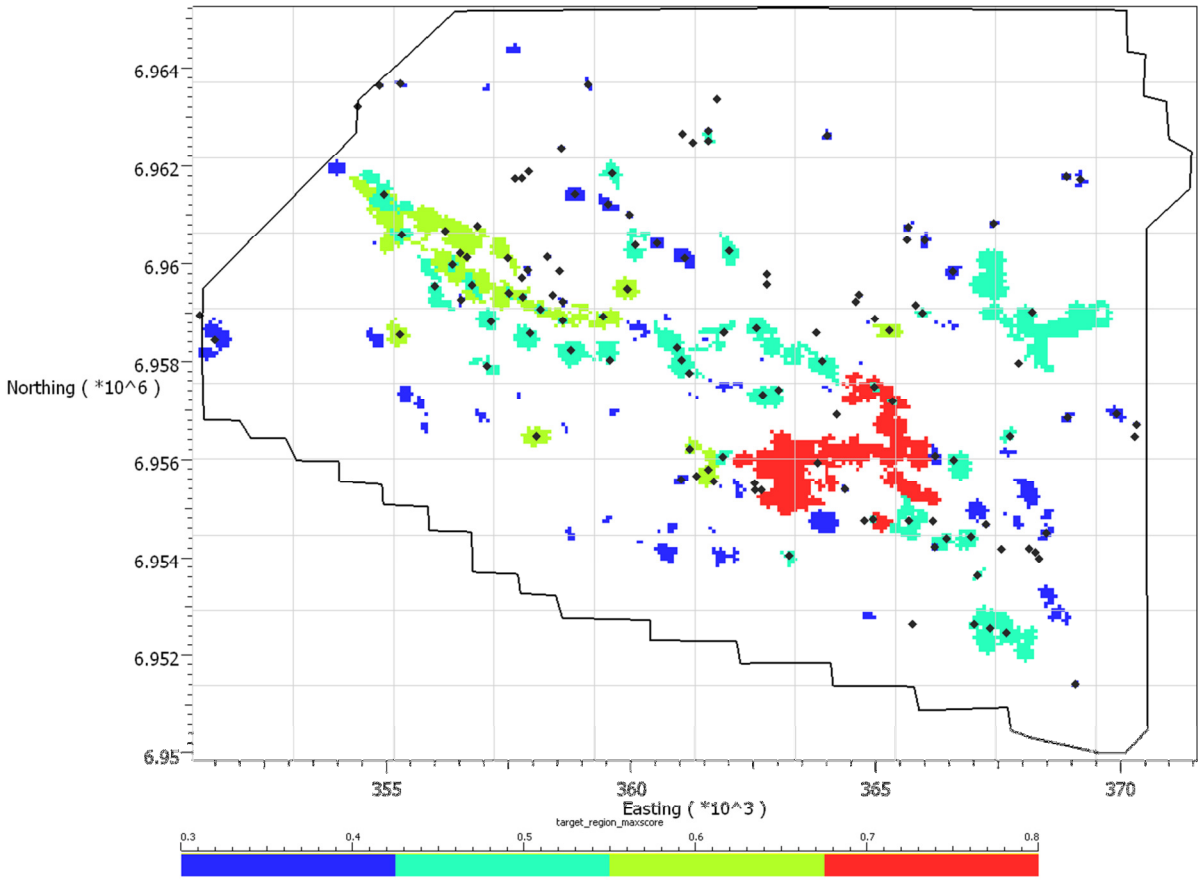

Figure 50: Targeting result for the K Block showing the 98% cut-off with the target centroid locations displayed as black diamonds.

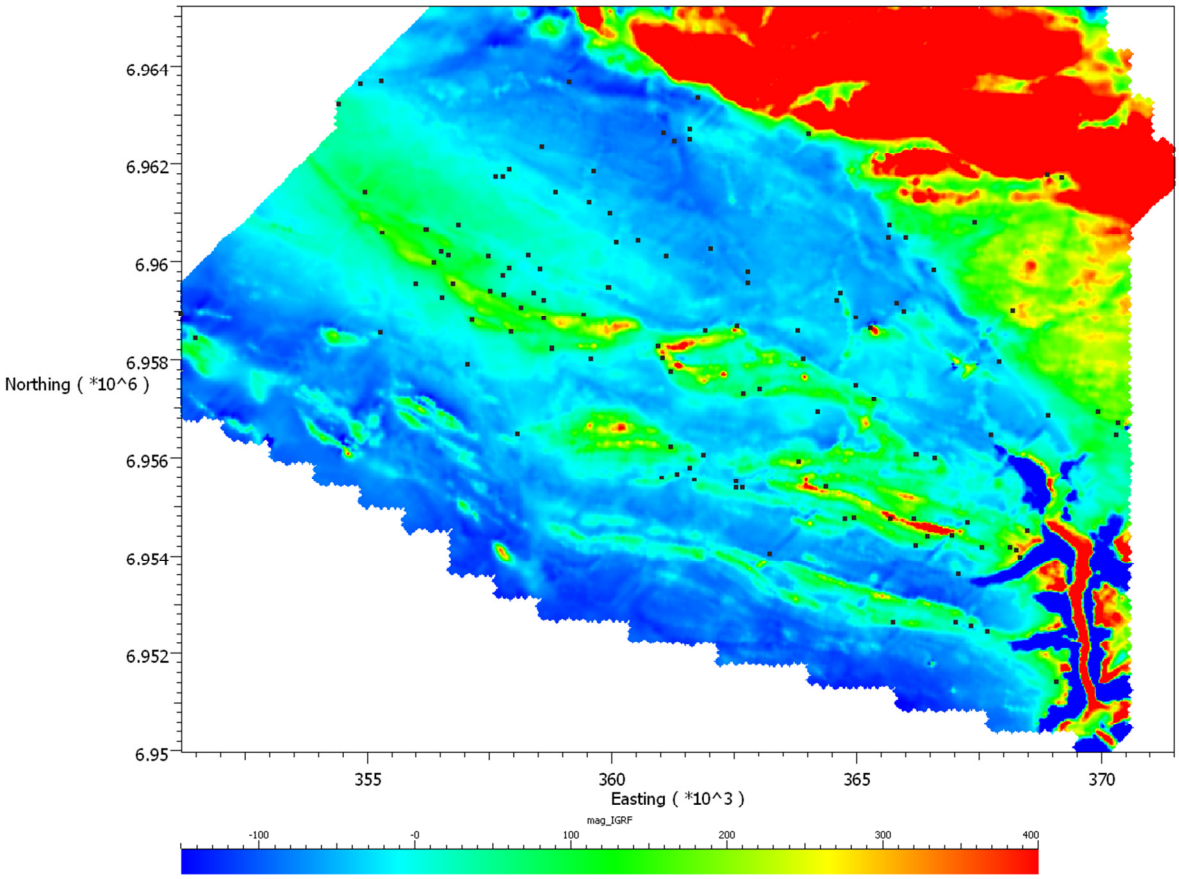

Figure 51: K Block IGRF corrected magnetic data with the target centroid locations displayed as black points.

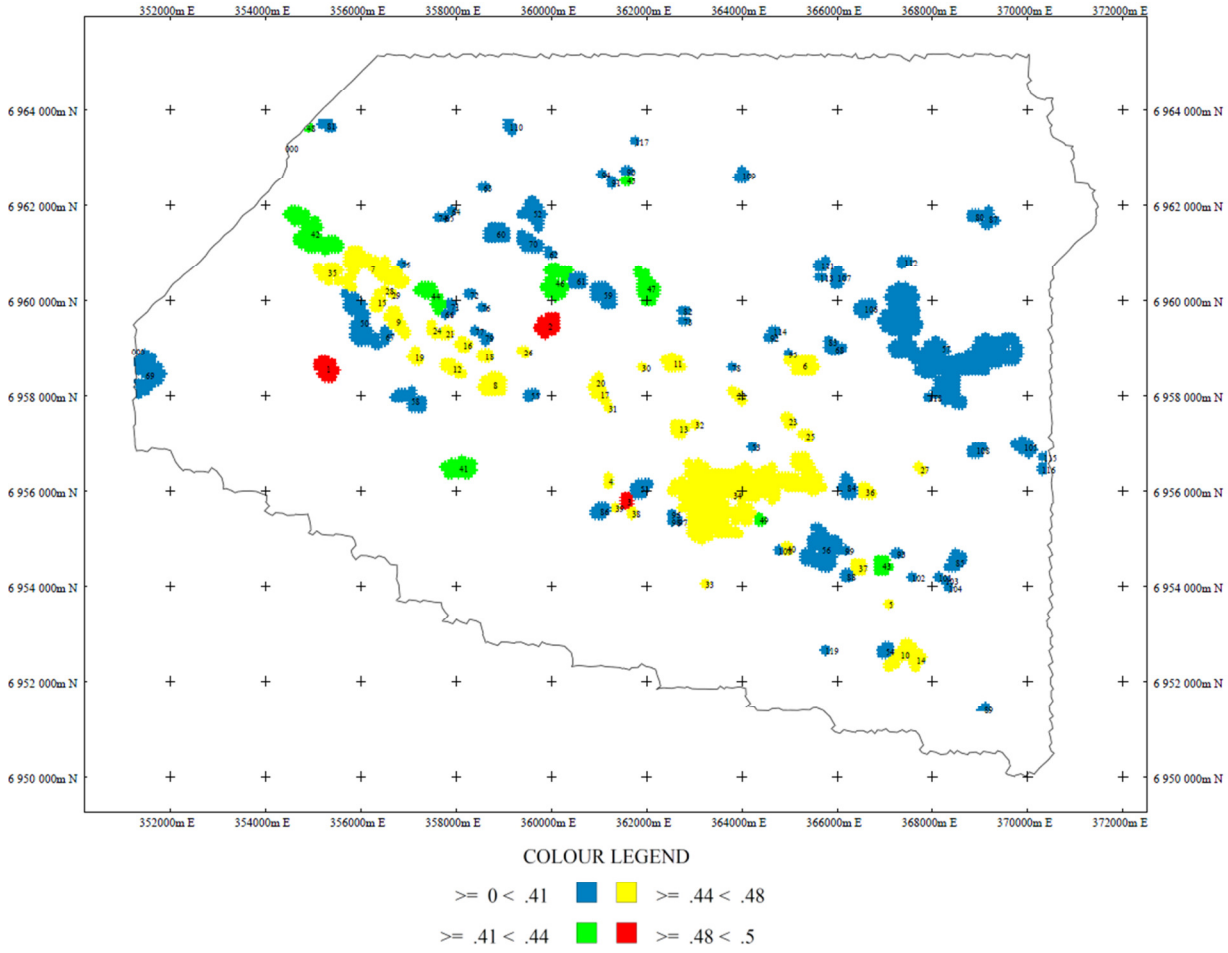

Figure 52: Targeting result for the K Block showing the 98% cut-off with the target centroid locations ranked by mean score then size.

Table 6: K Block target centroids ranked by mean score and number of cells.

Rank (based on Mean then size)	X	Y	Z	Target_Mean_Score	Number of cells in region
1	355276	6958557	658	0.497619	24
2	359931	6959488	715	0.495238	24
3	361585	6955795	871	0.485714	6
4	361200	6956215	957	0.473469	3
5	367080	6953625	771	0.473469	1
6	365283	6958636	786	0.470748	27
7	356205	6960669	580	0.470554	77
8	358780	6958228	740	0.465306	28
9	356752	6959561	798	0.465306	20
10	367336	6952558	792	0.465306	20
11	362563	6958674	849	0.465306	15
12	357933	6958578	846	0.465306	12
13	362688	6957312	974	0.465306	12
14	367668	6952463	766	0.465306	10
15	356354	6959972	738	0.465306	9
16	358150	6959075	763	0.465306	7
17	361030	6958025	798	0.465306	7
18	358610	6958840	695	0.465306	6
19	357140	6958817	851	0.465306	6
20	360943	6958280	771	0.465306	6
21	357784	6959323	743	0.465306	5
22	363902	6958007	840	0.465306	5
23	364980	6957475	780	0.465306	5
24	357508	6959400	787	0.465306	4
25	365348	6957178	767	0.465306	4

26	359427	6958922	749	0.465306	3
27	367745	6956460	668	0.465306	2
28	356510	6960205	690	0.465306	1
29	356650	6960135	681	0.465306	1
30	361900	6958595	765	0.465306	1
31	361200	6957755	860	0.465306	1
32	363020	6957405	991	0.465306	1
33	363230	6954045	928	0.465306	1
34	363818	6955926	1005	0.463678	454
35	355310	6960590	593	0.460408	20
36	366598	6955989	822	0.453515	9
37	366450	6954395	901	0.453515	9
38	361690	6955550	835	0.457143	2
39	361340	6955655	854	0.457143	1
40	364945	6954780	997	0.45102	4
41	358069	6956473	931	0.438002	29
42	354956	6961416	538	0.437877	75
43	366951	6954427	922	0.432025	13
44	357484	6960100	659	0.430427	22
45	361585	6962515	589	0.428571	2
46	360091	6960380	842	0.421482	38
47	362008	6960260	705	0.421398	33
48	354865	6963635	511	0.420408	2
49	364373	6955398	1029	0.416327	3
50	355986	6959546	690	0.409694	56
51	361870	6956050	874	0.40933	14
52	359621	6961846	694	0.408466	27
53	364210	6956915	927	0.408163	1

54	367019	6952636	823	0.406122	8
55	359573	6958018	868	0.406122	4
56	365684	6954756	979	0.403695	74
57	368198	6959010	819	0.402464	401
58	357057	6957908	852	0.397032	22
59	361101	6960114	850	0.395918	27
60	358855	6961420	722	0.395918	22
61	360535	6960415	875	0.395918	12
62	359963	6960998	795	0.395918	3
63	358575	6962375	677	0.395918	2
64	357910	6961885	640	0.395918	1
65	357770	6961745	627	0.395918	1
66	357770	6959715	703	0.395918	1
67	356524	6959267	780	0.394286	5
68	365960	6958999	737	0.393651	9
69	351489	6958442	904	0.391837	58
70	359532	6961216	807	0.391837	18
71	357893	6959873	639	0.391837	4
72	358295	6960135	668	0.391837	2
73	362775	6959575	757	0.391837	2
74	357630	6961745	602	0.391837	1
75	356860	6960765	610	0.391837	1
76	358540	6959855	651	0.391837	1
77	358400	6959365	700	0.391837	1
78	363790	6958595	906	0.391837	1
79	358610	6959225	667	0.389796	4
80	368900	6961780	530	0.387755	6
81	355292	6963677	441	0.387755	5

82	362775	6959785	757	0.387755	2
83	365820	6959155	732	0.387755	1
84	366217	6956075	806	0.383674	15
85	368491	6954508	772	0.383673	13
86	361025	6955585	887	0.383673	10
87	369188	6961722	547	0.383673	9
88	366205	6954220	844	0.383673	4
89	369087	6951408	717	0.383673	3
90	361585	6962725	589	0.383673	2
91	361270	6962480	579	0.383673	2
92	364595	6959225	770	0.383673	2
93	367255	6954675	917	0.383673	2
94	361060	6962655	591	0.383673	1
95	364980	6958875	743	0.383673	1
96	362530	6955515	810	0.383673	1
97	362670	6955375	820	0.383673	1
98	362530	6955375	808	0.383673	1
99	366170	6954745	979	0.383673	1
100	364770	6954745	975	0.383673	1
101	368130	6954185	774	0.383673	1
102	367570	6954185	837	0.383673	1
103	368270	6954115	743	0.383673	1
104	368340	6953975	729	0.383673	1
105	369927	6956920	780	0.379592	15
106	366575	6959835	646	0.379592	14
107	366009	6960471	668	0.379592	10
108	368923	6956845	791	0.379592	9
109	364012	6962632	675	0.379592	6

110	359128	6963663	586	0.379592	5
111	365666	6960751	693	0.379592	5
112	367413	6960818	603	0.379592	4
113	365645	6960485	651	0.379592	2
114	364665	6959365	764	0.379592	2
115	370335	6956705	776	0.379592	2
116	370300	6956460	741	0.379592	2
117	361760	6963355	585	0.379592	1
118	367920	6957965	714	0.379592	1
119	365750	6952645	970	0.379592	1

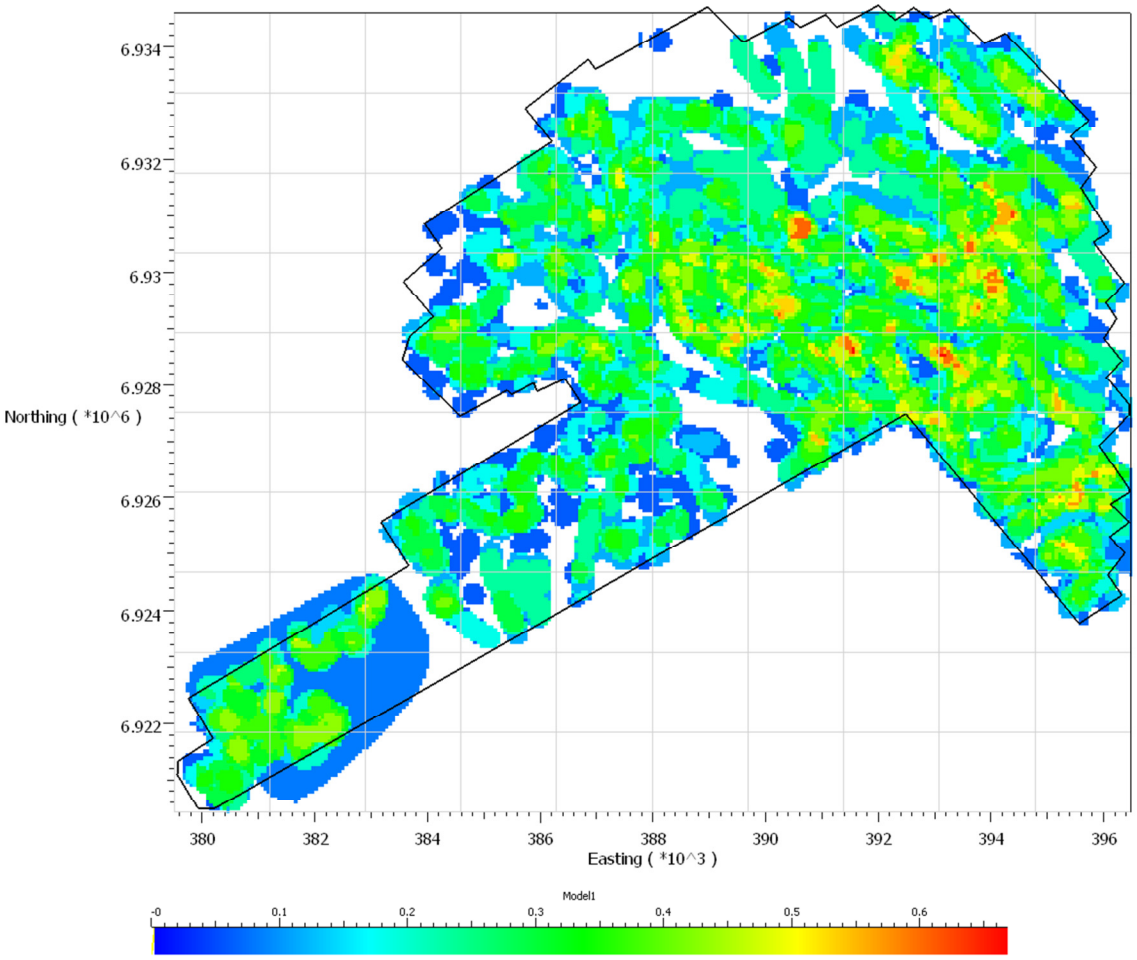

Figure 53: Targeting result for the O Block showing model cells coloured by score.

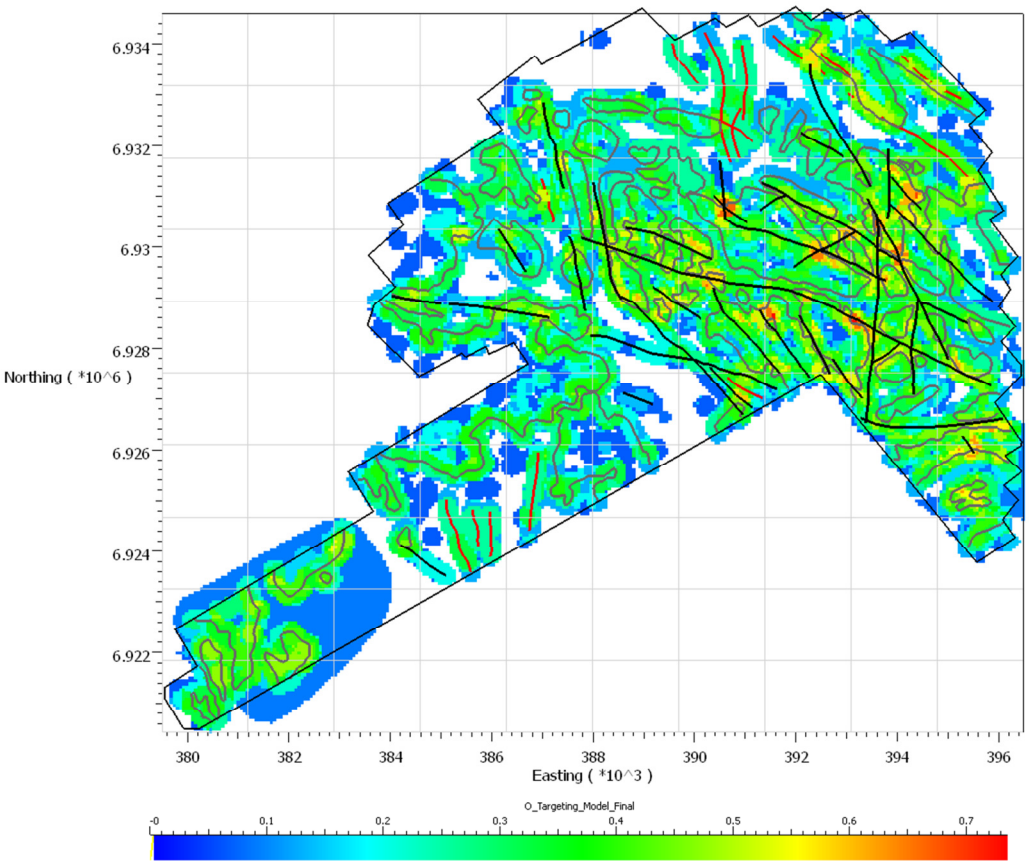

Figure 54: Targeting result for the O Block showing model cells coloured by score showing the structural interpretation layers.

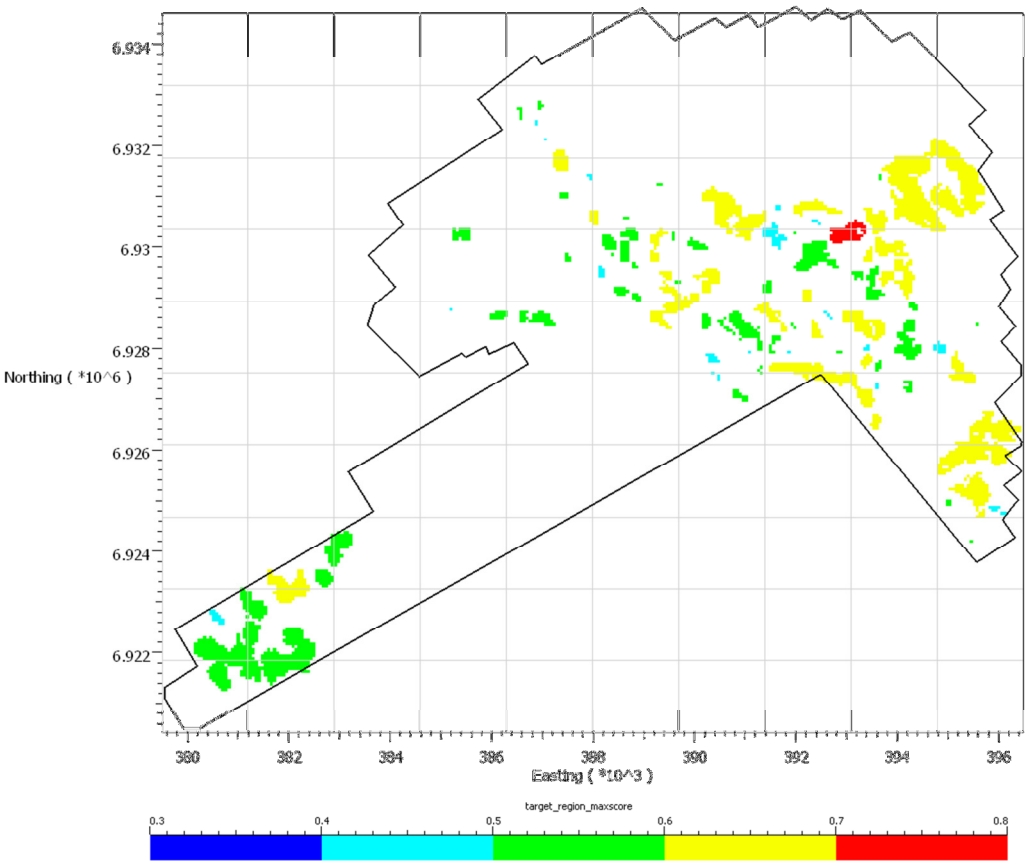

Figure 55: Targeting result for the O Block showing the 98% cut-off. Targets are coloured by score.

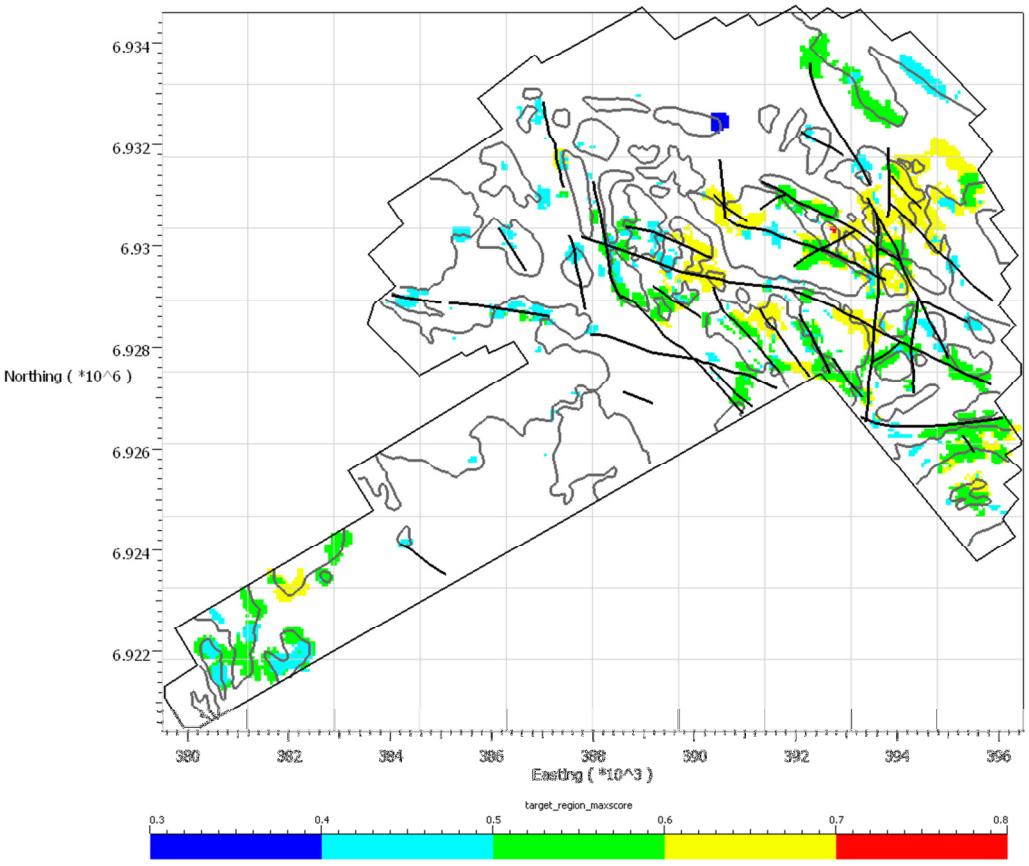

Figure 56: Targeting result for the O Block showing the 98% cut-off with structural interpretation layers.

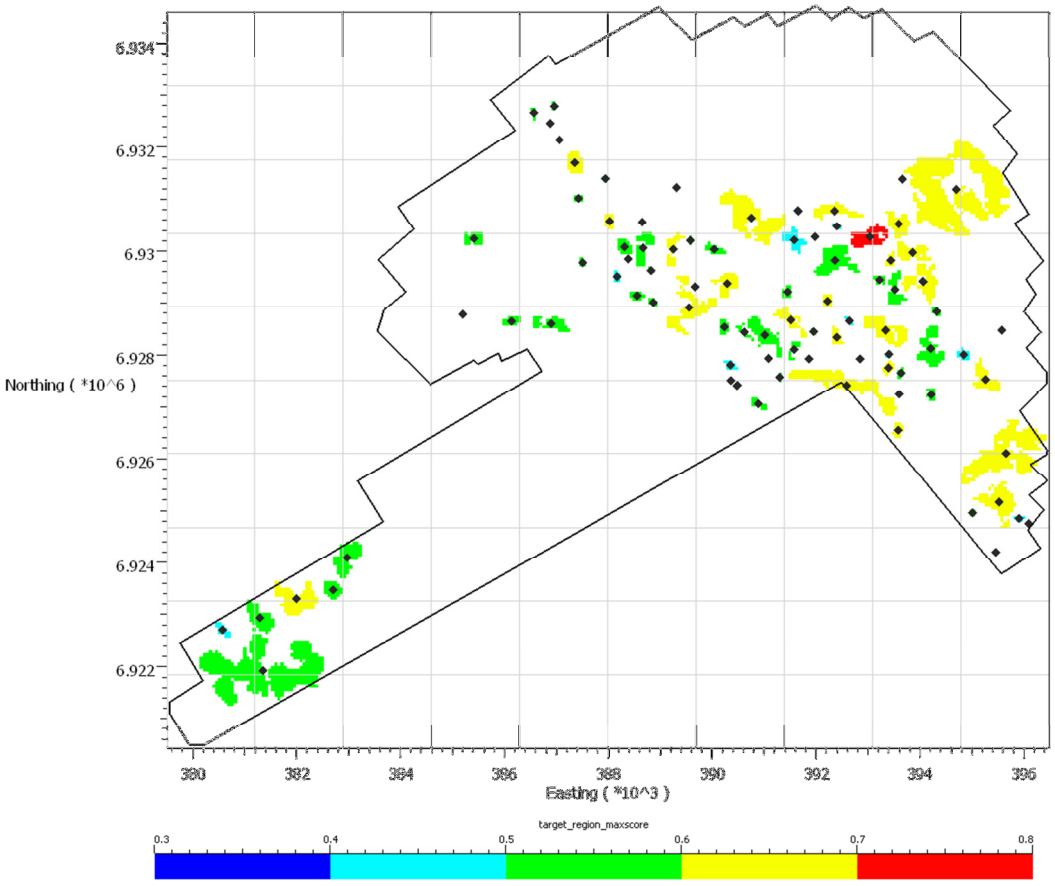

Figure 57: Targeting result for the O Block showing the 98% cut-off with the target centroid locations displayed as black diamonds.

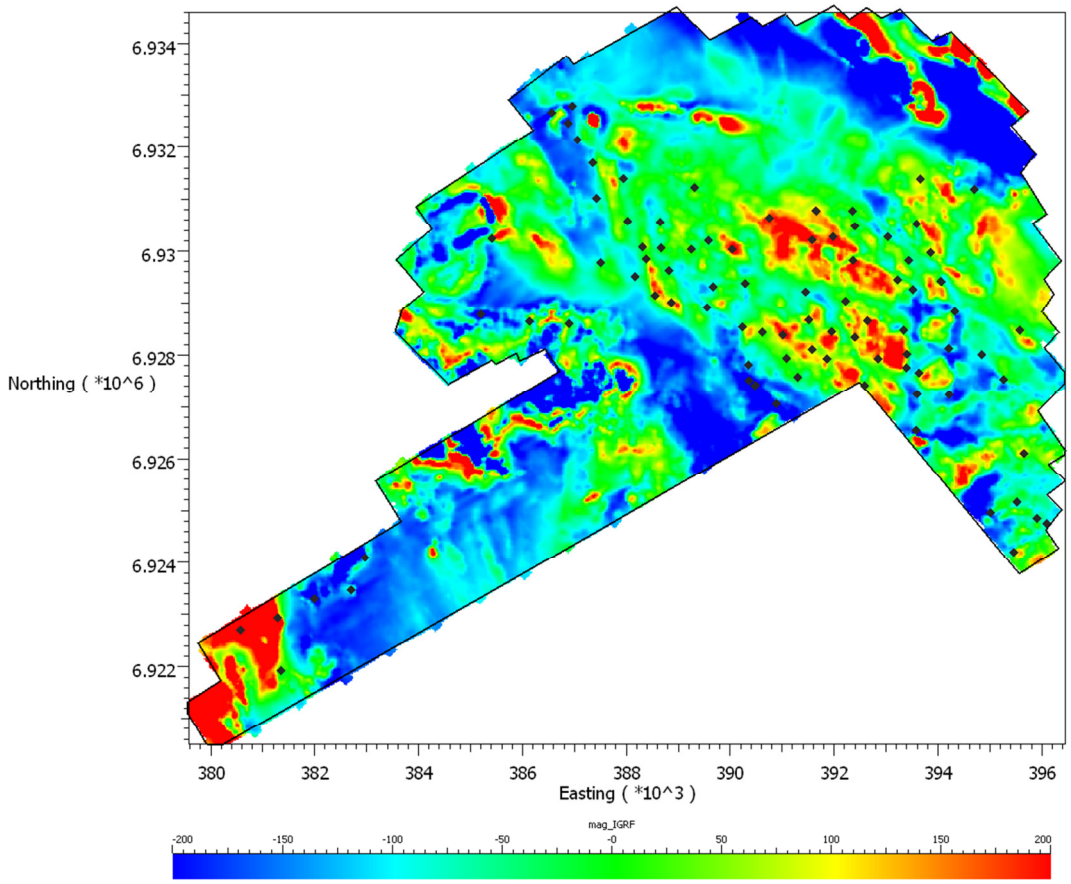

Figure 58: O Block IGRF corrected magnetic data with the target centroid locations displayed as black diamonds.

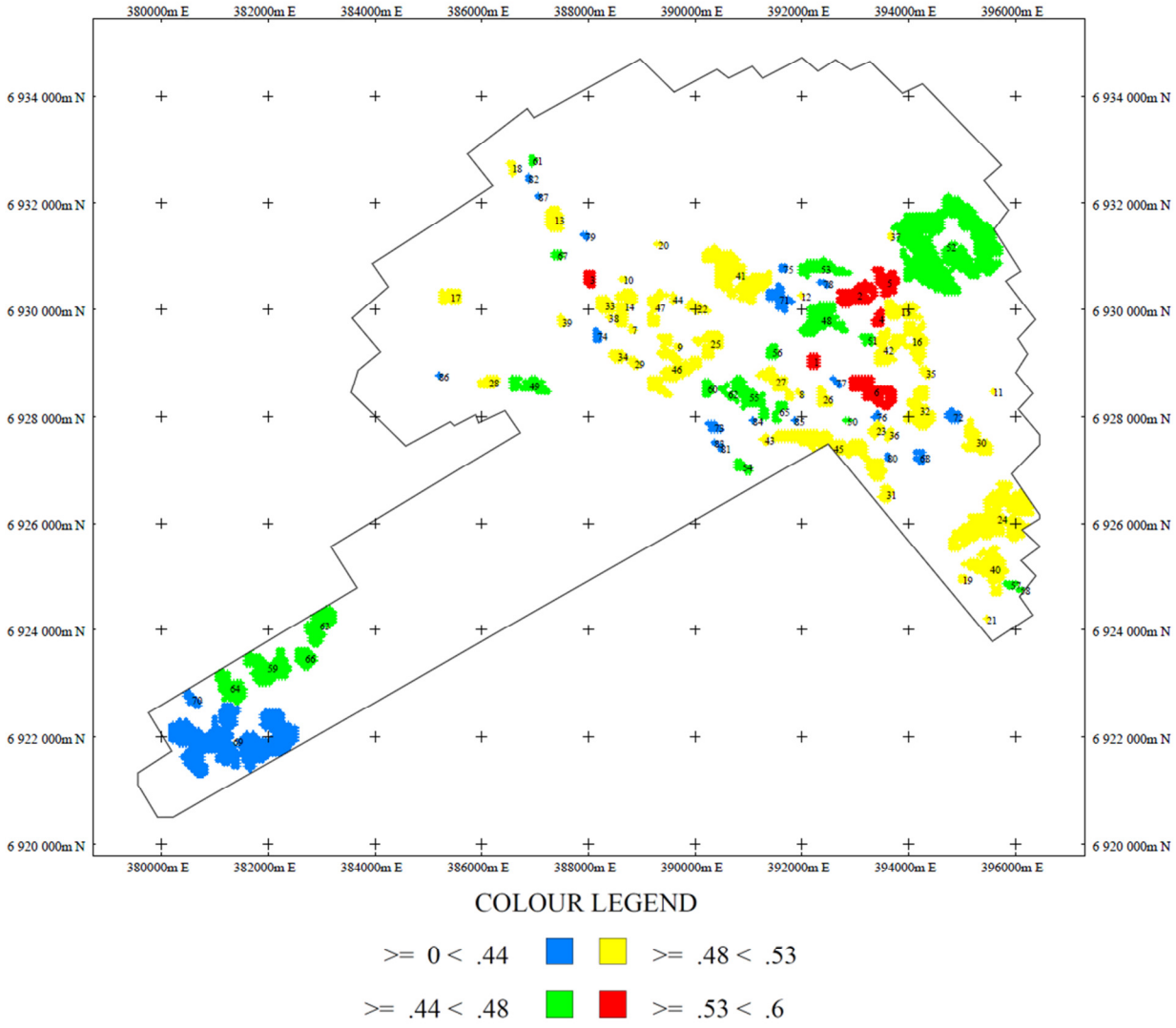

Figure 59: Targeting result for the O Block showing the 98% cut-off with the target centroid locations ranked by mean score then size.

Table 7: O Block target centroids ranked by mean score and number of cells.

Rank (based on Mean then size)	X	Y	Z	Target_Mean_Score	Number of cells in region
1	392220	6929040	714	0.578054	12
2	393031	6930274	749	0.570612	57
3	388024	6930579	817	0.542017	14
4	393436	6929823	710	0.533937	11
5	393584	6930524	756	0.533721	42
6	393344	6928471	694	0.531308	74
7	388820	6929630	982	0.524887	3
8	391950	6928440	799	0.524887	2
9	389670	6929310	886	0.524887	2
10	388650	6930570	881	0.524887	2
11	395580	6928470	694	0.524887	1
12	391980	6930270	811	0.524887	1
13	387360	6931700	837	0.524157	31
14	388671	6930062	955	0.522335	39
15	393853	6929976	701	0.522151	43
16	394058	6929414	644	0.521048	66
17	385415	6930240	925	0.520362	22
18	386568	6932658	890	0.520362	5
19	395010	6924960	748	0.520362	4
20	389310	6931230	857	0.520362	2
21	395460	6924210	776	0.520362	1
22	390038	6930034	866	0.518665	16
23	393390	6927750	627	0.516591	12

24	395655	6926104	820	0.516526	243
25	390288	6929370	823	0.516301	39
26	392396	6928342	760	0.514027	15
27	391510	6928662	843	0.513769	35
28	386136	6928646	968	0.511614	15
29	388860	6929010	1033	0.510666	7
30	395263	6927538	715	0.510005	45
31	393577	6926550	607	0.50818	13
32	394207	6928125	574	0.507937	63
33	388311	6930081	895	0.506787	21
34	388550	6929135	997	0.506787	12
35	394320	6928830	596	0.506787	7
36	393630	6927660	607	0.506787	6
37	393660	6931380	729	0.506787	2
38	388380	6929850	933	0.506787	1
39	387504	6929778	890	0.504977	5
40	395524	6925159	798	0.502426	83
41	390756	6930647	884	0.502205	158
42	393524	6929257	686	0.492414	34
43	391300	6927570	746	0.491704	3
44	389580	6930210	855	0.491704	3
45	392591	6927416	631	0.49073	144
46	389561	6928908	964	0.490114	92
47	389250	6930036	902	0.485779	28
48	392365	6929814	763	0.476774	79
49	386895	6928590	994	0.475113	36

50	392850	6927930	715	0.475113	2
51	393227	6929443	736	0.469583	9
52	394700	6931184	543	0.466153	500
53	392353	6930778	812	0.46017	43
54	390885	6927055	762	0.458522	12
55	391009	6928379	899	0.456602	55
56	391445	6929212	747	0.454957	11
57	395910	6924850	876	0.452489	6
58	396090	6924750	886	0.452489	2
59	381991	6923298	1061	0.452439	90
60	390231	6928530	835	0.4504	13
61	386955	6932790	854	0.450226	4
62	390620	6928437	836	0.447461	9
63	382970	6924097	936	0.44556	64
64	381288	6922937	1106	0.445084	55
65	391576	6928110	837	0.443439	11
66	382696	6923474	983	0.443104	27
67	387420	6931020	832	0.441931	6
68	394213	6927243	561	0.4364	9
69	381346	6921926	1095	0.434796	422
70	380576	6922706	1223	0.434389	14
71	391575	6930212	839	0.425339	31
72	394835	6928005	644	0.425339	12
73	390354	6927804	757	0.425339	10
74	388166	6929507	986	0.425339	7
75	391650	6930780	870	0.425339	4

76	393400	6928010	683	0.425339	3
77	392640	6928650	740	0.425339	3
78	392400	6930490	779	0.425339	3
79	387940	6931390	776	0.425339	3
80	393600	6927240	600	0.425339	2
81	390480	6927420	705	0.425339	2
82	386880	6932460	915	0.425339	2
83	390360	6927510	717	0.425339	1
84	391080	6927930	807	0.425339	1
85	391860	6927930	783	0.425339	1
86	385200	6928770	892	0.425339	1
87	387060	6932130	939	0.425339	1

6. Conclusions and Recommendations

The knowledge-driven weights targeting applied to porphyry Cu-Au-Mo exploration near Carmacks, Yukon was successful. The exploration criteria were successfully built as a quantitative property into the exploration model encompassing each survey property. This required the import of several datasets, including structural interpretation of the magnetics, interpretation of radiometrics, and 3D inversion of magnetic data. The mineral potential models developed are meaningful as potential guides to exploration drillhole targeting.

A review of the geology near Carmacks, Yukon was completed to aid with the geological understanding of the G, K and O Block properties and to determine an appropriate exploration model for the targeting process. The review suggests that the G, K and O Block properties are located in a highly prospective area for Cu-Au-Mo mineralization. Nearby deposits in the Carmacks area, including the high-grade copper-gold Minto Mine and Carmacks Copper deposit, lie along the same northwest-trending belt as the G, K, and O Block properties and are hosted by the same early Jurassic magmatic suite. Other deposits, located further to the west, host mineralization associated with a younger Cretaceous phase of magmatism. Many of the nearby deposits are porphyry-type deposits.

Based on the sparse geochemistry and regional geologic mapping available, it is beyond the limits of the geophysical data to draw any conclusions about the style of deposits that may be present at the G, K and O Blocks or whether the properties share the same ore deposit model. The targeting method used in this study follows the intrusive-related porphyry deposit model proposed by Holister (1976). Using the same intrusive-related porphyry deposit model for targeting allows for direct comparison of the three properties which would not be possible if different models were used.

The targeting results show that there is the potential for a large deposit to be found on the G, K and O Block properties. All three properties show that a significant number of criteria are satisfied for intrusive-porphyry style mineralization at numerous locations on the properties. A target list has been generated for each survey area for follow up.

Despite the lack of detailed data present on the survey blocks, the interpretation of the geophysical data and subsequent targeting performed on the survey areas represent a very thorough review. Completing such an in-depth review prior to conducting ground work is important as work can be focused on target areas with the highest potential for mineralization, thus maximizing exploration budgets for field work programs.

The best target found in this study is target 1 in G block. However, one should not ignore the other targets identified when following up. These targets are primarily based on the interpretation of the magnetic and radiometric airborne data. The addition of geochemical data, even from quite limited surveys, will rapidly upgrade and change the rank of targets and will focus exploration on a few excellent targets for drilling. Geological traversing in the areas of high prospectivity identified in this work may also upgrade targets and solidify the ranking of targets on the basis of a more complete set of geological knowledge.

In the K block a region of strong potassium enrichment has been identified where basalts are interpreted on the NE portion of the property. Potassium enrichment is consistent with the alteration and whole rock geochemistry of alkaline volcanics around Kuroko deposits in ophiolitic basaltic sequences. It would be prudent to check this area (marked 1 in figure 20) for possible mineralization. Whole rock geochemistry to map VMS alteration indices would be a practical method of follow-up.

Geochemical sampling is recommended as a primary follow-up method in the target regions. Depending upon the size of the target area and the local morphology, either soil grids or stream sediment sampling can be used. The topographic relief is quite rugged in the survey areas. Weathering and sediment transport should be analyzed with respect to the topography and watersheds.

Ground geophysics is an important next step to define drill targets. Induced Potential (IP) is an effective ground method for the prospection and characterization of mineral deposits, particularly Cu-Au porphyry deposits. Measured chargeability and apparent resistivity data have proven successful for detecting favourable Cu-Au mineralization. The surveys can be designed as

conventional 2D arrays or 3D arrays and the data can be inverted in both 2D and 3D. The modelling results of IP surveys can be put into the targeting workflow as new targeting criteria to refine existing targets and generate new ones. If it is a future goal to integrate data in 3D, it would be wise to collect physical property data as well. This data can be used to constrain the inversions to better represent the geology.

It is important to recognize that the targeting process is dynamic. As new data is collected, the exploration criteria can be redefined for a more specific ore deposit model. In this case, the application of a common model to all three survey blocks enables comparison between the properties and is therefore appropriate given the lack of detailed data available. As Figure 6 shows, targeting is a continual process that allows the user to test the exploration model, when new data is received, or with existing data but different criteria. If the results are what we would expect, then the exploration model is likely correct. If the results are not what are expected, the model needs to be changed. It is an interactive and iterative process.

Finally, the models produced in this study have ongoing value to Canadian Dehua International Mines. Modifications to exploration criteria or target type, definition of training data, or simply the addition of new drilling or other data can all be used to update the existing model easily now that the investment in the model framework for the Carmacks area is complete.

References and Related Reading

Bineli Betsi, T. and Bennett, V., 2010. New U-Pb age constraints at Freegold Mountain: evidence for multiple phases of polymetallic mid- to Late Cretaceous Mineralization. *In:* Yukon Exploration and Geology 2009, K.E. MacFarlane, L.H. Weston and L.R. Blackburn (eds.), Yukon Geological Survey, p. 57-84.

Bennett, V., Colpron, M. and Burke, M., 2010. Current thinking on Dawson Range tectonics and metallogeny. Yukon Geological Survey, Miscellaneous Report 2.

Campbell, A. N., V. F. Hollister, R. O. Duda and P. E. Hart, "Recognition of a Hidden Mineral Deposit by an Artificial Intelligence Program", SCIENCE , Vol. 217, No. 4563, pp 927-929 (3 September 1982).

Cook, F.A., Clowes, R.M., Snyder, D.B., van der Velden, A.J., Hall, K.W., Erdmer, P. and Evenchick, C.A., 2004. Precambrian crust beneath the Mesozoic northern Canadian Cordillera discovered by Lithoprobe seismic reflection profiling. Tectonics, vol. 23.

Deklerk, R. (compiler), 2002. Yukon MINFILE 2002 – A database of mineral occurrences. Exploration and Geological Services Division, Yukon Region, Indian and Northern Affairs Canada.

Gabrielse, H., Murphy, D.C., and Mortensen, J.K., 2006. Cretaceous and Cenozoic dextral orogen-parallel displacements, magmatism and paleogeography, north-central Canadian Cordillera. In: Paleogeography of the North American Cordillera: Evidence For and Against Large-Scale Displacements, J.W. Haggart, J.W.H. Monger and R.J. Enkin (eds.), Geological Association of Canada, Special Paper 46, p. 255-276.

Hart, P. E., "Progress on a Computer-Based Consultant," Proc. International Joint Conference on Artificial Intelligence, Vol. 2, pp 831-841, (Tbilisi, USSR, September 1975).

Holister, V. F. and Seraphim, R., H (1976) Intrusive rocks associated with porphyry copper mineralization in island arc areas, Economic Geology, v. 71, no. 3; p. 678-679

Hood, S., Hickey, K., Colpron, M. and Mercer, B., 2009. High-grade hydrothermal copper-gold mineralization in foliated granitoids at the Minto mine, central Yukon. *In:* Yukon Exploration and Geology 2008, L.H. Weston, L.R. Blackburn and L.L. Lewis (eds.), Yukon Geological Survey, p. 137-146.

Johnston, S.T., 1999. Large-scale coast-parallel displacements in the Cordillera: a granitic solution to a paleomagnetic dilemma. Journal of Structural Geology, vol. 21, p. 1103-1108.

Mortensen, J.K., Appel, V.L. and Hart, C.J.R., 2003. Geological and U-Pb age constraints on base and precious metal vein systems in the Mount Nansen area, eastern Dawson Range, Yukon. *In:* Yukon Exploration and Geology 2002, D.S. Emond and L.L. Lewis (eds.), Exploration and Geological Services Division, Yukon Region, Indian and Northern Affairs Canada, p. 165-174.

Lelievre, P. G., and D. W. Oldenburg, 2006, Magnetic forward modelling and inversion for high susceptibility, Geophys. J. Int., **166**, 76–90.

Lelievre, P. G., D. W. Oldenburg, and N. D. Phillips, 2006, 3D magnetic inversion for total magnetization in areas with complicated remanence. SEG Expanded Abstracts, **25**, 953.

Li, Y., and D. W. Oldenburg, 1996, 3-D inversion of magnetic data, Geophysics, **61**, 394-408.

Li, Y., and D. W. Oldenburg, 1998, Separation of regional and residual magnetic field data, Geophysics, **63**, 431-439.

MAG3D Manual 2005, from http://www.eos.ubc.ca/ubcgif/ or http://www.eos.ubc.ca/ubcgif/iag/sftwrdocs/mag3d/mag3d-manual.pdf

Tafti, R. and Mortensen, J.K., 2004. Early Jurassic porphyry(?) copper (-gold) deposits at Minto and Williams Creek, Carmacks Copper Belt, western Yukon. *In:* Yukon Exploration and Geology 2003, D.S. Emond and L.L. Lewis (eds.), Yukon Geological Survey, p. 289-303.

Verduzco, B., Fairhead, J. D., Green, C., and MacKenzie, C., 2004, New insights into magnetic derivatives for structural mapping, The Leading Edge*;* v. 23; no. 2; p. 116-119.

Wallace, Y., 2007, 3D modelling of banded iron formation incorporating demagnetisation – a case study at the Musselwhite Mine, Ontario, Canada, Exploration Geophysics, **38**(4), 254–259.

Appendix 1. Project Deliverables

Table 8: Project Deliverables

FORMAT	FILENAME	DESCRIPTION
REPORT	Mira_AGIC_Dehua_Targeting_Report_3486.pdf	Logistics report detailing the magnetic, radiometric interpretation, magnetic inversion, and targeting process
UBC	G_Mag_Sus_Inv_Mesh.msh, G_Mag_Sus_Inv_Model.sus K_Mag_Sus_Inv_Model.msh, K_Mag_Sus_Inv_Model.sus O_Block_Mag_Sus_Inversion_Model.msh, O_Block_Mag_Sus_Inversion_Model.sus	MAG3D inversion results in ASCII data format
GOCAD	G_Targeting_Final.gprj and G_Targeting_Final.prj folder K_Targeting_Final.gprj and K_Targeting_Final.prj folder O_Targeting_Final.gprj and O_Targeting_Final.prj folder (objects listed separately below)	Gocad project with all data and model results
BINARY GRID	*.grd - sections of the magnetic susceptibility inversion model	2D Geosoft grid

DXF	*.dxf - Interpretation layers and isosurfaces	Autocad dxf
ASCII	*.xyz, *.txt – target lists	Point data

Table 9: G Block Gocad Objects

NAME	TYPE	DESCRIPTION
G_2D_axes	Voxet	2D axes (padded mesh)
G_2D_core_axes	Voxet	2D axes (core mesh)
G_Au_Stream_Drainage_Watershed_Limits	Curve	Au Stream Drainage Watershed Limits
G_axes	Voxet	3D axes (padded mesh)
G_Batholith_Limits	Curve	Outer Limits of Interpreted Batholith
G_Batholith_Limits_Ridges	Curve	Backbone (Ridges) of Interpreted Batholith
G_Faults_from_Mag_Interp	Curve	Interpreted faults from mag data
G_Contacts_from_Mag_Interp	Curve	Interpreted contacts from mag data
G_core_axes	Voxet	3D axes (core mesh)
G_Dikes_from_Mag_Interp	Curve	Interpreted dikes from mag data

G_Dilational_Zones_AOI	PointsSet	Areas of interest from mag interp
G_Dilational_Zones_Contact_Jogs	PointsSet	Locations where contacts jog or change strike
G_Dilational_Zones_Dike_Jogs	PointsSet	Locations where dikes jog or change strike
G_Dilational_Zones_Faults_Jogs	PointsSet	Locations where faults jog or change strike
G_Dilational_Zones_Surf_Mag_Interp_Highs	PointsSet	Potential Dilational Zone Interpreted from Surface Mag High
G_Dilational_Zones_Surf_Mag_Interp_Jogs_and_pinch_outs	PointsSet	Potential Dilational Zone Interpreted from jogs, strike changes or pinch-outs in Surface Mag
G_Evidence_Layer_BU	Voxet	Back-up of Evidential Layers Used in Targeting Workflow (property names not changed)
G_Fault_Intersections	PointsSet	Locations of fault intersections
G_Mag_Data_Downsampled	PointsSet	IGRF corrected magnetic data as a pointset

G_Mag_Data_Downsampled_as_surface	Surface	IGRF corrected magnetic data as a surface
G_Mag_Sus_core	SGrid	Core Mag Sus Inversion Model
G_Mag_Sus_Iso_0_0030_curves	Curve	Mag Sus 0.0030 SI Isosurface Contours
G_Mag_Sus_Iso_0_0040_curves	Curve	Mag Sus 0.0040 SI Isosurface Contours
G_Mag_Sus_Iso_0_0050_curves	Curve	Mag Sus 0.0050 SI Isosurface Contours
G_Mag_Sus_Iso_0_0060_curves	Curve	Mag Sus 0.0060 SI Isosurface Contours
G_Mag_Sus_Iso_0_0070_curves	Curve	Mag Sus 0.0070 SI Isosurface Contours
G_Mag_Sus_Iso_0_0080_curves	Curve	Mag Sus 0.0080 SI Isosurface Contours
G_Mag_Sus_Iso_0_0090_curves	Curve	Mag Sus 0.0090 SI Isosurface Contours
G_Mag_Sus_Iso_0_0100_curves	Curve	Mag Sus 0.0100 SI Isosurface Contours
G_Mag_Sus_Iso_0_0110_curves	Curve	Mag Sus 0.0110 SI Isosurface Contours

G_Mag_Sus_Iso_0_0120_curves	Curve	Mag Sus 0.0120 SI Isosurface Contours
G_Mag_Sus_Iso_0_0130_curves	Curve	Mag Sus 0.0130 SI Isosurface Contours
G_Mag_Sus_Iso_0_0140_curves	Curve	Mag Sus 0.0140 SI Isosurface Contours
G_Mag_Sus_Iso_0_0150_curves	Curve	Mag Sus 0.0150 SI Isosurface Contours
G_Mag_Sus_Iso_0_0160_curves	Curve	Mag Sus 0.0160 SI Isosurface Contours
G_Mag_Sus_Iso_0_0170_curves	Curve	Mag Sus 0.0170 SI Isosurface Contours
G_Mag_Sus_Iso_Curves_at_Surface	Curve	Mag Sus Isosurface Intersections with Topo Surface
G_Mag_Sus_Iso0_0030	Surface	Mag Sus 0.0030 SI Isosurface
G_Mag_Sus_Iso0_0040	Surface	Mag Sus 0.0040 SI Isosurface
G_Mag_Sus_Iso0_0050	Surface	Mag Sus 0.0050 SI Isosurface
G_Mag_Sus_Iso0_0060	Surface	Mag Sus 0.0060 SI Isosurface

G_Mag_Sus_Iso0_0070	Surface	Mag Sus 0.0070 SI Isosurface
G_Mag_Sus_Iso0_0080	Surface	Mag Sus 0.0080 SI Isosurface
G_Mag_Sus_Iso0_0090	Surface	Mag Sus 0.0090 SI Isosurface
G_Mag_Sus_Iso0_0100	Surface	Mag Sus 0.0100 SI Isosurface
G_Mag_Sus_Iso0_0110	Surface	Mag Sus 0.0110 SI Isosurface
G_Mag_Sus_Iso0_0120	Surface	Mag Sus 0.0120 SI Isosurface
G_Mag_Sus_Iso0_0130	Surface	Mag Sus 0.0130 SI Isosurface
G_Mag_Sus_Iso0_0140	Surface	Mag Sus 0.0140 SI Isosurface
G_Mag_Sus_Iso0_0150	Surface	Mag Sus 0.0150 SI Isosurface
G_Mag_Sus_Iso0_0160	Surface	Mag Sus 0.0160 SI Isosurface
G_Mag_Sus_Iso0_0170	Surface	Mag Sus 0.0170 SI Isosurface

G_Mag_Sus_Iso0_0180	Surface	Mag Sus 0.0180 SI Isosurface
G_Radiometrics_KbyTh_1sigma	PointsSet	K:Th radiometric anomalies
G_Radiometrics_KbyTh_2sigma	PointsSet	K:Th radiometric anomalies
G_Survey_Limits	Curve	Survey Outline
G_Target_Region_Centroids	PointsSet	Geometric centroids of 2D target regions (NOTE: Depending on target region geometry, these points may or may not lie within the target regions with which they are associated. Please see the full targeting map for guidance to target extents.)
G_Targeting_All	PointsSet	Targeting Results for every cell in model
G_Targeting_Evidence_Layers	Voxet	Targeting Model
G_Targeting_Target_Regions_Only	PointsSet	Targeting results for target regions only
G_Topo_Used	Surface	Survey DTM merged with SRTM Topography

G_Topo_Used_Masked_to_Survey	Surface	Survey DTM merged with SRTM Topography masked to Survey area
MINFILE_Showings	PointsSet	Yukon Geological Survey geochem data
Stream_Sediment_Au_Anomalies	PointsSet	Yukon Geological Survey geochem data
Yukon_Bedrock_Geology_PF_Yukon_Bedrock_Geology_Curve	Curve	Yukon Geological Survey bedrock data
Yukon_Faults_250K_ta_SPF_FAULT_LN_250K_SVW_Curve	Curve	Yukon Geological Survey fault data

Table 10: K Block Gocad Objects

NAME	TYPE	DESCRIPTION
K_Dilational_Zones_Contact_Jogs	PointsSet	Locations where contacts jog or change strike
K_Dilational_Zones_Dike_Jogs	PointsSet	Locations where dikes jog or change strike
K_Fault_Intersections	PointsSet	Locations of fault intersections
K_Dilational_Zones_Faults_Jogs	PointsSet	Locations where faults jog or change strike

K_Dilational_Zones_Surf_Mag_Interp_Jogs_and_pinch_outs	PointsSet	Potential Dilational Zone Interpreted from jogs, strike changes or pinch-outs in Surface Mag
K_Dilational_Zones_Surf_Mag_Interp_Highs	PointsSet	Potential Dilational Zone Interpreted from Surface Mag High
K_Au_Stream_Drainage_Watershed_Limits	Curve	Au Stream Drainage Watershed Limits
MINFILE_Showings	PointsSet	Yukon Geological Survey geochem data
Stream_Sediment_Au_Anomalies	PointsSet	Yukon Geological Survey geochem data
K_Batholith_Limits_Part_A	Curve	Outer Limits of Interpreted Batholith
K_Batholith_Limits_Part_B	Curve	Outer Limits of Interpreted Batholith
K_Batholith_Limits_Part_C	Curve	Outer Limits of Interpreted Batholith
K_Batholith_Limits_Ridges	Curve	Backbone (Ridges) of Interpreted Batholith
K_Contacts_from_Mag_Interp	Curve	Interpreted contacts from mag data
K_Dikes_from_Mag_Interp	Curve	Interpreted dikes from mag data
K_Faults_from_Mag_Interp	Curve	Interpreted faults from mag data
K_Most_Reliable_Mag_Inv_Limits	Curve	Area showing magnetic data least affected by remanence
K_Survey_Limits	Curve	Survey Outline
K_Topography	Surface	Survey DTM merged with SRTM Topography

K_Mag_Sus_Inversion_Model	SGrid	Core Mag Sus Inversion Model
K_Targeting_Evidence_Layers_Model4	Voxet	Targeting Model
K_Radiometrics_KbyTh_1sigma	PointsSet	K:Th radiometric anomalies
K_Radiometrics_KbyTh_2sigma	PointsSet	K:Th radiometric anomalies
K_Target_Region_Centroids	PointsSet	Geometric centroids of 2D target regions (NOTE: Depending on target region geometry, these points may or may not lie within the target regions with which they are associated. Please see the full targeting map for guidance to target extents.)
K_Targeting_All	PointsSet	Targeting Results for every cell in model
K_Targeting_Target_Regions_Only	PointsSet	Targeting results for target regions only
K_Dilational_Zones_AOI	PointsSet	Areas of interest from mag interp
K_Mag_Sus_Iso0_0030_curves	Curve	Mag Sus 0.0030 SI Isosurface Contours
K_Mag_Sus_Iso0_0040_curves	Curve	Mag Sus 0.0040 SI Isosurface Contours
K_Mag_Sus_Iso0_0050_curves	Curve	Mag Sus 0.0050 SI Isosurface Contours
K_Mag_Sus_Iso0_0060_curves	Curve	Mag Sus 0.0060 SI Isosurface Contours
K_Mag_Sus_Iso0_0070_curves	Curve	Mag Sus 0.0070 SI Isosurface Contours
K_Mag_Sus_Iso0_0080_curves	Curve	Mag Sus 0.0080 SI Isosurface Contours
K_Mag_Sus_Iso0_0090_curves	Curve	Mag Sus 0.0090 SI Isosurface Contours

K_Mag_Sus_Iso0_0100_curves	Curve	Mag Sus 0.0100 SI Isosurface Contours
K_Mag_Sus_Iso0_0110_curves	Curve	Mag Sus 0.0110 SI Isosurface Contours
K_Mag_Sus_Iso0_0120_curves	Curve	Mag Sus 0.0120 SI Isosurface Contours
K_Mag_Sus_Iso0_0130_curves	Curve	Mag Sus 0.0130 SI Isosurface Contours
K_Mag_Sus_Iso0_0140_curves	Curve	Mag Sus 0.0140 SI Isosurface Contours
K_Mag_Sus_Iso0_0150_curves	Curve	Mag Sus 0.0150 SI Isosurface Contours
K_Mag_Sus_Iso0_0160_curves	Curve	Mag Sus 0.0160 SI Isosurface Contours
K_Mag_Sus_Iso0_0170_curves	Curve	Mag Sus 0.0170 SI Isosurface Contours
K_Mag_Sus_Iso_Curves_at_Surface	Curve	Mag Sus Isosurface Intersections with Topo Surface
K_Mag_Data_Downsampled	PointsSet	Downsampled IGRF corrected magnetic data
K_Mag_IGRF	Voxet	IGRF corrected magnetic data
K_Mag_Sus_Isosurface_0_0170	Surface	Mag Sus 0.0170 SI Isosurface
K_Mag_Sus_Isosurface_0_0160	Surface	Mag Sus 0.0160 SI Isosurface
K_Mag_Sus_Isosurface_0_0150	Surface	Mag Sus 0.0150 SI Isosurface
K_Mag_Sus_Isosurface_0_0140	Surface	Mag Sus 0.0140 SI Isosurface
K_Mag_Sus_Isosurface_0_0130	Surface	Mag Sus 0.0130 SI Isosurface
K_Mag_Sus_Isosurface_0_0120	Surface	Mag Sus 0.0120 SI Isosurface
K_Mag_Sus_Isosurface_0_0110	Surface	Mag Sus 0.0110 SI Isosurface
K_Mag_Sus_Isosurface_0_0100	Surface	Mag Sus 0.0100 SI Isosurface

K_Mag_Sus_Isosurface_0_0090	Surface	Mag Sus 0.0090 SI Isosurface
K_Mag_Sus_Isosurface_0_0080	Surface	Mag Sus 0.0080 SI Isosurface
K_Mag_Sus_Isosurface_0_0070	Surface	Mag Sus 0.0070 SI Isosurface
K_Mag_Sus_Isosurface_0_0060	Surface	Mag Sus 0.0060 SI Isosurface
K_Mag_Sus_Isosurface_0_0050	Surface	Mag Sus 0.0050 SI Isosurface
K_Mag_Sus_Isosurface_0_0040	Surface	Mag Sus 0.0040 SI Isosurface
K_Mag_Sus_Isosurface_0_0030	Surface	Mag Sus 0.0030 SI Isosurface
K_survey_outlines	Curve	Survey Outline

Table 11: O Block Gocad Objects

NAME	TYPE	DESCRIPTION
O_Block_dikes_from_mag_interp	Curve	Interpreted dikes from mag data
O_Mag_IGRF	Voxet	IGRF corrected magnetic data
O_Block_contacts_from_mag_interp	Curve	Interpreted contacts from mag data
O_Block_faults_from_mag_interp	Curve	Interpreted faults from mag data
O_block_fault_jogs	PointsSet	Locations where faults jog or change strike
O_Block_Dike_jogs	PointsSet	Locations where dikes jog or change strike
O_Block_survey_outline	Curve	Survey Outline
O_mag_sus_iso_surface_0_0300	Surface	Mag sus isosurface

O_mag_sus_iso_surface_0_0250	Surface	Mag sus isosurface
O_mag_sus_iso_surface_0_0200	Surface	Mag sus isosurface
O_mag_sus_iso_surface_0_0150	Surface	Mag sus isosurface
O_mag_sus_iso_surface_0_0100	Surface	Mag sus isosurface
O_mag_sus_iso_surface_0_0050	Surface	Mag sus isosurface
O_mag_sus_iso_surface_0_0040	Surface	Mag sus isosurface
O_mag_sus_iso_surface_0_0030	Surface	Mag sus isosurface
O_mag_sus_iso_surface_0_0020	Surface	Mag sus isosurface
O_fault_intersections	PointsSet	Location of fault intersections
O_mag_sus_iso_surface_0_0300_pl	Curve	Mag sus isosurface outline
O_mag_sus_iso_surface_0_0250_pl	Curve	Mag sus isosurface outline
O_mag_sus_iso_surface_0_0200_pl	Curve	Mag sus isosurface outline
O_mag_sus_iso_surface_0_0150_pl	Curve	Mag sus isosurface outline
O_mag_sus_iso_surface_0_0100_pl	Curve	Mag sus isosurface outline
O_mag_sus_iso_surface_0_0050_pl	Curve	Mag sus isosurface outline
O_mag_sus_iso_surface_0_0040_pl	Curve	Mag sus isosurface outline
O_mag_sus_iso_surface_0_0030_pl	Curve	Mag sus isosurface outline
O_mag_sus_iso_surface_0_0020_pl	Curve	Mag sus isosurface outline
O_mag_highs	PointsSet	Local magnetic highs.
O_mag_anomaly_pinch_outs	PointsSet	Interpreted changes in mag anomalies

O_rad_anomalies_sigma1	PointsSet	K:Th radiometric anomalies
O_rad_anomalies_sigma2	PointsSet	K:Th radiometric anomalies
AOI_Au_stream_drainage	Curve	Yukon Geological Survey data
AOI_Dehua_stream_sed_Au_anomalies	PointsSet	Yukon Geological Survey geochem data
AOI_showing_1000m	Curve	Yukon Geological Survey geochem data
AOI_Dehua_MINFILE_showings	PointsSet	Yukon Geological Survey geochem data
O_block_contact_bends	PointsSet	Locations where contacts jog or change strike
O_Block_AOI_from_mag_interp	Curve	Areas of interest from mag interp
O_block_AOI	PointsSet	Areas of interest from mag interp
O_core_axes	Voxet	3D Coordinate axes
O_Evidence_Layer	Voxet	Targeting Model
O_Block_Mag_Sus_Inversion_Model	SGrid	3D magnetic susceptibility inversion model
O_drillhole_target_centroids	PointsSet	Centre point of target regions
O_DTM	Voxet	Survey DTM
O_survey_DTM	Surface	Survey DTM
O_Targeting_Results_All_Points	PointsSet	Targeting Results for every cell in model
O_Targeting_Results_Target_Areas_Only	PointsSet	Targeting results for target regions only
O_Topo_Used	Surface	SRTM topography

Appendix 2. Magnetization and Modelling

Magnetization

Local magnetic anomalies in the data are due to the magnetic field produced by magnetically susceptible material beneath the surface that has been magnetized by the Earth's ambient magnetic field. The majority of the response comes from shallow material due to the fast fall-off nature of the magnetic field. For low susceptibilities (< ~0.2 S.I.) the strength of the magnetization vector, and resulting field, is a linear relationship between the Earth's field flux intensity and susceptibility. This makes interpretation relatively intuitive and modelling a less complex process.

Self-Demagnetization

For high magnetic susceptibilities (> ~0.2 S.I) the relationship between the strength of magnetization and susceptibility is non-linear. This non-linear relationship is the cause of the phenomena known as self-demagnetization where a component of the magnetization opposes the Earth's field. The effect of self-demagnetization, which aligns the magnetization vector with the long-axis of the magnetic body, is to reduce the amplitude of the anomaly and change the anomaly location and shape, thus making traditional interpretation unreliable (Wallace, 2007). A typical result of considering only linear magnetization in modelling routines when non-linear magnetization is present is for the resulting dip of a magnetic body to be too shallow.

Remanent Magnetization

Remanent magnetization (or remanence) is a permanent magnetization that can be obtained by ferromagnetic material through several phenomena including thermo-, chemical and detrital remanence. Often, the remanence obtained in the past becomes oriented in a direction different from the Earth's field today; this can occur through movement of the Earth's magnetic poles or through tilting of the stratigraphic units containing the permanently magnetized material. Hence, the induced and remanent components can be oriented in different directions. Typical magnetic

inversion routines assume no remanent component exists and employ a magnetization direction aligned with the current Earth's inducing field, and erroneous results can be obtained from this incorrect assumption (Lelievre et al., 2006). Typical artefacts from inversions where remanence is not accounted for results in model features with very low susceptibility increasing in width with depth.

Appendix 3. MAG3D Modelling Software

MAG3D is a program library (version 4.0 as of August 2005) for carrying out forward modelling and inversion of surface, airborne, and/or borehole magnetic data in the presence of a three dimensional Earth. The program library carries out the following functions:

Forward modelling of the magnetic field anomaly response to a 3D volume of susceptibility contrast.

Data are assumed to be the anomalous magnetic response to buried susceptible material, not including Earth's ambient field. The model is specified using a mesh of rectangular cells, each with a constant value of susceptibility, and topography is included. The magnetic response can be calculated anywhere within the model volume, including above the topography, simulating ground or airborne surveys, and inside the ground simulating borehole surveys. This code assumes susceptibilities are "small". This means results will be wrong when susceptibilities are high enough to cause self-demagnetization. There is no method for incorporating remanent magnetization in this code.

Inversion of surface, airborne, and/or borehole magnetic data to generate 3D models of susceptibility contrast.

The inversion is solved as an optimization problem with the simultaneous goals of (i) minimizing an objective function on the model and (ii) generating synthetic data that match observations to within a degree of misfit consistent with the statistics of those data. To counteract the inherent lack of information about the distance between source and measurement, the formulation incorporates a depth or distance weighting term. By minimizing the model objective function, distributions of subsurface susceptibility contrast are found that are both close to a reference model and smooth in three dimensions. The degree to which either of these two goals dominates is controlled by the user by incorporating *a priori* geophysical or geological information into the inversion. Explicit prior information may also take the form of upper and lower bounds on the susceptibility contrast in any cell (as of version 4.0). The regularization parameter (controlling

relative importance of objective function and misfit terms) is determined in either of three ways, depending upon how much is known about errors in the measured data. The large size of useful 3D inversion problems is mitigated by the use of wavelet compression. Parameters controlling the implementation of this compression are available for advanced users (MAG3D Manual).

Appendix 4. Regional Removal

Regional magnetic responses often dominate weaker, local magnetic responses. By removing the regional magnetic response, an inversion can be produced that is just concerned with a local volume of investigation, and data is produced with easier to discern local features that are not superimposed on the signal of larger responses. Two inversions are performed. The first inversion is the regional inversion which covers the entire data set, uses a coarse cell size, and represents all geologic sources of the magnetic response including large-scale and deeper geology. A second inversion is performed that just focuses on a locally defined volume of interest after regional responses are removed. This modelling-based approach to the subjective process of regional signal removal provides a more robust result that is consistent with the modelling objectives.

The modelling workflow is outlined below:

1. Regional Inversion: Invert the entire data set using a coarse mesh.
2. Regional Response: Define a local volume of interest with lateral extents and a depth of interest (partially based on the regional inversion model results). Forward model the regional model response using the inverted regional model without the local volume of interest.
3. Regional Removal: Calculate a residual by removing the regional response from the original data.
4. Invert the residual data using a refined mesh over the local volume of interest.

For a detailed explanation of the regional removal process, refer to Li and Oldenburg (1998).

Appendix 5. Magnetic Inversion – Regional models removed

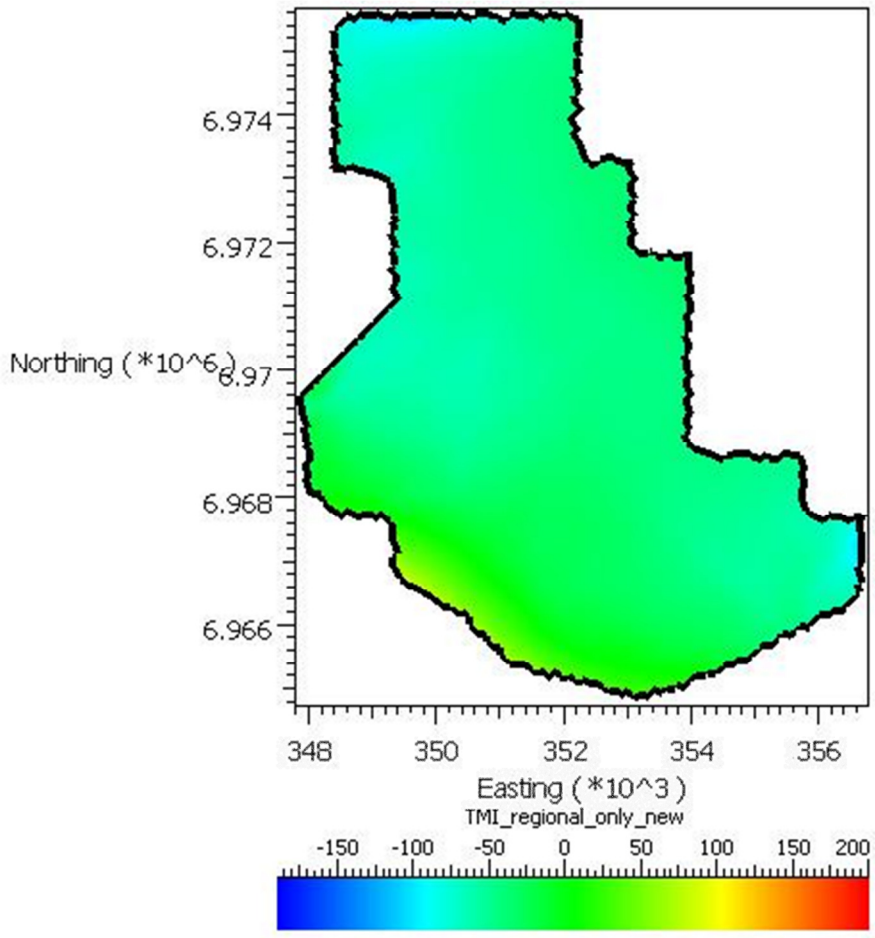

Figure 60: Estimate of Regional Magnetic Intensity for the G Block Property.

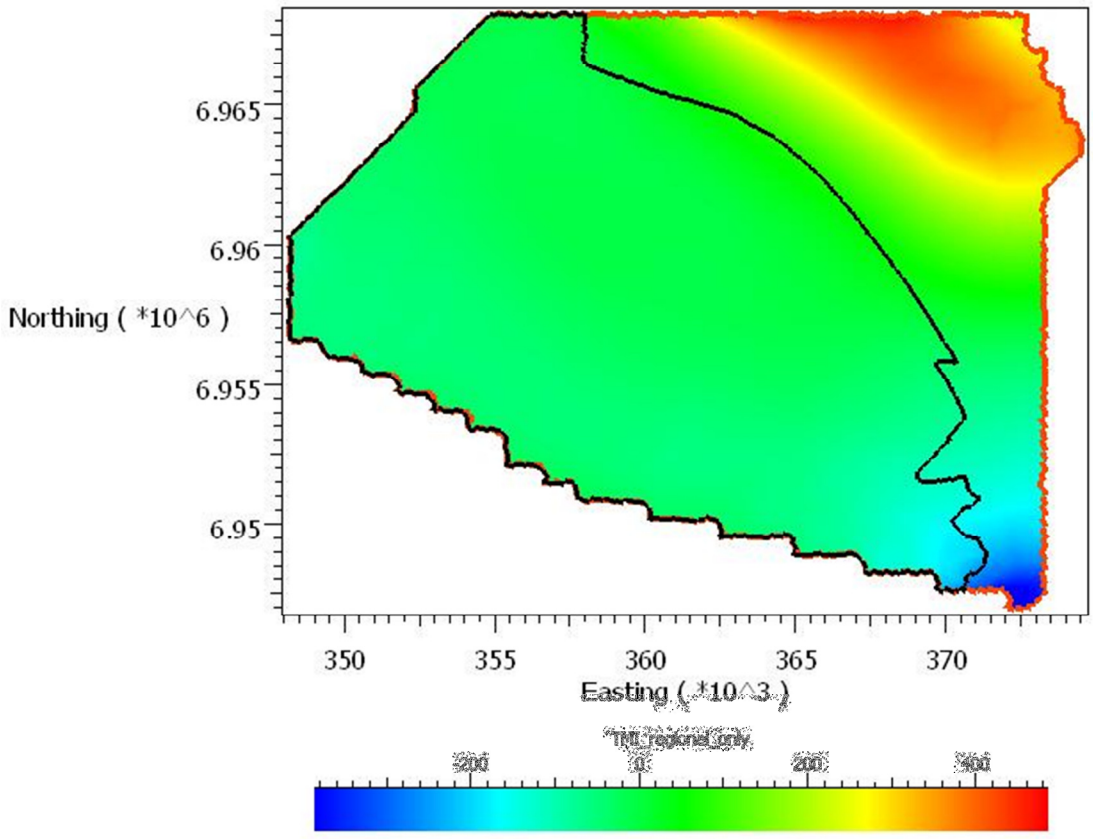

Figure 61: Estimate of Regional Magnetic Intensity for the K Block Property.

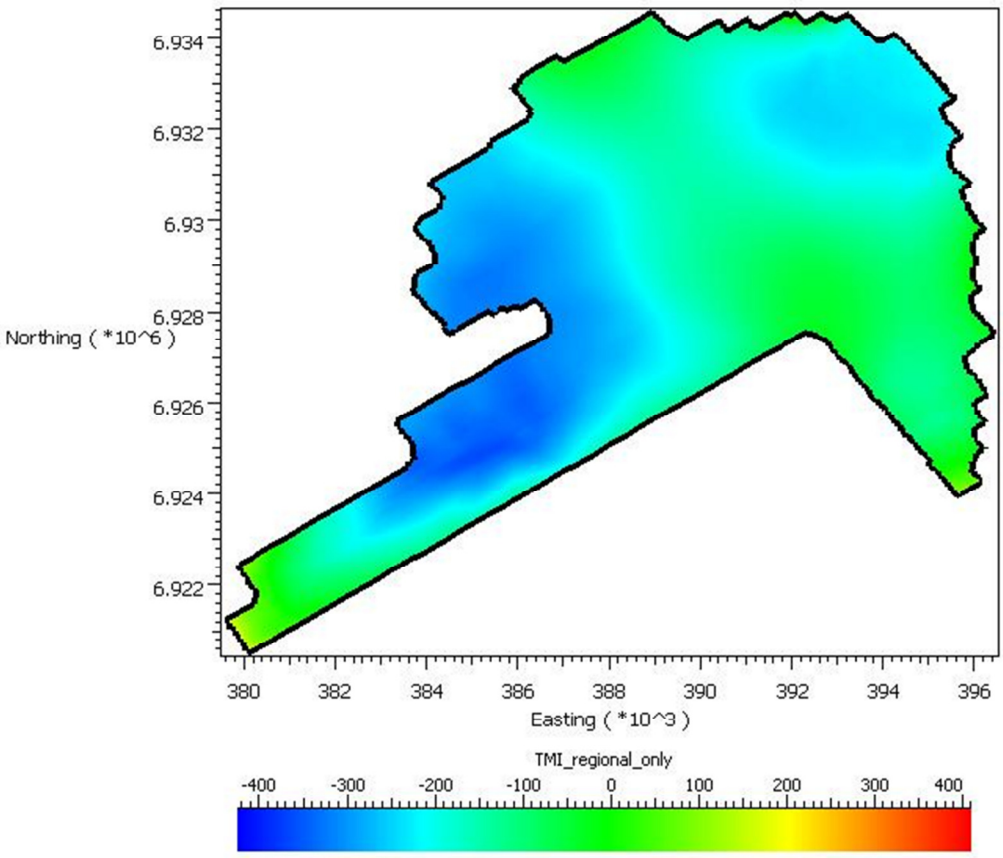

Figure 62: Estimate of Regional Magnetic Intensity for the G Block Property.

Appendix 6. Targeting Criteria for G Block

Evidential property settings used as targeting criteria for Block O. Red indicates that the area is favourable and will be used as an evidence layer.

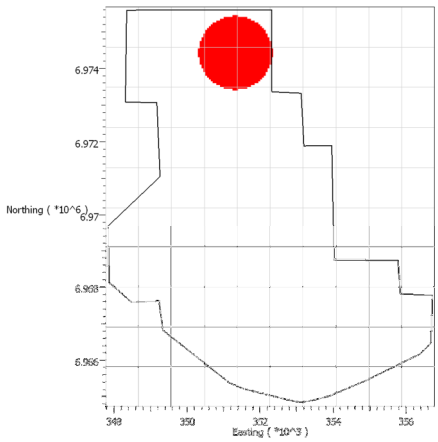

Figure 63: Distance to MINFILE showing = 1000m

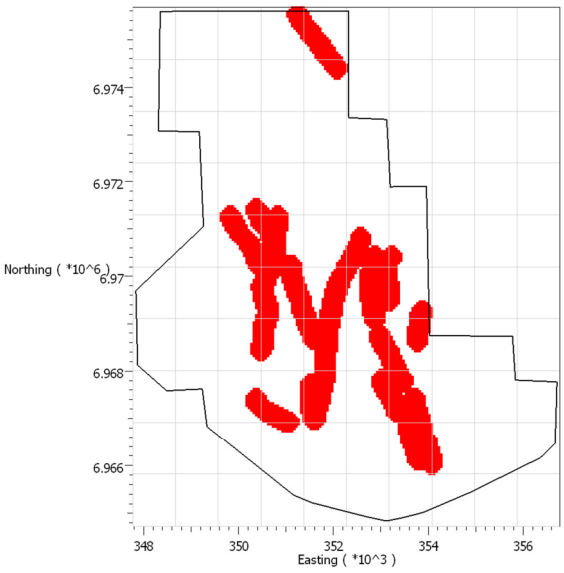

Figure 64: Distance to faults

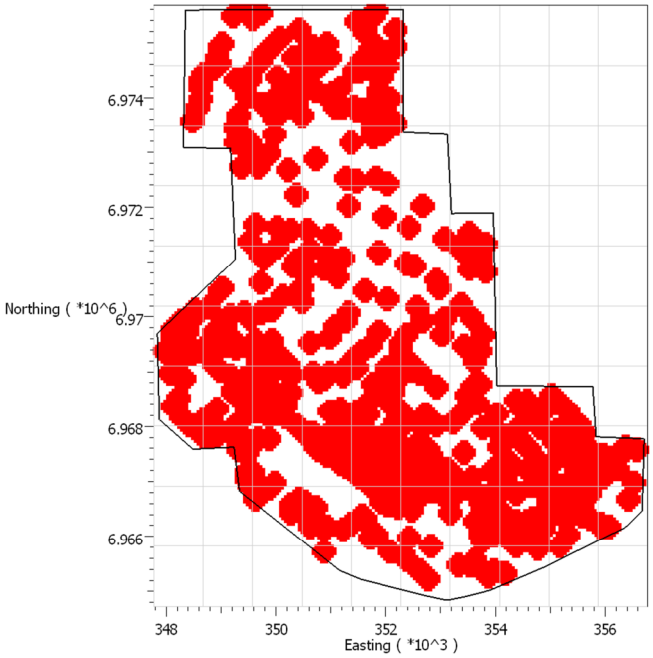

Figure 65: Distance to magnetic highs near surface

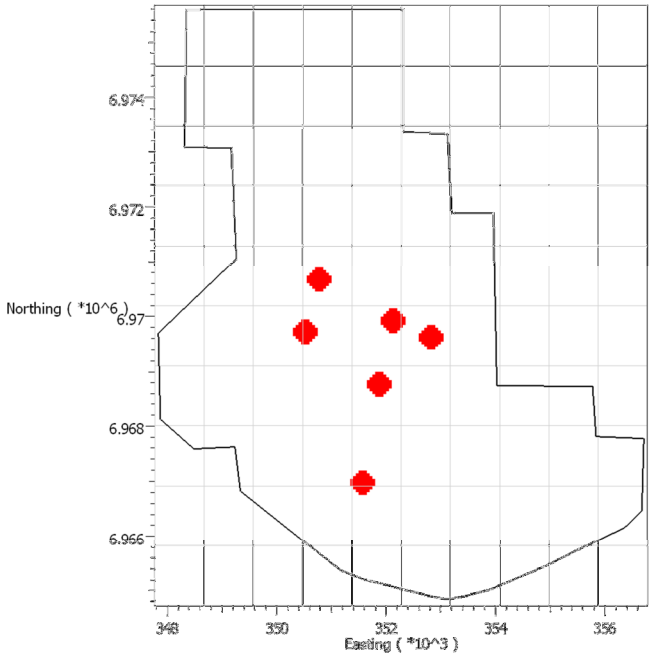

Figure 66: Distance to fault intersections

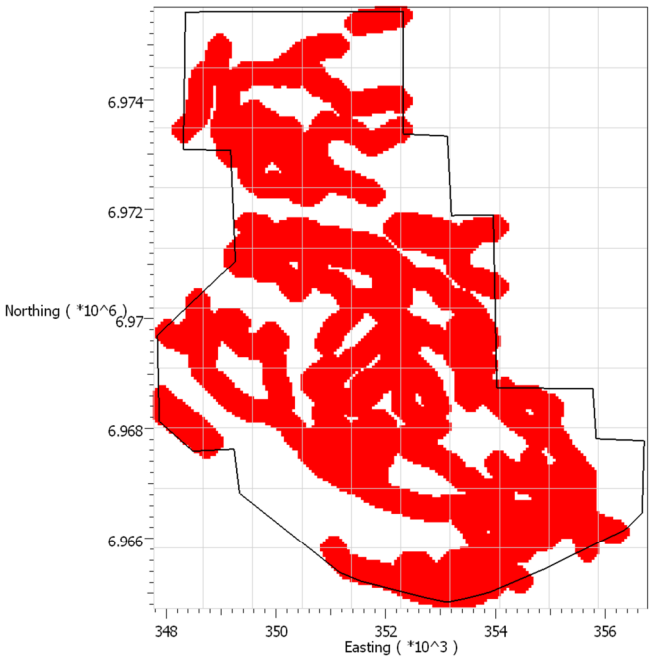

Figure 67: Distance to contacts and dikes

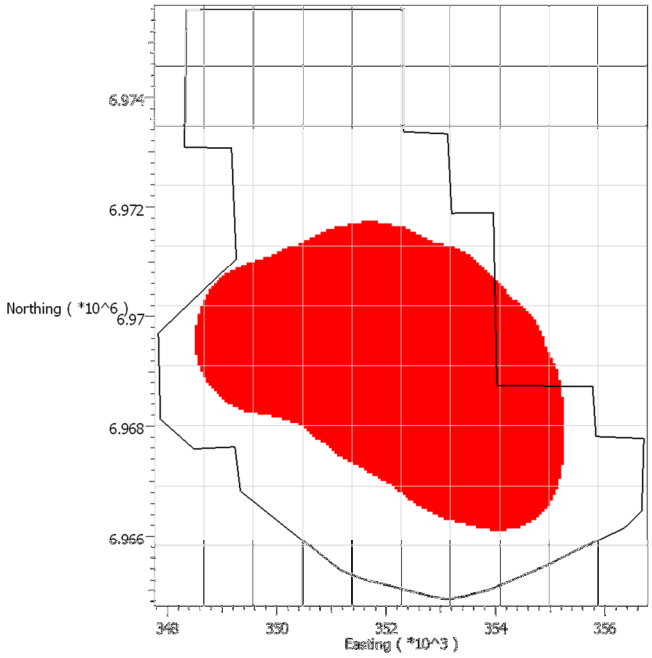

Figure 68: Distance to batholith contact

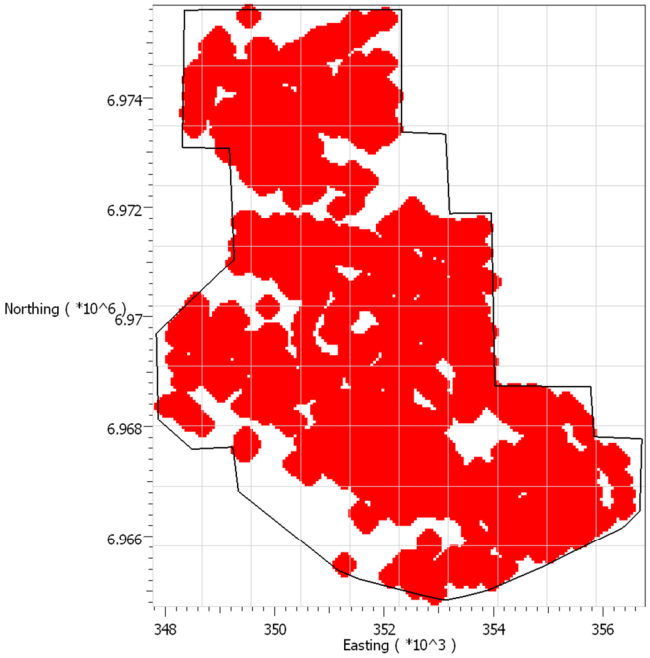

Figure 69: Distance to bends and pinch outs in contacts, dikes, faults, and magnetic anomalies

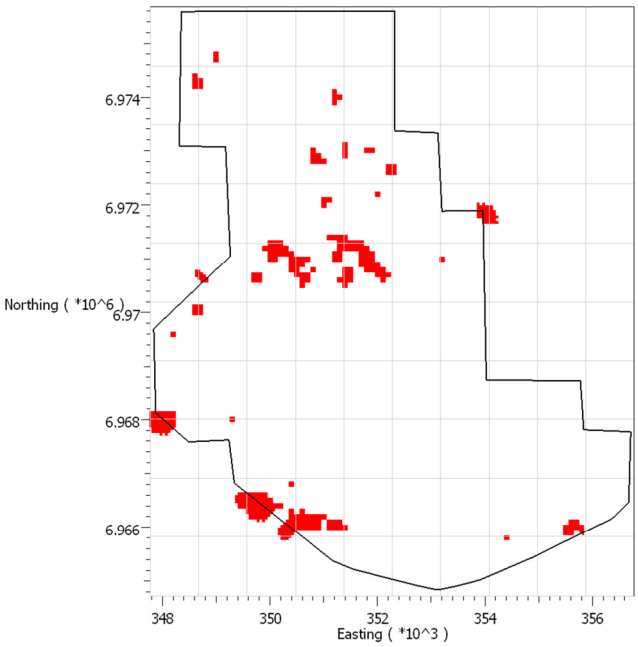

Figure 70: K:Th_anomalies_sigma_1

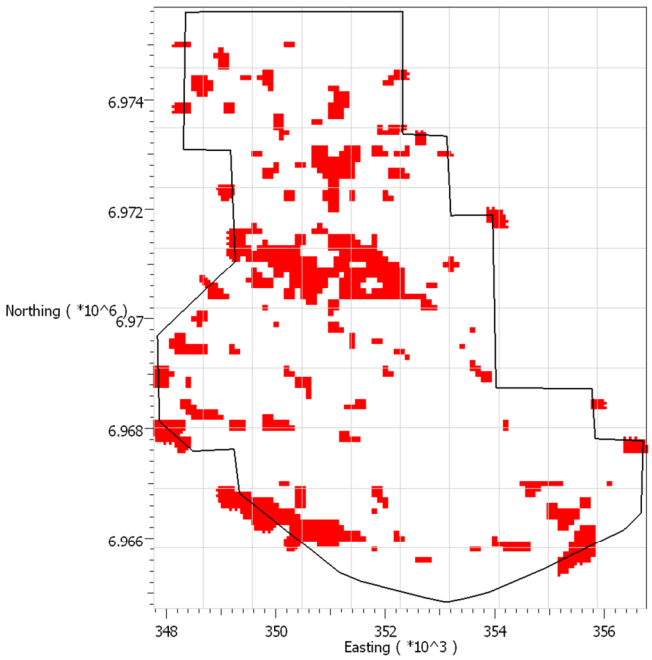

Figure 71: K:Th_anomalies_sigma_2

Appendix 7. Targeting Criteria for K Block

Evidential property settings used as targeting criteria for Block O. Red indicates that the area is favourable and will be used as an evidence layer.

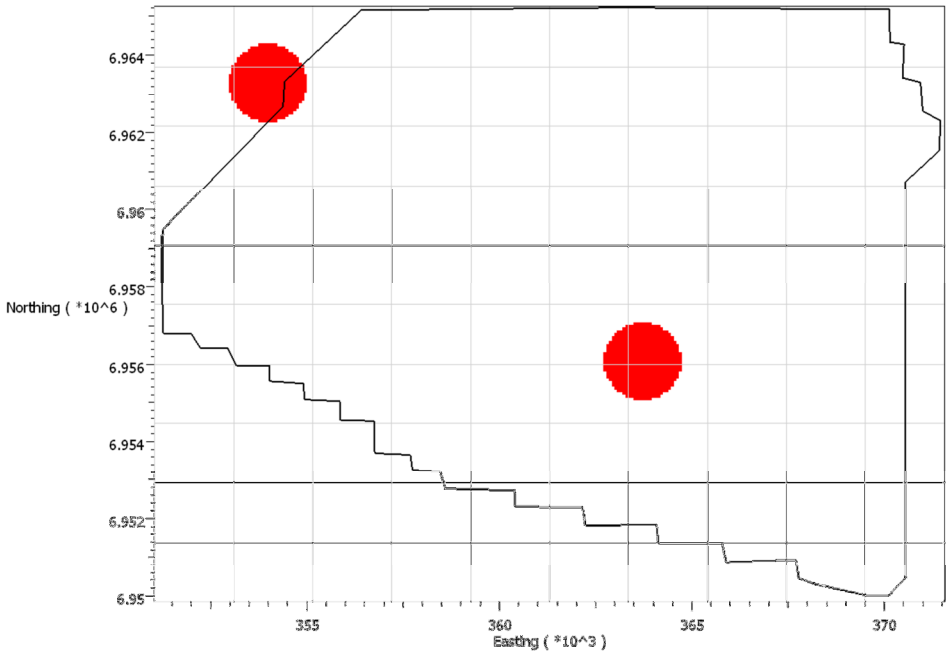

Figure 72: Distance to MINFILE showing = 1000m

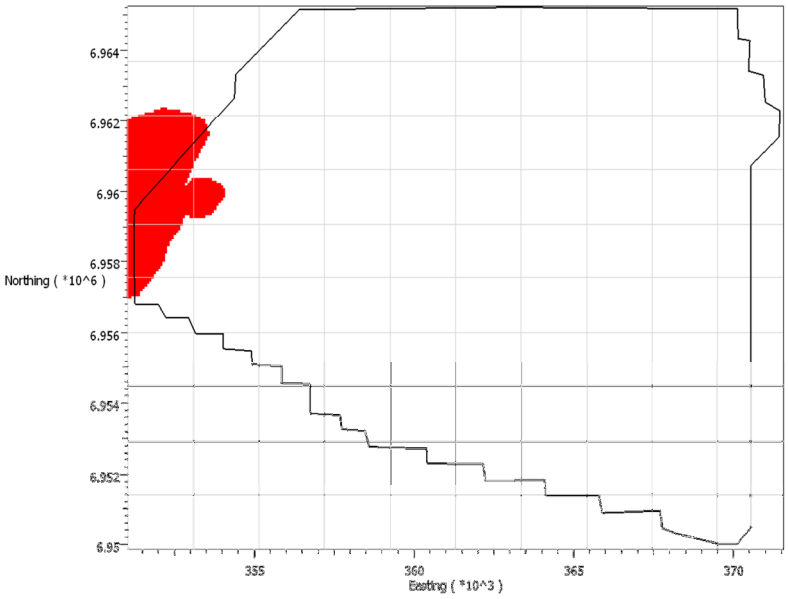

Figure 73: Au stream drainage

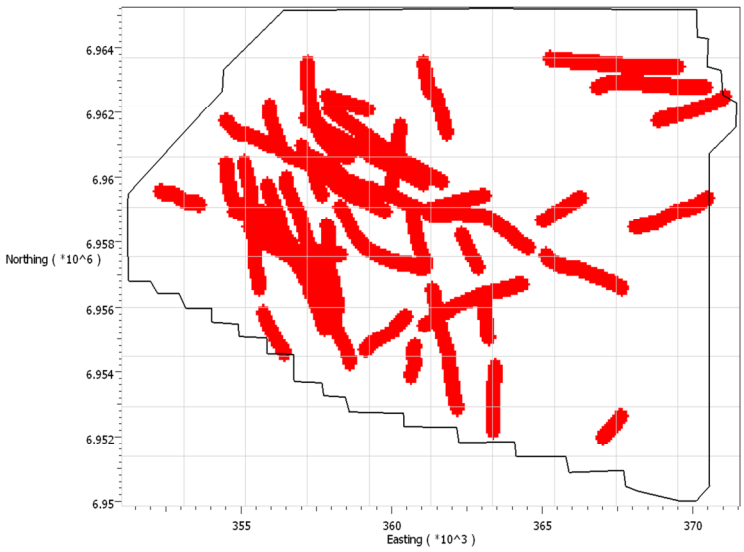

Figure 74: detailed faults

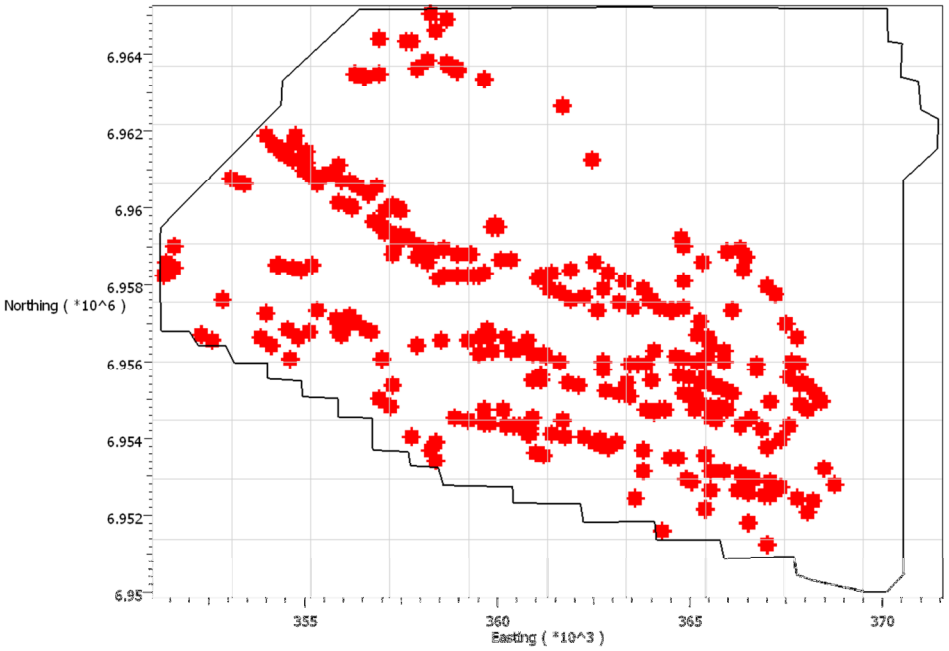

Figure 75: mag highs

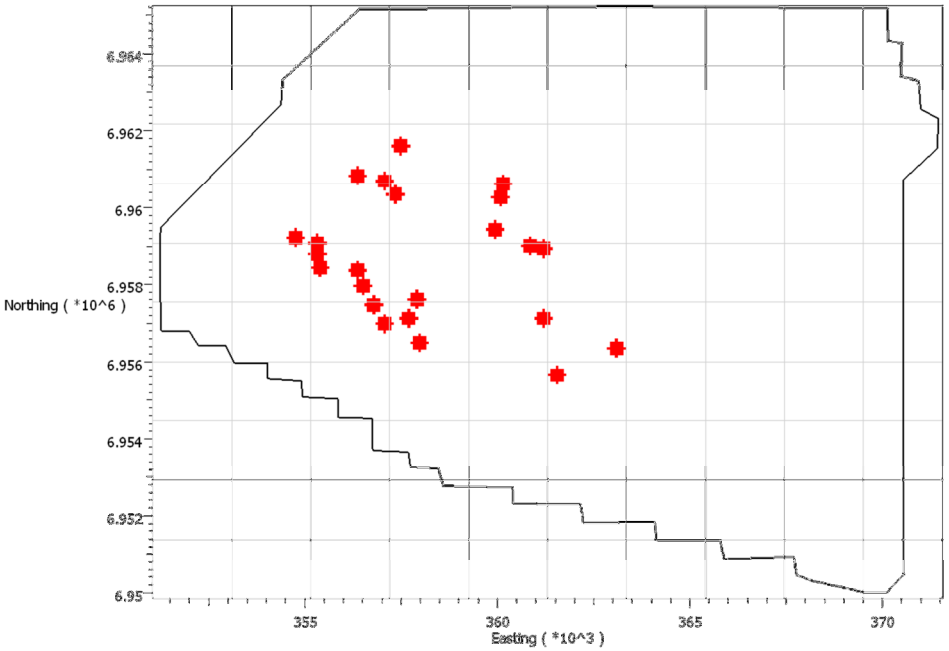

Figure 76: fault intersections

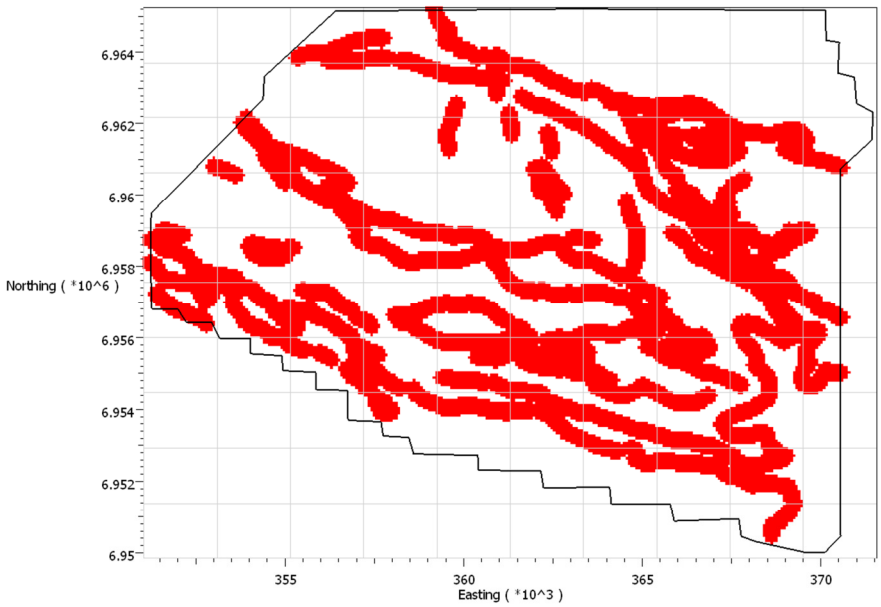

Figure 77: Distance to contacts and dikes

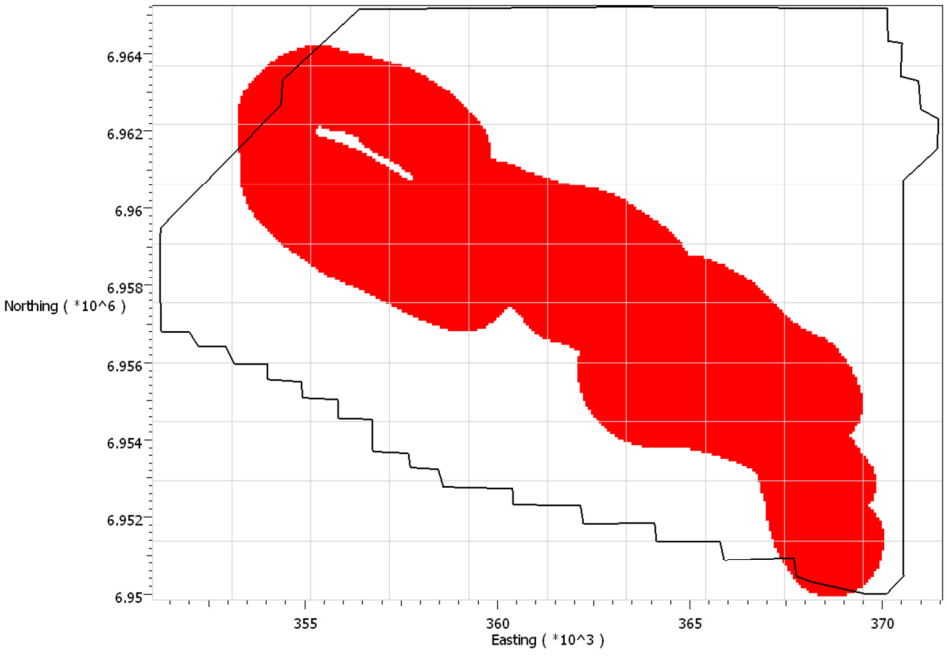

Figure 78: Distance to batholith contact

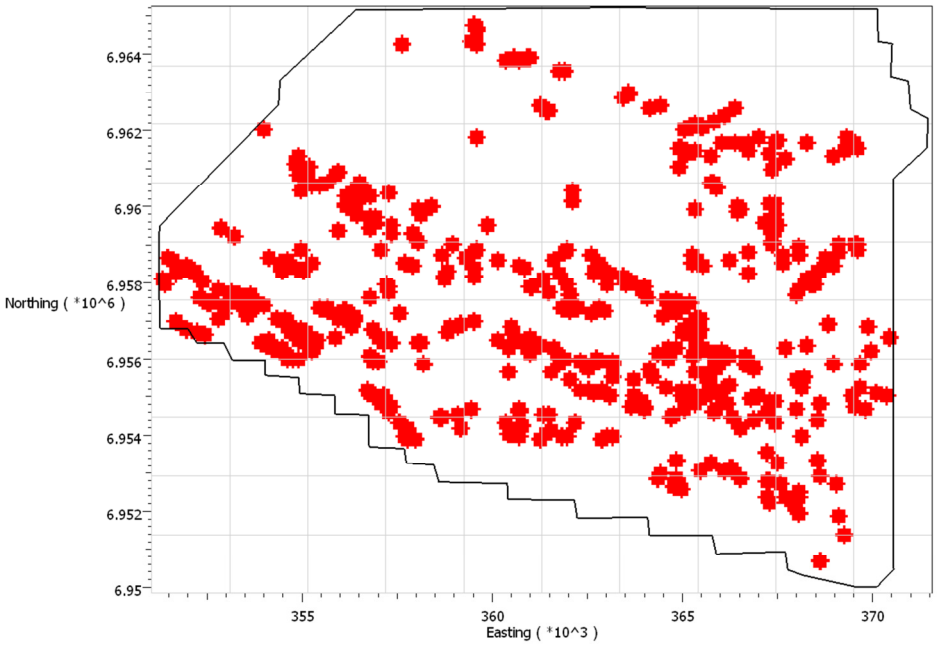

Figure 79: K_Block_bends and pinch outs

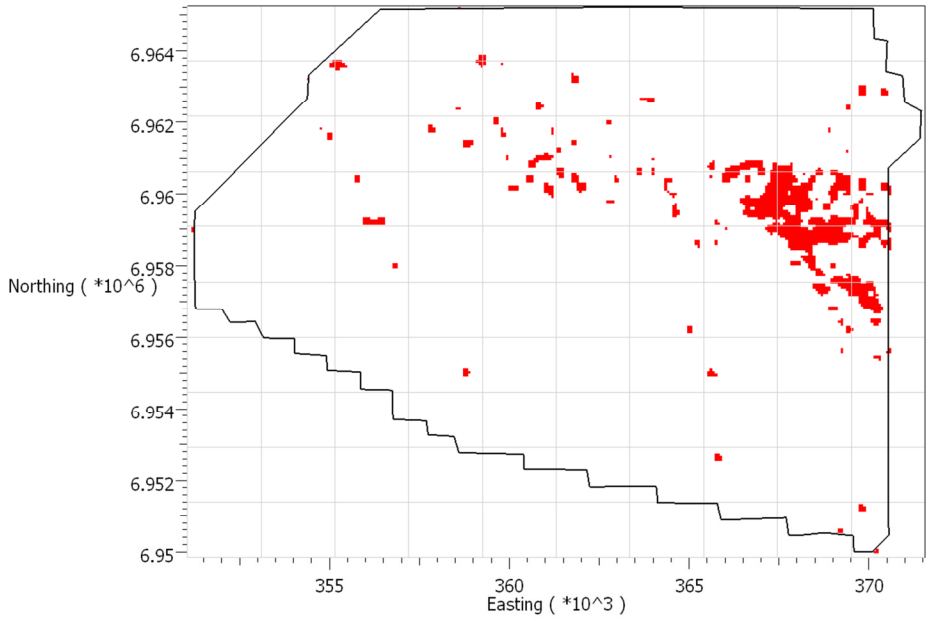

Figure 80: K_Block_K:Th_anomalies_sigma_1

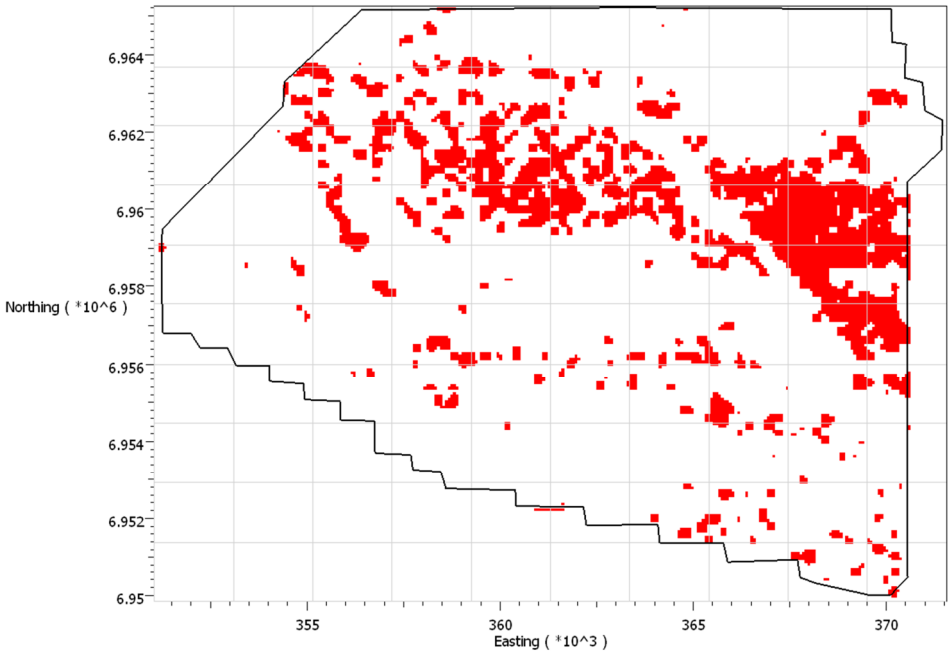

Figure 81: K_Block_K:Th_anomalies_sigma_2

Appendix 8. Targeting Criteria for O Block

Evidential property settings used as targeting criteria for Block O. Red indicates that the area is favourable and will be used as an evidence layer.

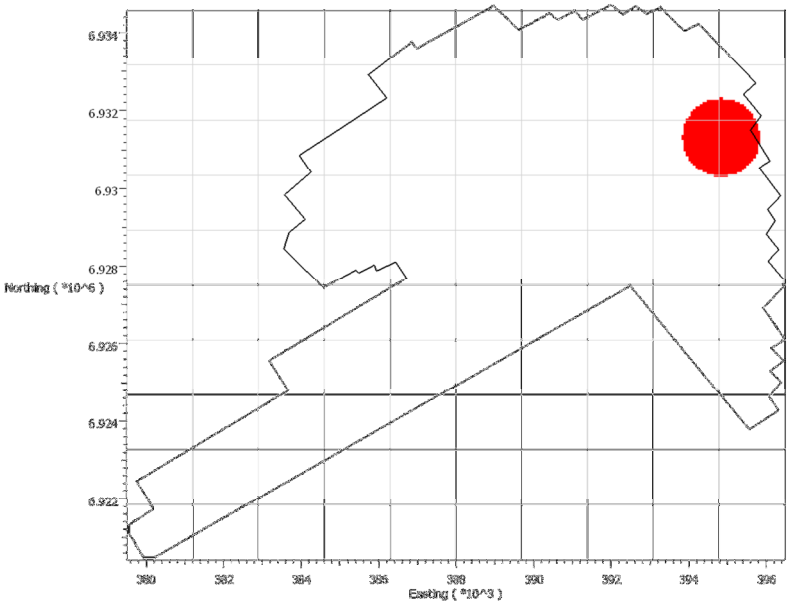

Figure 82: Distance to MINFILE showing = 1000m

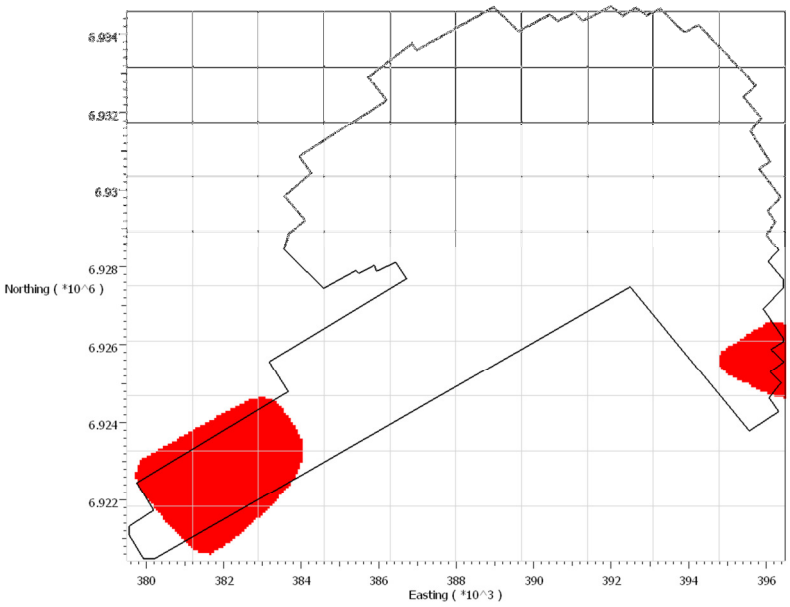

Figure 83: Au stream sediment drainage

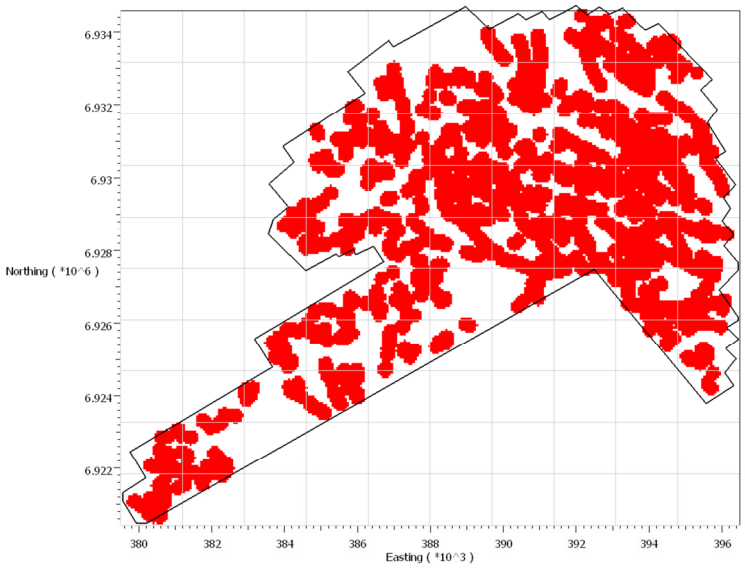

Figure 84: Distance to bends and pinch outs in contacts, dikes, faults, and magnetic anomalies

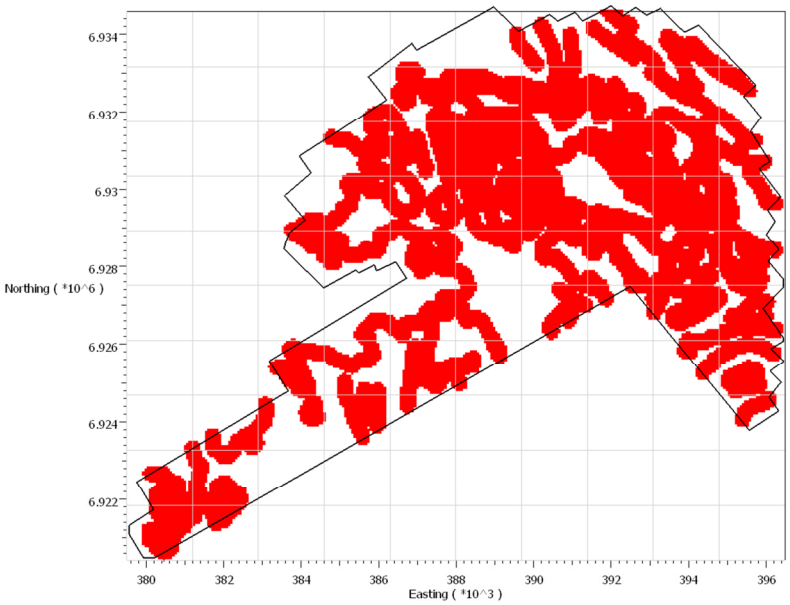

Figure 85: Distance to contacts and dikes

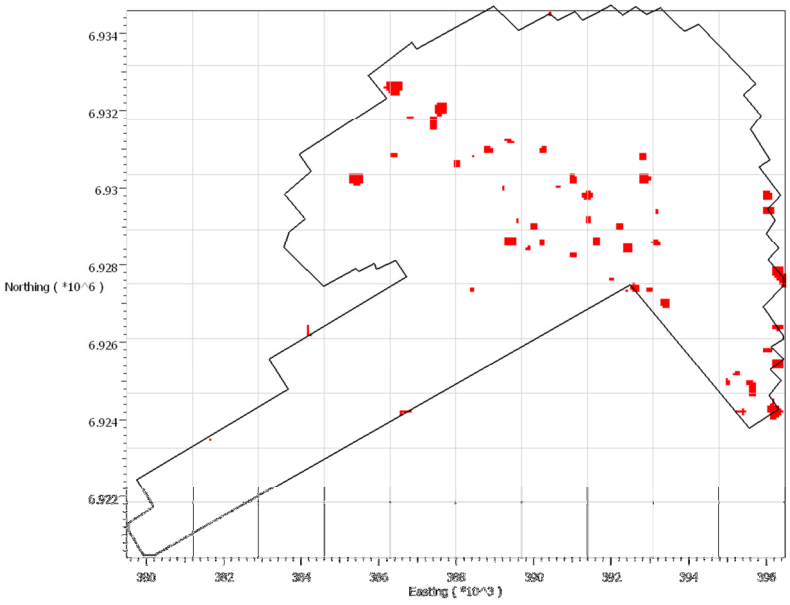

Figure 86: K:Th_anomalies_sigma_1

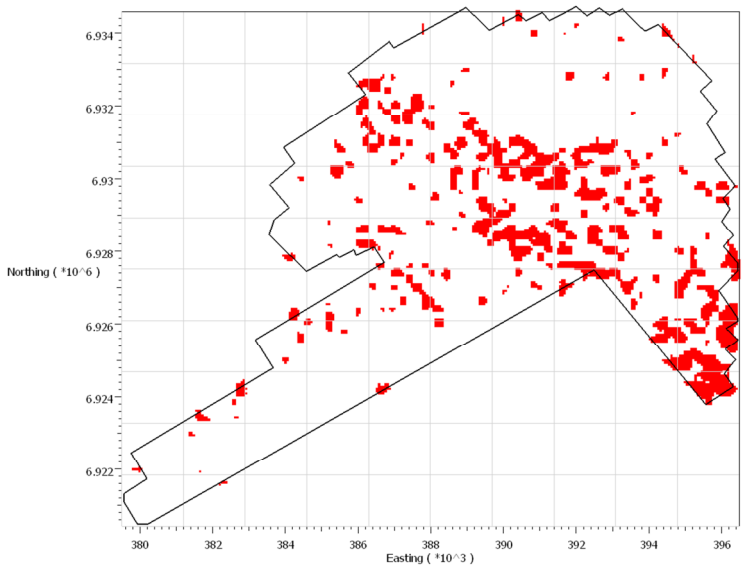

Figure 87: K:Th_anomalies_sigma_2

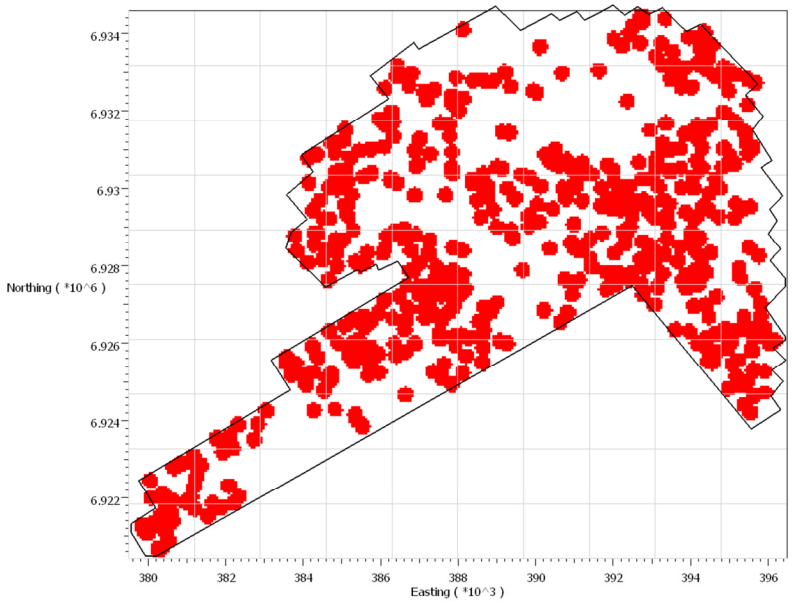

Figure 88: Distance to magnetic highs near surface

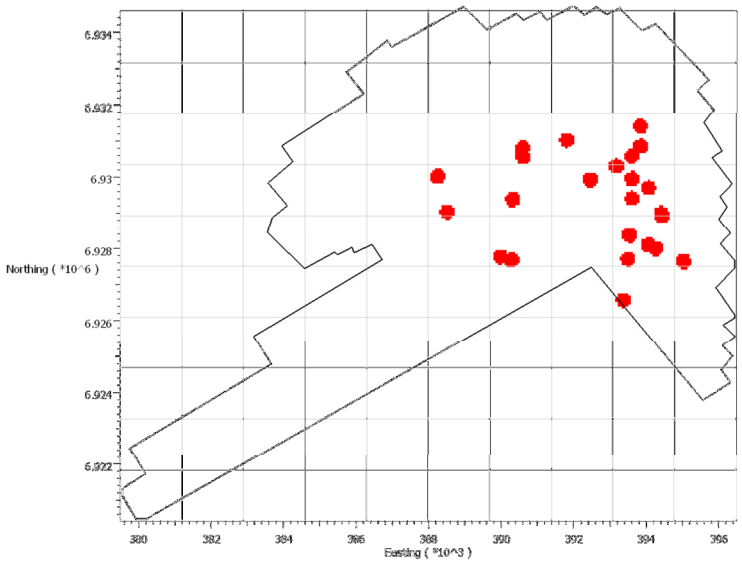

Figure 89: Distance to fault intersections

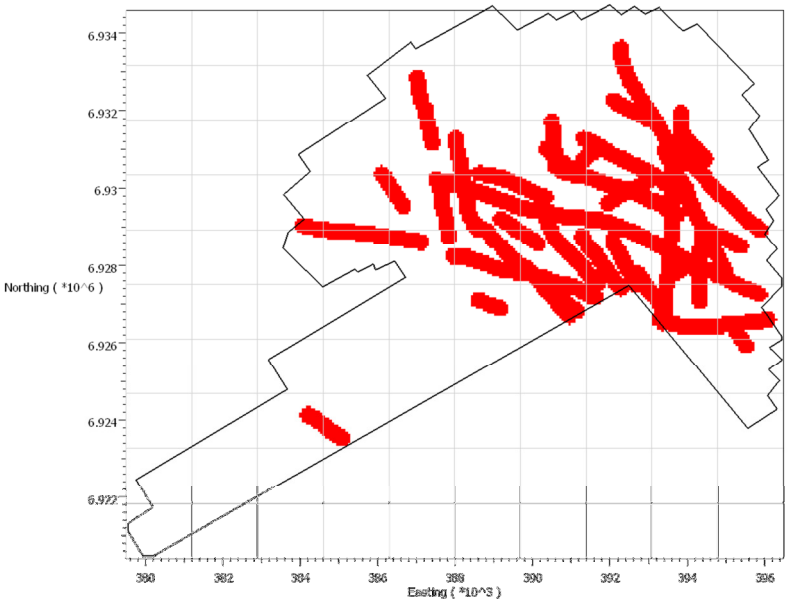

Figure 90: Distance to faults

Appendix 9. Statement of Qualifications

I, Peter L. Kowalczyk of 14717 16A Ave, Surrey, British Columbia V4A 5M6 do hereby certify that:

1) I am a principal consultant at Mira Geoscience Advanced Geophysical Interpretation Centre, a geophysical consulting group that is a part of Mira Geoscience, a geological and geophysical consulting company registered in the province of Quebec.
2) The offices of the Mira Geoscience Advanced Geophysical Interpretation Centre are at Suite 512 B, 409 Granville Street, Vancouver, BC. V6C 1T2.
3) I am a graduate of the University of British Columbia, Vancouver British Columbia (1970 B.Sc. Geophysics).
4) I have been employed in my profession as a mineral exploration geophysicist since graduation.
5) I am duly registered as a Professional Geoscientist (Geophysics) in British Columbia within the Association of Professional Engineers and Geoscientists of British Columbia, registration #20141.
6) I have no interest in the property described as the Carmacks project of Canadian Dehua International Mines Group Inc., nor do I have any plans to acquire any such interest.

Signed at Vancouver, British Columbia this 23rd of December 2010

Peter Kowalczyk, P. Geo.